Bulgarian Academy of Sciences

Bulgarian Geophysical Journal

2013 Volume 39

BGJ

Bulgarian Geophysical Journal (BGJ) is an interdisciplinary journal containing original contributions on physics of the atmosphere and ionosphere, geomagnetism and gravimetry, seismology and physics of the Earth's interior, as well as those dealing with applied geophysics, instrumentation and observations in these scientific fields. BGJ is a joint publication of National Institute of Geophysics, Geodesy and Geography at the Bulgarian Academy of Sciences and the Bulgarian Geophysical Society. BGJ is now published in 1 issue per year.

Address of the Editorial Board:
Bulgarian Geophysical Journal, NIGGG - BAS,
Acad. G. Bonchev Street, bl.3, Sofia 1113, Bulgaria
e-mail: bgj@geophys.bas.bg
Technical Editor: M. Palapeshkova, tel. 979 3330

Bulgarian Academy of Sciences **ISSN 1311-753X**

Bulgarian Geophysical Journal

2013, Vol. 39

Contents

CONTEMPORARY CRUSTAL MOVEMENTS FROM GPS AND TRIANGULATION DATA

N. Dimitrov

National Institute of Geophysics, Geodesy and Geography, Department Geodesy

Abstract. The article discussed a method for joint processing of GPS and classical triangulation measurements to estimate the crustal movements in Central Western Bulgaria region. It was examined the possibility of combining GPS with angular measurements of the first class triangulation network in Bulgaria during the period 1923 - 1930 year. As a result of the processing of GPS and angular measurements are derived horizontal velocities of 15 points. The obtained results indicate the possibility of using the angular measurement of first class triangulation points, together with the GPS, to obtain estimates of the horizontal crustal movements.

Key words: GPS, geodynamics, crustal movements

Introduction

GPS technology is widely used in geosciences. Static GPS measurements are used to determine the crustal movements. Dynamic navigation and GPS definitions are used in geophysics, satellite altimetry, the determination of orbits, physical oceanography, the study of the atmosphere and precise navigation. GPS measurements allow the study of modern tectonics because they provide quantitative assessments of crustal movements in the studied areas. The GPS data provide a good opportunity to study the current geodynamic processes, but the question remains how far back in time can be results interpolated. Combining old triangulation measurements from the twenties of the last century with the GPS measurements made during the last decade can answer this question (Dimitrov, 2011).

In this article a method is discussed for obtaining estimates of the contemporary movement of the crust by processing classical GPS measurements and in the region of central west Bulgaria. This area is of particular interest because of the high population density and high concentration of industrial resources. The results can be used to locate a modern active faults and fault structures.

Processing method

Method of treatment consists in determining the three-dimensional velocity vector at each node of a predefined grid of two-dimensional rectangular region containing measurement data. Having identified the three dimensional velocities of nodes of the grid, the values of the velocity of any point within the region can be adequately approximated by interpolation (Drew and Snay, 1989). Deformations of the corners of the rectangular grid are determined by bilinear function using information from measurements of the geodetic points.

Let P(n,t), L(n,t) and h(n,t) is respectively geodetic latitude, longitude and ellipsoidal height at the moment - t. It is assumed that for a predetermined moment to, there are velocities of the points for which:

$$P(n,t) = P(n,t_0) + u(L(n,t), P(n,t))(t - t_0) \tag{1}$$

$$L(n,t) = L(n,t_0) + v(L(n,t), P(n,t))(t - t_0) \tag{2}$$

$$h(n,t) = h(n,t_0) + w(L(n,t), P(n,t))(t - t_0) \tag{3}$$

Also it is assumed that in a two-dimensional rectangular region it is known three dimensional velocities of the points of vertices of the area, then the velocities at each point in the grid can be calculated by bilinear function.

$$u(L(n,t), P(n,t)) = [u(L_i, P_j)BD + u(L_{i+1}, P_j)AD + u(L_i, P_{j+1})BC + \\ + u(L_{i+1}, P_{j+1})AC] / [(A+B)(C+D)] \tag{4}$$

with:

$$A = L(n,t_0) - L_i \qquad B = L_{i+1} - L(n,t_0) \tag{5}$$

$$C = P(n,t_0) - P_j \qquad D = P_{j+1} - P(n,t_0) \tag{6}$$

Similar equations can be written for speeds - v(L,P) and w(L,P).

Data

GPS measurements of eight points in the region of central western Bulgaria conducted by specialists from the Central Laboratory of Geodesy (CLG) in several periods between 1997 and 2006 is used in estimation. Points of the network are stabilized with metal bolts in typical rocks after geological field study Additional GPS measurements were carried out of seven points of the first class Bulgarian triangulation network. Also it is included angular measurements triangulation network conducted during 1926 1930. (Tabl. 1).

Joint processing of GPS and angular measurements from first class Bulgarian

triangulation network has been done with the software Dynapg (DYNamic Adjustment Program using a Grid).

GPS	epoch				
	1	2	2	2	2
	9	0	0	0	0
	9	0	0	0	0
ID	7	0	3	5	6
BREZ	X	X			
BUHO	X	X			
LOZE	X	X			
SLIV	X	X			
VERI	X	X			
VLAD	X	X			
PLA1	X	X			
0081			X		
0082			X		
0083			X		
0011			X		
0012			X		
0016			X		
0017			X		
0026			X	X	X

Table 1. GPS campaign

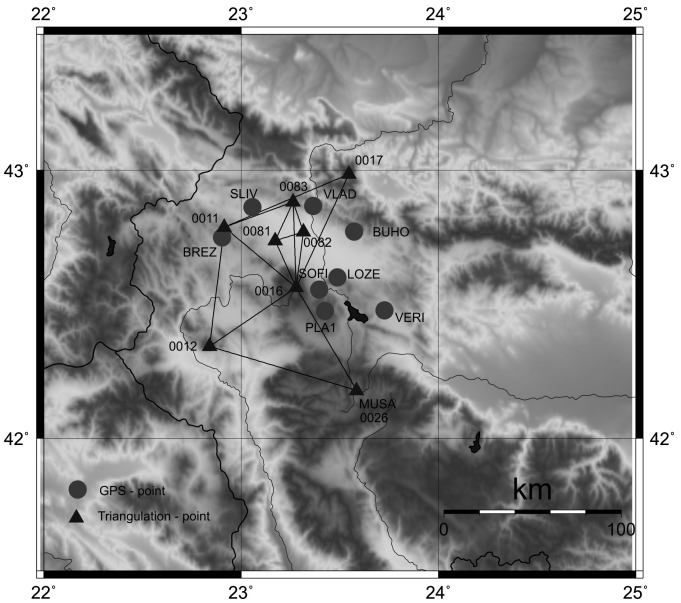

Fig. 1. Network sketch

DYNAPG (Snay, 1996) is a software for estimation of the velocities field of points associated with the movement of the Earth's crust. The program processes the different types of measurements: horizontal directions, distances, azimuths, zenith distance, and vectors derived from measurements with the global positioning system (GPS), and also with very long baseline interferometry (VLBI).

DYNAPG (Snay, 1996) is a software for estimation of the velocities field of points associated with the movement of the Earth's crust. The program processes the different types of measurements: horizontal directions, distances, azimuths, zenith distance, and vectors derived from measurements with the global positioning system (GPS), and also with very long baseline interferometry (VLBI).

Dynapg was developed by modifying software Dynap (Drew and Snay, 1989), which in turn is a modification of the software Adjust (Milbert and Kass, 1987). While Ajust assumed that the coordinates of the points remain fixed in time, it Dynapg can calculate both the coordinates of the points, and the parameters characterizing the movements in the earth's crust.

Dynapg uses format NGS – bbook. There are three input files :

Afile – choice of different options and the adjustment data.

Bfile – contains horizontal directions, angles, distances, azimuths and information

about the approximate coordinates of the measured points.

Gfile – contains information about the GPS measurements and related information.

Result interpretations

In processing are included measurements of five permanent network stations from IGS with the coordinates and velocities in the coordinate system ITRF2000. As a result were obtained velocities of the points (Tabl. 2). After transformation is obtained velocities of points in a coordinate system ETRF2000 (Tabl. 3).

ST	VN	m	VE	m
	мм/г	мм	мм/г	мм
81	10.4	0.4	24.5	0.4
82	10.2	0.4	24.6	0.4
83	10.0	0.4	25.1	0.4
17	10.5	0.4	24.7	0.4
12	11.5	0.4	23.1	0.4
11	10.5	0.4	24.7	0.4
26	11.3	0.5	22.1	0.5
16	11.5	0.4	23.1	0.4
VERI	10.5	0.4	23.3	0.4
PLA1	10.7	0.4	23.4	0.4
BUHO	9.9	0.5	24.6	0.5
LOZE	10.4	0.4	23.9	0.4
VLAD	9.9	0.5	24.9	0.5
BREZ	10.6	0.4	24.6	0.4
SLIV	10.2	0.5	25.0	0.5

Table 2. Velocities of points from the GPS and triangulation measurements in coord. system ITRF2000

ST	VNE	m	VEE	m
	мм/г	мм	мм/г	мм
81	-2.6	0.4	0.9	0.4
82	-2.7	0.4	1.0	0.4
83	-2.9	0.4	1.4	0.4
17	-3.3	0.4	1.8	0.4
12	-1.6	0.4	-0.7	0.4
11	-2.5	0.4	1.1	0.4
26	-1.6	0.5	-1.8	0.5
16	-2.3	0.4	0.1	0.4
VERI	-2.3	0.4	-0.5	0.4
PLA1	-2.2	0.4	-0.4	0.4
BUHO	-2.9	0.5	0.9	0.5
LOZE	-2.5	0.4	0.2	0.4
VLAD	-2.9	0.5	1.3	0.5
BREZ	-2.4	0.4	1.1	0.4
SLIV	-2.8	0.5	1.5	0.5

Table 3. Velocities of points from the GPS and triangulation measurements in coord. system ETRF2000

Conclusion

It is performed a joint processing of GPS measurements at 15 points in the period 1997-2006 and angular measurements of seven triangulation points in the period 1926 1930. Obtained horizontal velocities of the points in the region agree well with the field of horizontal velocities in Bulgaria and Eastern Mediterranean (Georgiev, 2010). The general movement of the points in the region of Central Western Bulgaria is in the south, which is consistent with extensional movement of southern Bulgaria and northern Greece – South-Balkan extensional area (Burchfiel et al. 2000).

The results of the joint processing of conventional and GPS measurements show

the possibility to define crustal movements in areas with relatively weak deformation, also indicate activity in the area and help to clarify the tectonic setting.

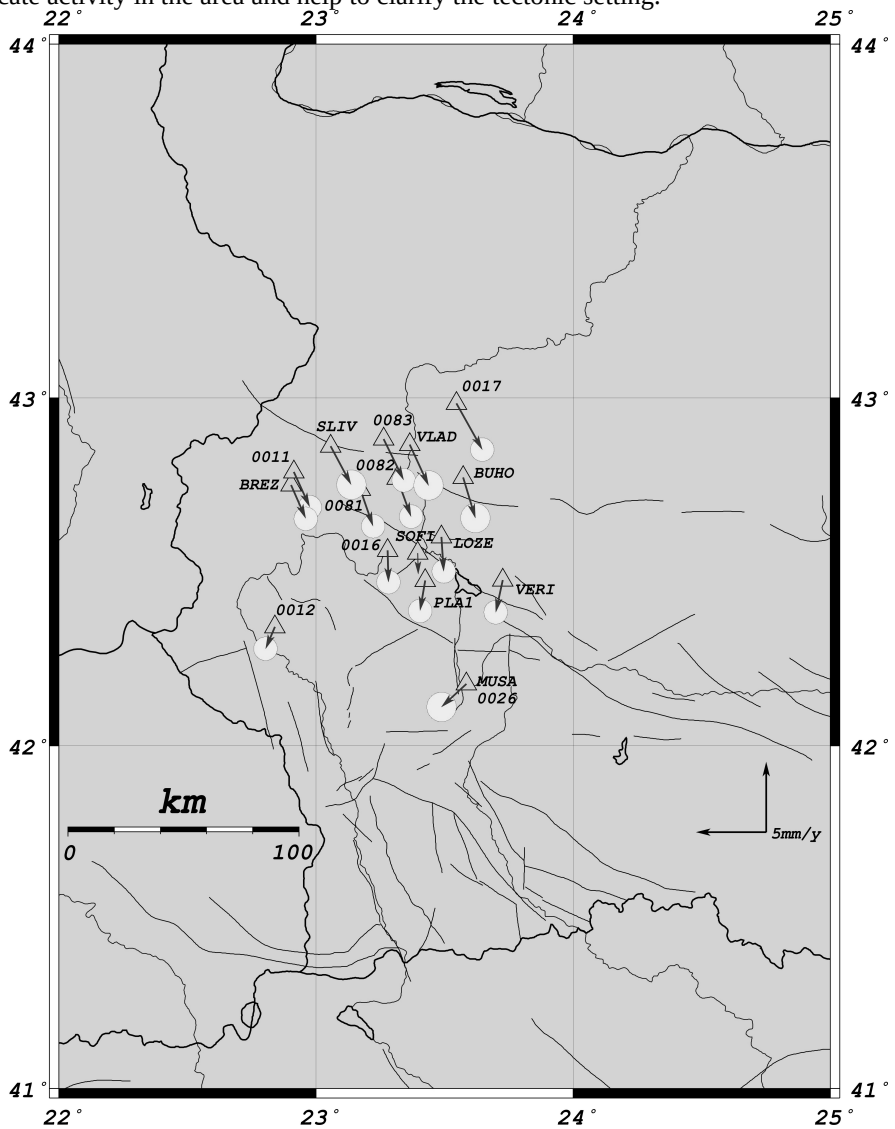

Fig.2. Velocities of points obtained from the analysis of GPS and triangulation measurements to stable Eurasia.

References

Burchfiel, B. C., R. Nakov, T. Tzankov, L. H. Royden, 2000. Cenozoic Extension in Bulgaria and Northern Greece: the northern part of the Aegean Extensional Regime.- In Tectonics and

Magmatism in Turkey and the Surrounding Area (E. Bozkurt, J.A. Winchester and J. D. A Piper, eds.), Geol. Soc., Sp. Publ. 173, 325-352.

Dimitrov, N., 2011. Study of contemporary crustal movements from GPS and classical geodetic measurements in the region of central western Bulgaria. Abstract for acquiring PhD degree, 49str., 14fig.

Drew, A.R. and R.A. Snay, 1989. DYNAP: software for estimating crustal deformation from geodetic data, Tectonophysics, 162, 331-343.

Georgiev, I., 2010. State and permanent GPS networks of Bulgaria - Processing of measurement, analysis and application in geodynamics. Abstract for obtaining the degree "Doctor of Science" 88str., 30 fig.

Milbert, D.G., and Kass, W.G., 1987. ADJUST: The Horizontal Observation Adjustment Program. NOAA Technical Memorandum NOS NGS-47, National Geodetic Information Branch, NOAA, Silver Spring,MD 20910, 53pp.

Snay, R.A., 1996. Documentation for Dynapg Software. NOAA/National Geodetic Survey.

Съвременни движения на земната кора от GPS и триангулачи данни

Н. Димитров

Резюме. В статията е разгледан един начин за съвместна обработка на GPS и класически триангулачни измервания за определяне на съвременните движения на земната кора в района на Централна западна България. Изследвана е възможноста за комбиниране на GPS с ъглови измервания на точки от първокласната триангулачна мрежа на България извършени през перида 1923 – 1930 година. Като резултат от съвместната обработка на GPS и ъгловите измервания са получени хоризонталните скоростите на 15 точки. Получените разултати показват възможността за използване на ъглови измервания на първокласни триангулачни точки, съвместно с GPS, за получаване на оценки на съвременните хоризонтални движения на земната кора.

CONDITION OF THE STRATOSPHERIC AND MESOSPHERIC OZONE LAYER OVER BULGARIA FOR THE PERIOD 1996-2012: Part 1 - TOTAL OZONE CONTENT, SEASONAL VARIATIONS

P. Kaleyna, Pl. Muhtarov, N. Miloshev

National Institute of Geophysics, Geodesy and Geography, str. Acad. G. Bonchev, bl 3, Sofia1113, Bulgaria, e-mail: pkaleyna@geophys.bas.bg, pmuhtarov@geophys.bas.bg, miloshev@geophys.bas.bg

Abstract. A detailed analysis of the variations of the stratospheric and mesospheric ozone over Bulgaria, in the period 1996-2012, is presented in the article on the basis of ground and satellite measurements of the Total Ozone Content (TOC). The move of the most important components: yearly running mean values, amplitudes and phases of the first four harmonics of the seasonal cycle. Their mean values for the period and the existing long term trends have been found.

Key words: total ozone content, seasonal curves, long term trend, trigonometric approximation, sliding time segment.

Introduction

The increased interest to the ozone layer condition of the Earth atmosphere, over the last decades, is due to the understanding that the protection of the whole biosphere from solar radiation UVB (280-315 nm) depends, to some extent, on this little atmospheric compound. Besides, the variations in its concentration have a substantial impact on the temperature regime and hence – on the whole dynamics of the middle atmosphere namely because of the property of ozone to absorb solar energy. In relation to the task assigned to NIGGG by governmental organs to study the condition of the ozone layer over Bulgaria, a daily monitoring of the Total Ozone Content was organized in 2008 with ground facilities working in Sofia also at present. Since it is not possible to obtain a continuous data row (measurements with ground appliances are possible only by clear weather), the data was complemented with measurements from satellite appliances. The output row of daily values allows tracking the condition of the ozone layer in the atmosphere over Bulgaria for a sufficiently long period: from 1996 to 2012 and to make some conclusions regarding the factors which have the greatest impact on it.

Total ozone content in years 1996-2012

The measurements of TOC in NIGGG are conducted with the sun photometer Microtops II, a production of Solar Light Company, USA, http://www.solarlight.com. The appliance is a 5-channel sun photometer with narrowband filters for five wave lengths in the field of ultraviolet solar radiation. The registering of solar radiation flux on the Earth's surface of three of the wave's lengths – 300, 305 and 312 nm allows to determine the total ozone content in the atmosphere by given geographical coordinates of the place of measurement, universal time, and by using the data of the built-in meter of atmospheric pressure. The special electronic with a low noise level and a built-in 20-bit analogue-to-digital converter with high linearity and a dynamic range provide for a high precision of the measurements. An original compensating algorithm for correction of the value received from the relations of the different channels is built in the appliance. The results are obtained fully automatically from the built-in microcomputer; the only manual operation by the measurement is targeting the sensors of the appliance to the Sun for the purpose of which an optical targeting system is provided in the appliance. The accuracy of the appliance, given by the manufacturer, is 1-2%. The error amounts to 6 DU by an average amount of the total content about 300 DU.

The measurements with Microtops II are complemented with data from Ozone Monitoring Instrument (OMI) working on AURA Satellite which are available on http://toms.gsfc.nasa.gov/. The data are presented in a grid with a step of one geographical degree by geographic latitude and longitude. Those which are in relation to the territory of Bulgaria are from 42 to 44°N and from 23 to 28°E. The measurement method of the total ozone is based on the reflection of solar radiation from the cloud cover by conditions close to local noon. The relation between the data obtained from Microtops II and OMI for the period September 2009 to June 2009 is displayed on Fig. 1.

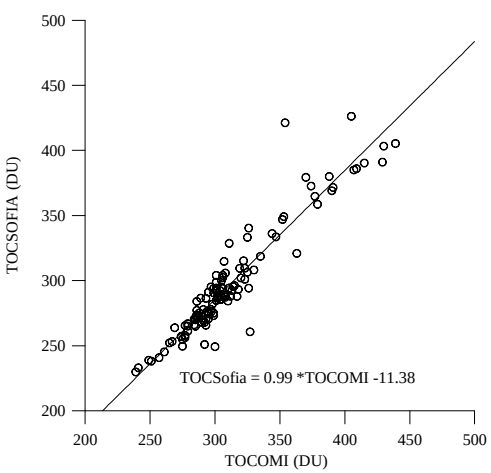

Fig. 1. Relation between the values of the total ozone obtained from the measurements in Sofia and the respective satellite data of OMI

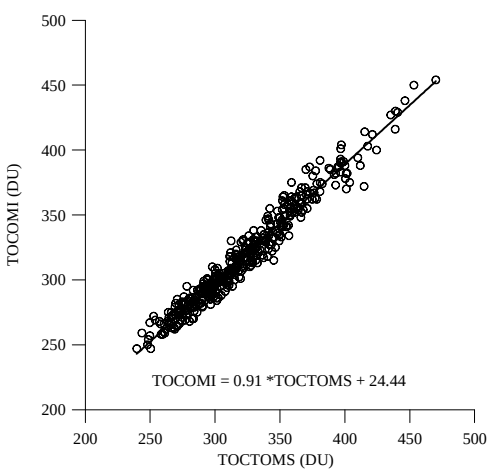

Fig. 2. Relation between the values of the total ozone from OMI and TOMS.

There is a little systematic bias between the two types of measurements, about 11 DU, which allows recalculating the data from OMI and tying them to the data of Microtops II. The data row was extended to 1996 with the data from Total Ozone Mapping Spectrometer (TOMS) aboard the Nimbus 7 polar-orbiting satellite. The simultaneous data from TOMS and OMI from October 2004 to December 2005 allow to calibrate the data of TOMS to OMI and then to the data of Microtops II (Fig. 2).

The resulting data row, notwithstanding that it is obtained from different appliances, should be considered free of systematic bias. The move of the annual monthly values of TOC over Bulgaria is displayed on Fig. 3. A certain seasonal cycle of the total ozone with a spring maximum and an autumn minimum may be readily seen. The initial value of ozone amounts to 305.4 DU by the indicated linear approximation. The resulting positive trend of 0.022 DU a month (0.26 DU a year) is insignificant and allows making the conclusion that the ozone layer over Bulgaria is generally stable in the period under consideration, and there are no reasons to expect trends towards its destruction. Stolarski et al, 1991, Fig. 1 defines a negative trend of the total ozone at 40N latitude of about 0.5 DU/year on the basis of data from TOMS from 1978 to 1990. The present study shows that the negative trend changed to positive in the period of time to follow.

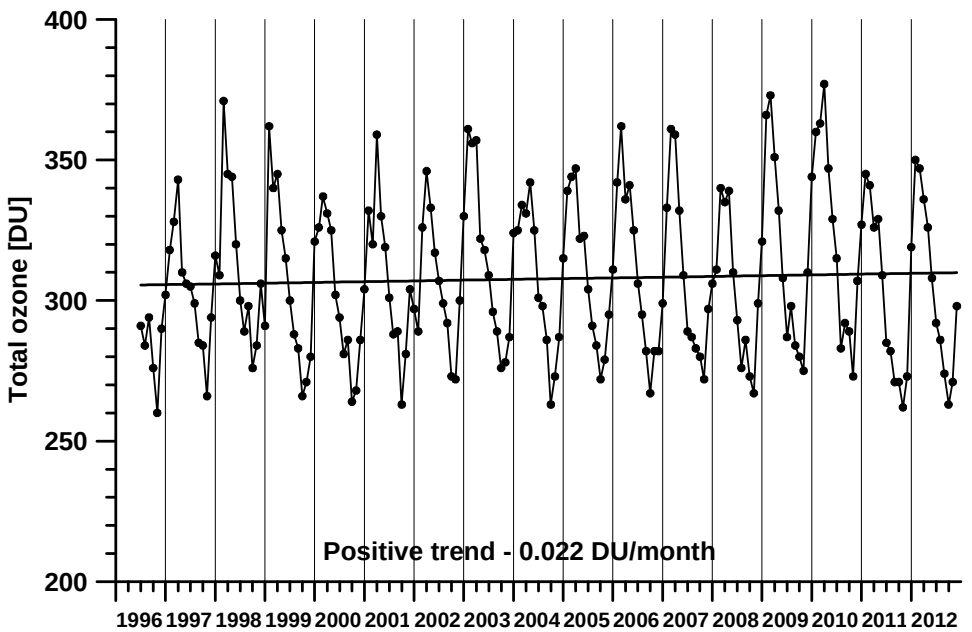

Fig. 3. Mean monthly values of TOC over Bulgaria 1996-2012.

A detailed study of the behavior of the total ozone is appropriate to make on the basis of the components of the seasonal cycle over the studied period. A decomposition of the daily values has been made with a sliding time segment of a year with a step of one day, and the components of the seasonal cycle from the first to the fourth harmonic have been included in the decomposition (that is mean annual value, yearly oscillation, semi-yearly oscillation, 4- and 3-month oscillation). This corresponds to a decomposition in Fourier

series but the amplitudes and phases have been defined by the least squares best fit (Bowman et Krueger, 1985) because of data gaps. The results are presented for the period 1997-2012 because 1996 is not complete, and we have the opportunity to use the data from 2013 until now for the second half of 2012.

The moves of the yearly running mean values of the total ozone displayed in Fig. 4 show three clearly pronounced height sections about 1998, about 2003-2007 and in 2009-2010 and the respective low ones in 2000, 2007 and in 2011. The difference between the highest and the lowest value is about 25 DU. The mean value, indicated with a dotted line, is 308.4 DU and practically coincides with that obtained above on the basis of mean monthly values. The polynomial best fit (degree 2) which shows an upward trend in the first half of the period that changes to a downward trend in the second half is shown as the most common characteristic of the trend to changes of the mean annual value but those trends are very weakly expressed and may hardly be interpreted as an impact, for example of the 11-year solar activity cycle displayed in Fig. 5 with smoothed monthly mean solar radio flux F107. The 16-year period used in the present work does not allow confirming the study (Kilifarska, 2011, 2012) which shows an impact of the solar activity and galactic cosmic rays on the total ozone measured in Arosa (Switzerland).

Fig. 4. Running yearly mean TOC.

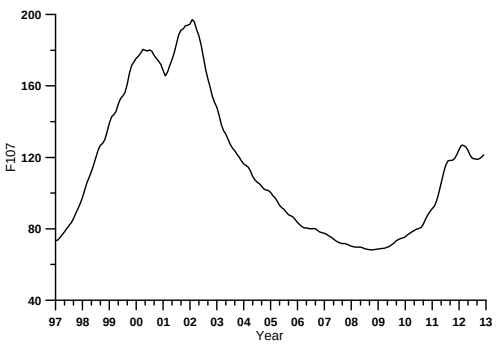

Fig. 5. Smooted monthly mean solar radio flux.

Certain similarity is observed between the running mean annual values of the total ozone and the analogous values of the mean zonal wind speed at 68hPa on Fig. 6 (about 21 km altitude, close to the level of maximal concentration of ozone) obtained from assimilated atmospheric data-set of UKMO for coordinates close to those of Sofia with an accuracy of 2.5° latitude and 3.5° longitude. There is no similarity with the move of temperature. A Quasi-Biennial Oscillation is readily seen in the move of temperature which cannot be observed in the move of TOC (Fig. 7).

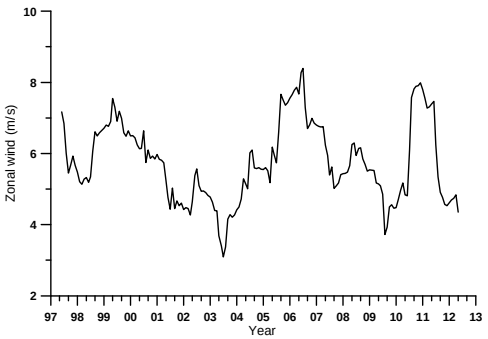

Fig. 6 Running yearly mean zonal wind at 68 hPa (21 km).

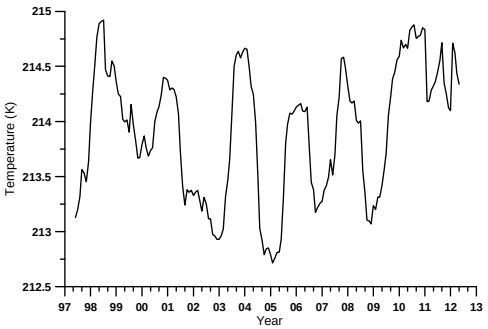

Fig. 7. Running yearly mean temperature at 68 hPa (21 km).

Huang et al, 2008 obtains distinctive Quasi-Biennial Oscillation in the concentration of ozone at altitudes between 30 and 40 km according to data of SABER/TIMED for the period 2002-2004 but predominantly in the equatorial region. The results shown confirm the stable character of the total ozone content over Bulgaria in the studied period. The question whether there is solar dependence of TOC cannot be solved on the basis of the data with which we dispose but it may be presumed that even if there is such dependence, it is sufficiently weak.

The curve of a 12-month amplitude and phase is displayed on Fig. 8 and Fig. 9. This is the strongest variation of the total ozone related to the seasonal cycle. The amplitude of the annual oscillation shows a steady upward trend in the studied period, for example from 30 to 40 DU. This means an increase in the maximal and a decrease in the minimal value over the year on condition that the mean annual value, as it turned out, has no significant upward or downward trend. It can be noticed that the temporary increases and decreases in the amplitude occur in the same periods in which there is an increase of the mean annual value. The linear regression of the amplitude displayed in the figure is: Amplitude=31.3 + 0.64.(year-1997). The mean value for the period, indicated with a dotted line, is 36.4 DU.

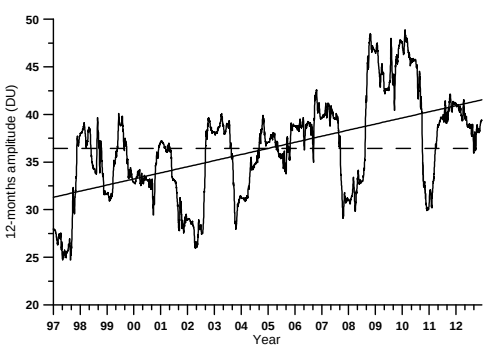

Fig. 8. 12-months amplitude.

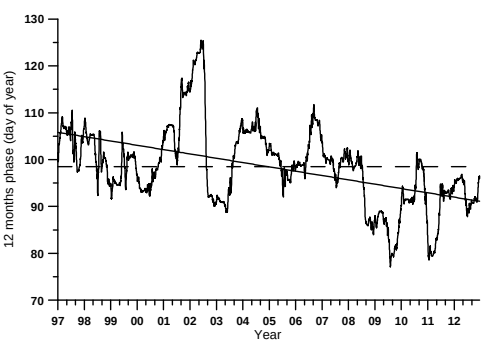

Fig. 9. 12-months phase.

The phase of the annual oscillation shows a distinctive downward trend. The phase (that is the maximal momentum of the annual amplitude) is about the 98th day of the year (the beginning of April) as an average for the period. The negative linear trend is 0.9 days/year. It is not possible to evaluate whether this trend will continue in the future and whether it is related to any long term atmospheric trends on the basis of the available material.

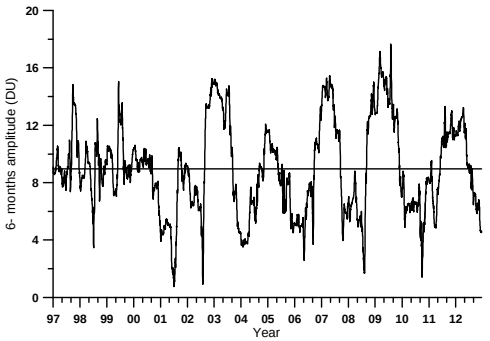

Fig. 10. 6-months amplitude.

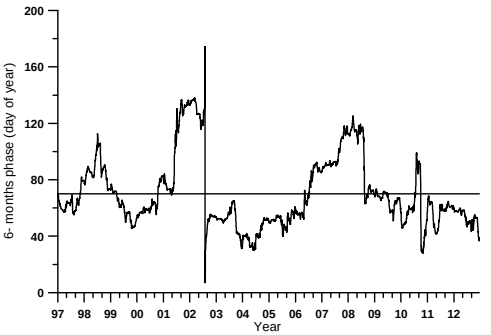

Fig. 11. 6-months phase.

The amplitude and the phase of the semi-annual oscillation of the seasonal cycle of TOC do not show significant trends for the studied period. The amplitude varies in wide ranges: almost from zero until about 16 DU while the mean value is 9 DU (Fig. 10). The mean value of the phase is the 70th day of the year (Fig. 11). A Quasi-Biennial Oscillation can readily be seen in the period 2001 to 2012 which period coincides well with the period of distinctive Quasi-Biennial Oscillations in the temperature of 68 hPa, displayed on Fig.7.

The dependency is, obviously, negative: a decrease in the amplitude of the semi-annual oscillation of TOC corresponds to an increase of the temperature. The amplitudes of the other two components of the seasonal cycle of TOC, with periods of 4 and 3 months, are displayed on Fig. 12, 13. Their values approximate the measurement error. Most probably, their variations are of a random character. Bowman et Krueger, 1985 obtain values of the annual amplitude for the period 1978 - 1982 of about 40 DU and of the semi-annual - about 5 DU, approximately the same values that have been obtained in the present research.

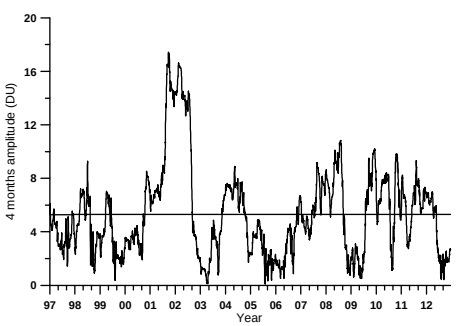

Fig. 12. 4-months amplitude.

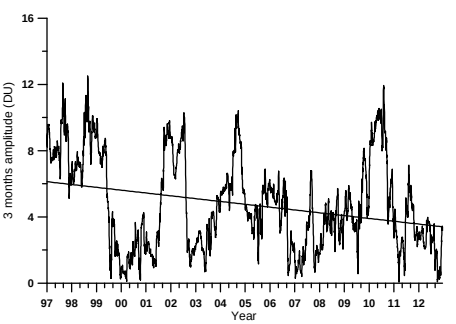

Fig. 13. 3-months amplitude**.**

Conclusions

The analysis of the seasonal cycle of the Total Ozone Content over Bulgaria, made on the basis of assimilated dataset of daily values, obtained by ground and satellite measurements and smoothed between each other with the use of regression fitting, shows that the condition of the stratospheric ozone which is the most important for the protection of the Earth's surface from the harmful impact of the ultraviolet solar radiation is stable during the studied 16-year period (1997-2012) and no trends towards its destruction are observed. The observed variations of the semi-annual value are most probably due to variations of the dynamic stratospheric row which have a purely internal atmospheric character. It has been found that that the natural seasonal cycle of TOC is described by a mean annual value and the amplitudes and phases of the 12-month and 6-month component. The annual component shows clear trends of the amplitude and phase which are, most probably, also due to long term variations in the stratospheric region while the most marked similarity is observed with the variations of the mean annual values of the zonal wind at 68 hPa.

Acknowledgements. The study was funded by FP7-PEOPLE-2009-IRSES (Grant No.247608) IGIT- Integrated geo-spatial information technology and its application to resource and environmental management towards the GEOSS.

References

Stolarski, R., P. Bloomfield, R. McPeters, J. Herman, 1991. Total Ozone Trends Deduced from Nimbus 7 Toms Data, *Geophysical Research Letters,* No 18 (6), 1015–1018, DOI: 10.1029/91GL01302.

Bowman, K. P., A. J. Krueger, 1985. A Global Climatology of Total Ozone from the Nimbus 7 Total Ozone Mapping Spectrometer, *J. Geophys. Res.,* No 90(D5), 7967–7976, doi:10.1029/JD090iD05p07967.

N. Kilifarska, 2011. Nonlinear Re-Assesment of the long-term Ozone variability during 20th century, *Reports of the Bulgarian Academy of Sciences,* Tome 64, No 10, 1479-1488.

N. Kilifarska, 2012. Climate sensitivity to the lower stratospheric ozone variations, *Journal of Atmospheric and Solar-Terrestrial Physics* 90–91, 9–14.

Huang, F. T., H. G. Mayr, C. A. Reber, J. M. Russell III, M. G. Mlynczak, and J. G. Mengel , 2008. Ozone quasi-biennial oscillations (QBO), semiannual oscillations (SAO), and correlations with temperature in the mesosphere, lower thermosphere, and stratosphere, based on measurements from SABER on TIMED and MLS on UARS, *J. Geophys. Res.,* No 113, A01316, doi:10.1029/2007JA012634.

Състояние на стратосферния и мезосферен озон над България за периода 1996-2012 г: Част 1 - Сезонни вариации на тоталното съдръжание на озон

П. Калейна, Пл. Мухтаров, Н. Милошев

Резюме: В статията е представен подробен анализ на вариациите на стратосферния и мезосферен озон над България през периода 1996 - 2012 на базата на наземни и спътникови измервания на тоталното съдръжание на озон (TCO). Изследван е ходът на най-важните компоненти - пълзяща средногодишна стойност, амплитуди и фази на четирите първи хармоника на сезонния ход. Установени са техните средни стойности за периода и съществуващите дългопериодични трендове.

CONDITION OF THE STRATOSPHERIC AND MESOSPHERIC OZONE LAYER OVER BULGARIA FOR THE PERIOD 1996-2012: PART 2 - TOTAL OZONE CONTENT, SHORT TERM VARIATIONS

P. Kaleyna, Pl. Muhtarov, N. Miloshev

National Institute of Geophysics, Geodesy and Geography, str. Acad. G. Bonchev, bl 3, Sofia1113, Bulgaria, e-mail: pkaleyna@geophys.bas.bg, pmuhtarov@geophys.bas.bg, miloshev@geophys.bas.bg

Abstract. An evaluation of the general characteristics of the short term variability of the Total Ozone Content (TOC) over Bulgaria has been made in the article. The impact of the planetary wave activity of the stratosphere on the total ozone has been studied and the climatology of the oscillation amplitudes with periods of 4, 7, 11 and 25 days has been defined.

Key words: total ozone content, short term variability, trigonometric approximation, sliding time segment, planetary waves, climatology.

Introduction

The seasonal cycle pattern of the Total Ozone over Bulgaria has been studied in the first part of the work with the means of its basic components corresponding to the components of the decomposition of one periodical (with a period of one year) process in Fourier series. There are also other types of oscillations in the atmosphere which are of a quasi-periodical character called planetary waves. They represent wave processes developing in an elastic medium as is the atmosphere. They originate from baric and thermal discontinuities arising at certain altitude regions. As a rule, those oscillations occur in random moments and continue for a relatively short time (several periods) in contrast to the oscillations which are generated by periodic influences related to the rotation of the Earth on its axis and around the Sun. The quasi-periods of the planetary waves, defined by the presence of resonant modes in the atmosphere, vary in wide ranges but are less than a month. Those waves are regarded as zonally (along a given geographic parallel) distributed variations of a given atmospheric characteristic (temperature, pressure, wind speed), sinusoidal by time and geographic longitude. The different types of waves posses different wave numbers and directions of propagations. The waves manifest themselves as an

oscillation in time in a point with given geographic coordinates.

A detailed resume of the studies in this area is given in Pancheva and Mukhtarov, 2011.

Variability of the total ozone content in years 1996-2012

For the purpose of the present research, the row of daily values of TOC, described in detail in the first part of the work, is filtered while the sliding mean value is extracted from every value in a segment of 31 days centered on the respective day. In this way, all variations with a temporary scale over 31 days (including the seasonal cycle) are filtered. The curve of the daily values received in this day is displayed on Fig. 1.

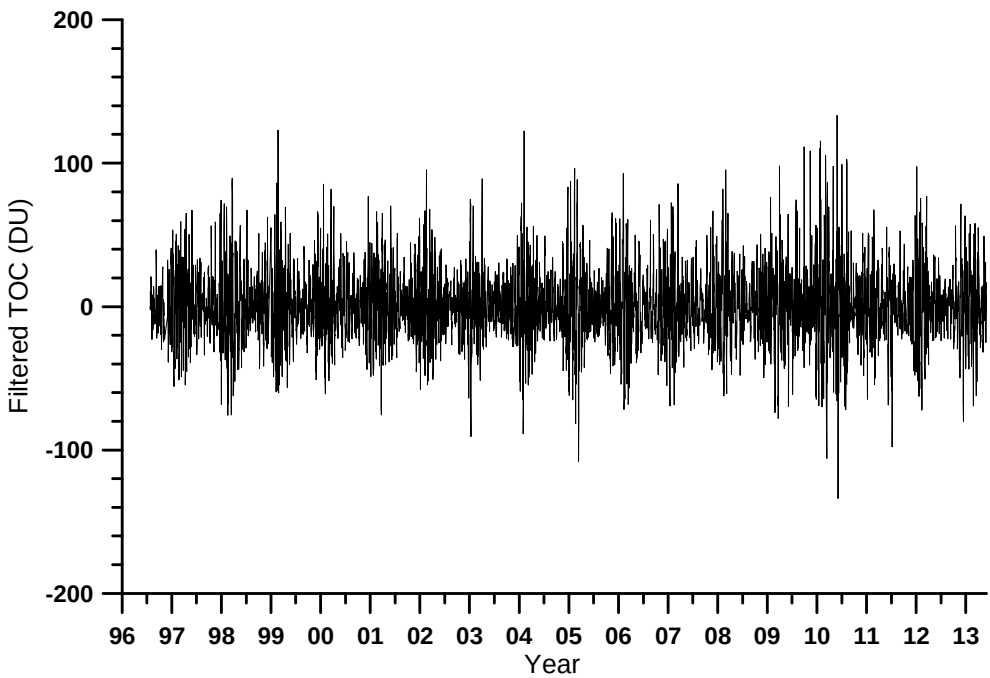

Fig. 1. Curve of the filtered values of the Total Ozone Content for 1996-2013.

It is obvious that short term variations have a considerable swing which is in the range of the mean seasonal cycle in some cases. Naturally, not only the assumed impact of the planetary wave activity but also local variations are included in those variations. A general characteristic of the total variability of the total ozone content over Bulgaria give the statistical characteristics displayed on Fig. 2: probability density, mean value and standard deviation.

Empirically, the output probability density deviates significantly from Gaussian model and shows a greater similarity to Laplacian model.

The mean value is practically zero which is a characteristic of the used filtering method. The probability of a short term variation in a given day in absolute value not more than the standard deviation, 24 DU, is 75% which value is obtained through integration of the empirical probability density.

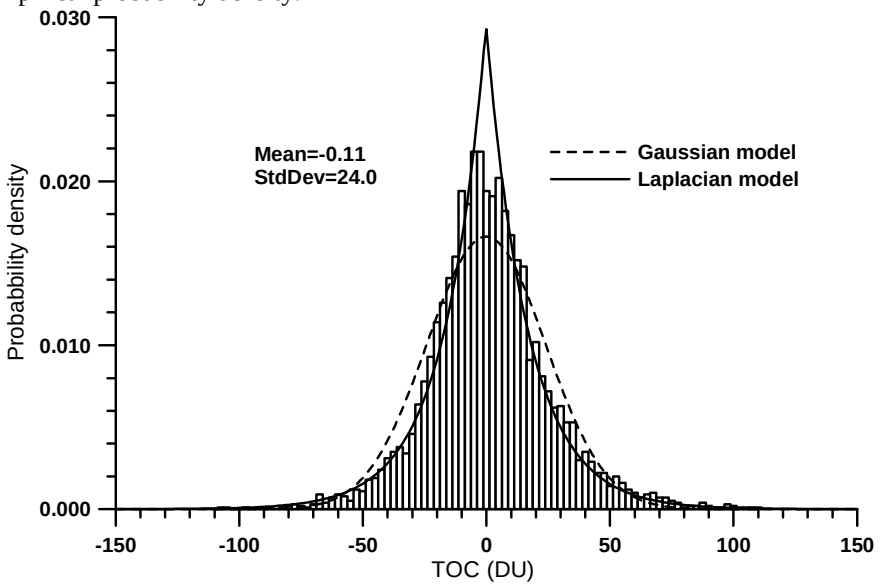

Fig. 2. Main statistical characteristics of the short term variability of Total Ozone Content over Bulgaria.

Influence of planetary waves over total ozone content

It is necessary to make an additional data filtering in order to evaluate the quality and quantity of the probable impact of the planetary wave activity on the total ozone. It is not feasible to use the strongest criterion for defining planetary waves, namely the analysis of the zonal structure which requires global data, by single-point data. The only opportunity is to look for such oscillations in time that will respond to the manifestation of planetary waves in one point – quasi-periodical oscillations with periods which correspond to the prevailing periods that are defined by the studies of global data. The move of the filtered data, displayed on Fig. 1, shows a distinctive nonstationarity expressed in a visible seasonal dependence of the amplitudes of the variations (increased during winter season) which does not allow to use effectively the different kinds of spectral analysis on the basis of Fourier transform. The wavelet analysis is suitable in this case (Pancheva and Mukhtarov, 2000) adjusted to the case when there are data gaps (Mukhtarov et all, 2010). Wavelet analysis based on the function of Morlet reveals oscillations with a given period which are expressed only in the area of a given moment of time.

A wavelet spectrum for two years of the studied period is displayed on Fig. 3. The presence of quasi-periodical oscillations with periods of about 7 days, about 10 days and

about 22 days is visible during winter periods. Those oscillations are of a localized character as it is characteristic for the planetary waves.

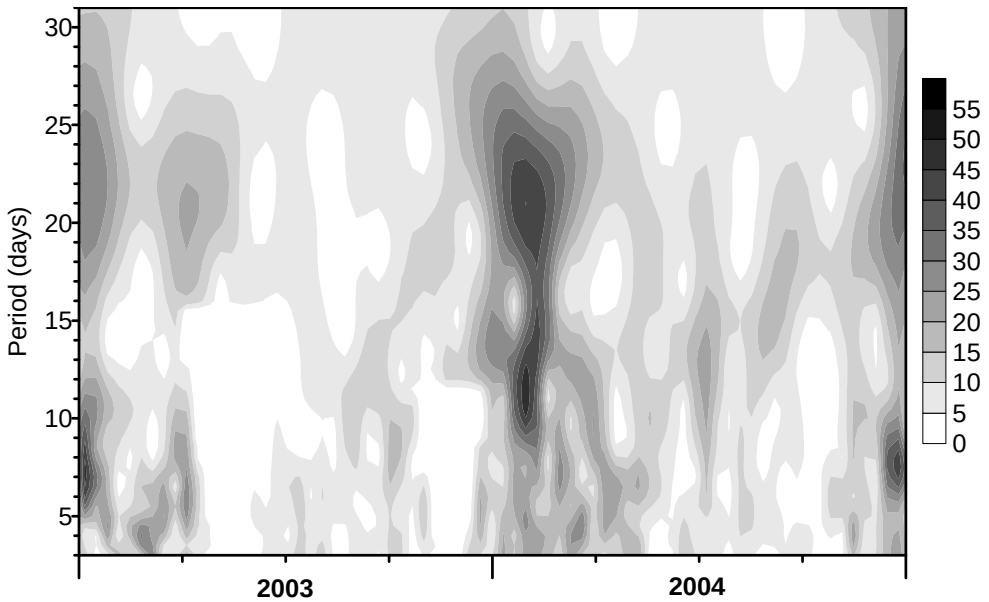

Fig. 3. Wavelet spectrum of filetered TOC in yeares 2003-2004.

A mean spectrum has been calculated to obtain a general idea of the prevailing periods by averaging the amplitudes of the oscillations with a given period in all the days of the years from 1997 to 2012, displayed on Fig. 4.

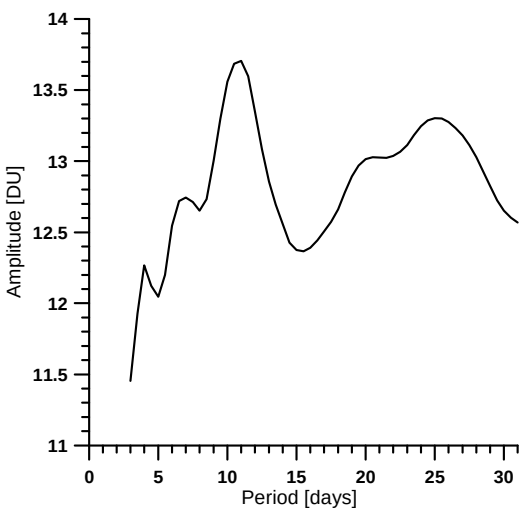

Fig.4. Mean wavelet spectrum of filetered TOC in yeares 1997-2012.

The spectrum is continuous which means that there are oscillations in the data within all periods from 3 to 31 days but there are readily seen prevailing ones about 4, 7, 11 and 25 days which periods are characteristic for the planetary waves in the stratosphere (Pancheva et al., 1994). The output mean spectrum confirms the assumption that the planetary wave activity is reflected in the concentration of ozone in the stratosphere (Fusco and Salby, 1999).

Having defined the prevailing periods, it is possible to study the curve of their amplitude with time by means of decomposition with sliding segments (Pancheva et al., 2009). Naturally, the method is used in its one dimensional version, in functions only of time. This filtering method of oscillations with predefined periods just like the wavelet-analysis has the property of localization in time. The simultaneous defining of the amplitudes and phases in the vicinity of a given moment of time (a sliding segment of 31 days has been used) makes the method effective in the cases when there are oscillations with different periods that are close by day of existence.

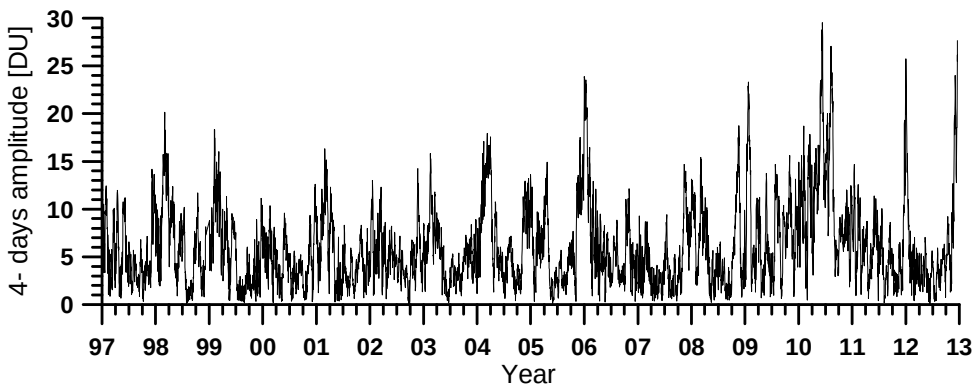

Fig. 5. 4- days amplitude.

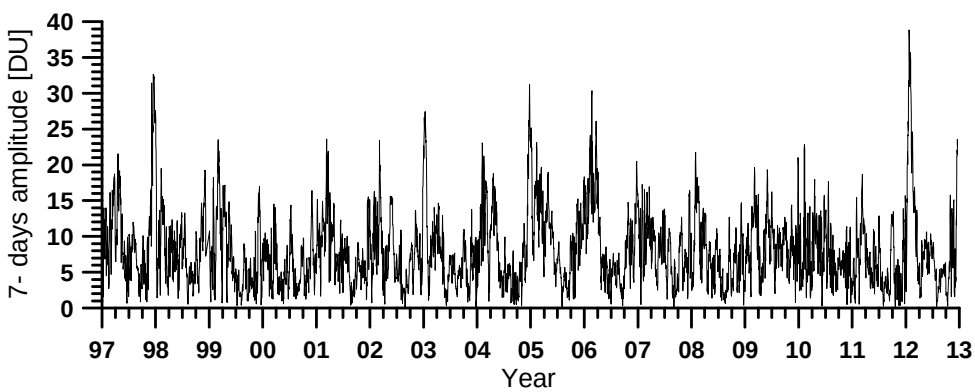

Fig. 6. 7- days amplitude.

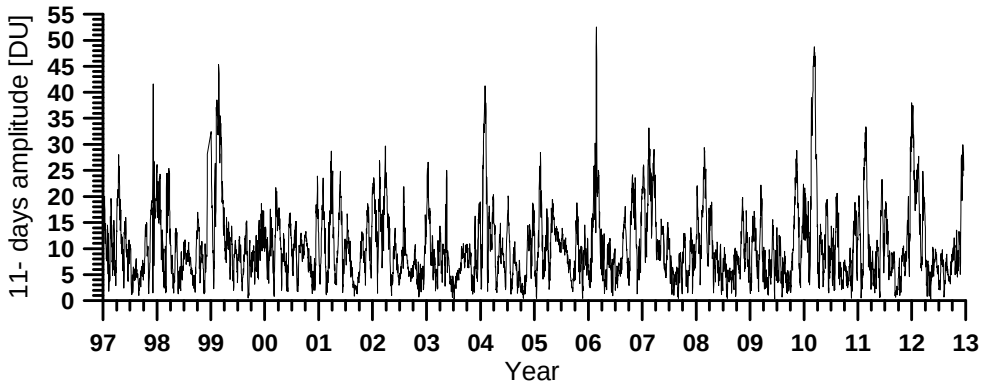

Fig. 7. 11- days amplitude.

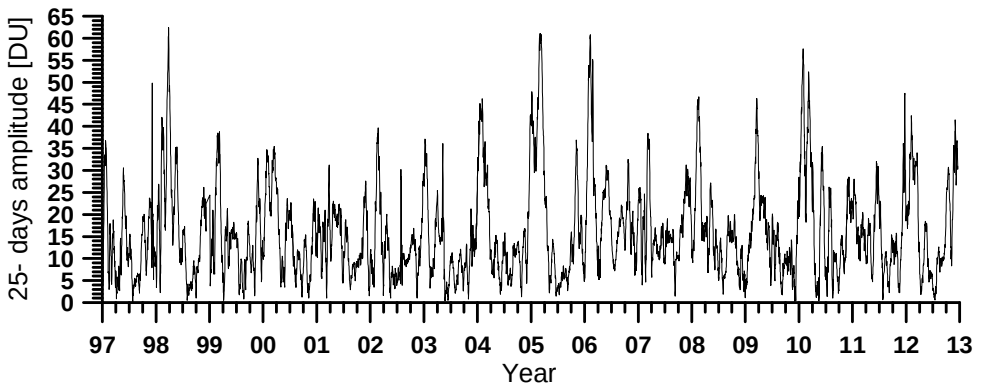

Fig. 8. 25- days amplitude.

The curve of the oscillation amplitudes by days with periods 4, 7, 11 and 25 days, for the period 1997-2912, is displayed on Fig. 5, 6, 7 and 8. An increase of the amplitudes in the winter season is noticed which is characteristic of the planetary wave activity as a whole. The amplitudes of the oscillations with longer periods are also bigger which is characteristic of the planetary wave activity, too. The mean amplitudes for every calendar month are calculated and displayed on Fig. 9. The interval of 16 years is long enough and provides statistical reliability of the obtained mean values (every mean monthly value is obtained from, for example, 30x16=480 values).

It may be assumed for the oscillation with a period of 4 days which was noted in the total ozone data is a reflection of the westward propagating Rossby wave (Pancheva et al., 2010). The climatology of this kind of waves in a temperature field, presented in this work, is expressed the strongest namely at latitude 40N but the seasonal cycle of Rossby wave shows seasonal maximums in the months of the equinox (March and September-October) in contrast to the present results for the total ozone while the climatology of the 4-day wave in the total ozone shows distinctive maximum values in December-March, and the annual minimum is in September. Besides, the average period in the total ozone proves to be smaller than the conventional Rossby waves' range of 5-7 days.

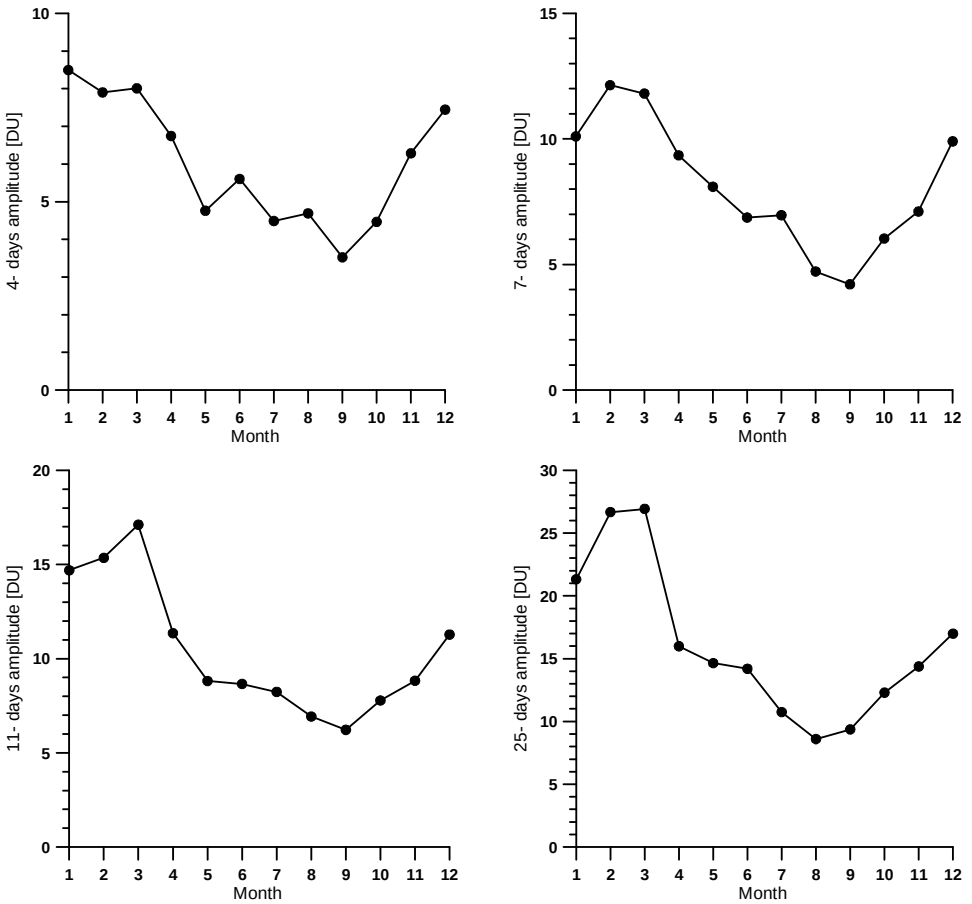

Fig. 9. Seasonal distribution of the amplitudes of the 4, 7, 11 and 25-day oscillations.

Oscillations with a period of 5-7 days are observed in ground and satellite data for the temperature and wind speed while their characteristics prove to be of Rossby (1,1) normal mode (Shepherd et al., 2007) but at low latitudes.

Eleven-day planetary waves with wave number 1 are observed in the field of stratospheric temperature (Pancheva and Mukhtarov, 2011). They activate themselves at middle latitudes and have maximal amplitudes in the winter season which coincides with the behavior of the 11-day oscillation in TOC over Bulgaria.

The studies of planetary waves with a period of about 25 days (Hua Lu et al., 2012) at geopotential height show that those waves in the stratosphere activate themselves in the winter season (from October to March) at middle latitudes which coincides with the climatology of the analogous oscillations in TOC (Fig. 9).

An offset in the seasonal cycle (the maximum is in February-March, and the minimum – in August-September) from that typical for the planetary waves in the other atmospheric characteristics is characteristic of the seasonal amplitude dependence of all

oscillations in TOC which coincides with the seasonal cycle of the very TOC. Global data are required to clarify this phenomenon.

Conclusions

The analysis of the short term variability of the Total Ozone Content over Bulgaria that has been made shows that short term deviations from the stationary seasonal cycle have significant values – 24 DU with 75% probability which is in the range of the annual wave amplitude of the seasonal cycle obtained in the first part of the present work (about 35 DU on the average for the studied period of time). The spectral analysis of the short term variations has shown that they are not of a completely random character and quasi-periodical variations in them are readily seen, the periods of which coincide with the periods of the planetary waves in the stratosphere (in the regions of temperature, pressure and wind speed). Certain caution is necessary by identifying the observed oscillations with periods of 4 and 7 days with Rossby waves because of the deviations of the seasonal cycle of the observed oscillations in TOC from the seasonal and latitudinal dependence of the analogous ones in the temperature and pressure. The behavior of the 11 and 25- day oscillations in TOC coincides better with the well-known characteristics of the analogous planetary waves with the exception of a certain offset (with about two months forward) of the seasonal cycle of the amplitudes in TOC.

Acknowledgements. The study was funded by FP7-PEOPLE-2009-IRSES (Grant No.247608) IGIT- Integrated geo-spatial information technology and its application to resource and environmental management towards the GEOSS.

References

Fusco, A., M. Salby, 1999. Interannual Variations of Total Ozone and Their Relationship to Variations of Planetary Wave Activity, *Journal of Climate*, V. 12, 1619- 1629.

Hua Lu, D. Pancheva, Pl. Mukhtarov, I Cnossen, 2012. QBO Modulation of Traveling Planetary Waves During Northern Winter, *Journal Of Geophysical Research*, VOL. 117, D09104, doi:10.1029/2011JD016901.

Mukhtarov Pl., B. Andonov, C. Borries, D. Pancheva, N. Jakowski, 2010. Forcing of the Ionosphere From Above and Below During the Arctic Winter of 2005/2006, *Journal of Atmospheric and Solar-Terrestrial Physics* 72, 193–205.

Pancheva D., Pl. Mukhtarov, M. Todorova, 1994. Simultaneous Observations of Quasi-Periodical Fluctuations in the TCO, Mesospheric Neutral Wind And Ionosperic Absorption, *Bulgarian Geophysical Journal*, Vol XX, No 3, 72- 81.

Pancheva, D., P. Mukhtarov, 2000. Wavelet Analysis on Transient Behaviour of Tidal Amplitude Fuctuations Observed by Meteor Radar in the Lower Thermosphere above Bulgaria, *Ann. Geophysicae* 18, 316±331.

Pancheva, D., P. Mukhtarov, B. Andonov, N.J. Mitchell, J.M. Forbes, 2009. Planetary Waves Observed by TIMED/SABER in Coupling the Stratosphere–Mesosphere–Lower

Thermosphere During the Winter of 2003/2004: Part 1— Comparison with the UKMO Temperature Results, *Journal of Atmospheric and Solar-Terrestrial Physics* 71, 61–74.

Pancheva, D., P. Mukhtarov, B. Andonov, N.J. Mitchell J.M. Forbes, 2010. Planetary Waves Observed by TIMED/SABER in Coupling the Stratosphere–Mesosphere–Lower Thermosphere During the Winter of 2003/2004: Part 2— Altitude and Latitude Planetary Wave Structure, *Journal of Atmospheric and Solar-Terrestrial Physics* 72, 26–37.

Pancheva, D., P. Mukhtarov, 2011. Atmospheric Tides and PlanetaryWaves: Recent Progress Based on SABER/TIMED Temperature Measurements (2002–2007) in Aeronomy of the Earth's Atmosphere and Ionosphere, edited by M.A. Abdu, D. Pancheva (eds.), A. Bhattacharyya (Coed.), *IAGA Special Sopron Book Series 2*, pp 19-56, DOI 10.1007/978-94-007-0326-1_2.

Shepherd, M.G., Wu, D.L., Fedulina, I.N., Gurubaran, S., Russell, J.M., Mlynczak, M.G., Shepherd, G.G., 2007. Stratospheric Warming Effects on the Tropical Mesospheric Temperature Field. *Journal of Atmospheric and Solar-Terrestrial Physics* 69, 2309–2337.

Сътояние на стратосферния и мезосферен озон над България за периода 1996-2012 г: Част 2 - Краткосрочни вариации на тоталното съдръжание на озон

П. Калейна, Пл. Мухтаров, Н. Милошев

Резюме: В статията е направена оценка на общите характеристики на краткосрочните вариации на тоталното съдържание на озон (TCO) над България. Изследвана е проявата на планетарната вълнова активност на стратосферата върху тоталния озон и е определена климатологията на амплитудите на колебанията с периоди 4, 7, 11 и 25 денонощия.

MODELLING SPATIAL DISTRIBUTION OF GLOBAL TOTAL COLUMN OZONE IN QGIS AND GRASS GIS ENVIRONMENT

E. Tcherkezova, P. Kaleyna, Pl. Mukhtarov

National Institute of Geophysics, Geodesy and Geography, str. Acad. G. Bonchev, bl 3, Sofia1113, Bulgaria, e-mail: et@geophys.bas.bg, pkaleyna@geophys.bas.bg, pmuhtarov@geophys.bas.bg

Abstract. Total Column Ozone (TCO) has an impact on the Earth's atmosphere. In this article the measurements are used for modelling the spatial distribution of the TCO in the atmosphere to observe the values of TCO and the state of the ozone layer as a whole. Spatial interpolation allows an extrapolation of large TCO point data sets to a larger area of interest and is an important method for such purpose. This article focuses on modelling spatial distribution of global TCO using two spatial interpolation methods applying the free open source software Quantum GIS (QGIS) and GRASS GIS. The priority is given to elaborate the workflow showing how to apply Quantum GIS and GRASS GIS and how to implement some spatial interpolation methods making a contribution to the use of geographic information systems (GIS) in modelling spatial distribution of the TCO in Earth's atmosphere. The main goal is, therefore, to demonstrate different means for integration of raw TCO data into GIS and modelling its spatial distribution using free and open source GIS software. The results show that QGIS and GRASS GIS are appropriate tools for modelling spatial distribution of TCO. There are two main advantages of this use: no-cost for software and GIS application that allow also more complex spatial analysis of TCO in GIS environment using additional geographic data and analytical tools for spatial analysis.

Key words: Total Column Ozone (TCO), spatial interpolation, Free and Open Source Software (FOSS), Quantum GIS (QGIS), GRASS GIS.

Introduction

The ozone is one of the so-called "small components" of the Earth's atmosphere (Schwartz et al. 2005). It represents allotropic form of oxygen gas with a triatomic molecule containing three oxygen atoms. In the atmosphere it is presented through very small concentrations, in total, the ozone makes up only 0.6 parts per million of the atmosphere. Despite these low concentrations, the ozone plays a vital role in the existence and development of the Earth's biosphere, because it has the ability to absorb this amount of

solar ultraviolet radiation that penetrates the Earth's stratosphere and prevents the ultraviolet radiation to reach dangerous quantity for living creatures. Absorption of solar energy, on the other hand, has an impact on temperature conditions of the stratosphere and its dynamics.

The part of the ultraviolet radiation of the Sun, which is absorbed by the ozone, depends on TCO (Total Column Ozone): a measurement of the total amount of atmospheric ozone in a given column. TCO is measured in Dobson Units (DU). One Dobson unit refers to a layer of gas that would be 10 μm thick under standard temperature and pressure, sometimes referred to as a 'milli-atmo-centimeter' (Schwartz et al. 2005). A baseline value of 220 DU is chosen as the starting point for an ozone hole since total ozone values of less than 220 Dobson Units were not found in the historic observations over Antarctica prior to 1979. Also, from direct measurements over Antarctica, a column ozone level of less than 220 Dobson units is a result of the ozone loss from chlorine and bromine compounds (Ozone Hole Watch 2007). The Dobson unit is named after Gordon Dobson, who was a researcher at the University of Oxford. In the 1920s, he built the first instrument to measure total ozone from the ground, now called the Dobson ozone spectrophotometer. The modern measurements of TCO are made through satellite equipment (Ozone Monitoring Instrument (OMI) Data User's Guide, 2008).

In this article TCO data is used from the Ozone Monitoring Instrument (OMI). OMI is a nadir-viewing near-UV/Visible CCD spectrometer aboard NASA's Earth Observing System's (EOS) Aura satellite. OMI measurements cover a spectral region of 264-504 nm (nanometers) with a spectral resolution between 0.42 nm and 0.63 nm and a nominal ground footprint of 13 x 24 km2 at nadir. The OMI instrument observes Earth's back scattered radiation with a wide-field telescope feeding two imaging grating spectrometers (Ozone Monitoring Instrument (OMI) Data User's Guide, 2008).

Essentially complete global coverage of TCO is achieved in one day (OMI Ozone). Those data is available as large data sets in tabular form (e. g. in delimited text format) which contain geographic coordinates (latitude and longitude) and TCO-value at each measured sample point. This format allows modelling spatial distribution of TCO using different methods of interpolation and software.

The main purpose of this work is to perform spatial interpolation methods for modeling global TCO using Free and Open Source Software (FOSS). The priority is given to elaboration of workflow showing in detail how to apply QGIS and GRASS GIS making a contribution to the use of geographic information systems (GIS) in modelling spatial distribution of global TCO. It includes processing precise tasks like data input into QGIS and GRASS GIS, spatial interpolation of TCO data, and 2D and 3D visualization.

Data

TCO data from OMI is available on the website http://ozoneaq.gsfc.nasa.gov/ in tabular form. OMI daily global data set is reproduced by using equal angle grid 1 degree × 1 degree cover the whole globe. The data for portion of the ground in many cases is missing due to technical reasons, which demands, when we need an overall picture of the distribution of TCO, to resort to interpolation. In this work is shown the global distribution

of TCO on 21.01.2009 during Stratospheric sudden warming. Stratospheric sudden warming (SSW) is one of the most prominent phenomena in the middle atmosphere. The selected day coincides with the maximum of SSW (Jin et al., 2012). This is a large-scale stratospheric anomaly that manifests itself in a sudden increase in stratospheric temperature in the North polar region with dozens of degrees and change the direction of the stratospheric zonal wind. During such anomalies is observed an uneven distribution of total ozone at high latitudes, which is evident in the figures in this article.

Additionally, we have used the free geographical data sets for land borders and for country boundaries on land and offshore for maps composition from the public domain map dataset 'Natural Earth' (Source: http://www.naturalearthdata.com/).

Software

Quantum GIS and GRASS GIS are free open source desktop GIS software projects. QGIS project is established as a project on SourceForge in June 2002 (QGIS Development Team 2004-2013). It is developed as separate projects for GNU/Linux, Windows, Mac OSX, and Androids. The current stable version of Quantum GIS on Windows is 2.0.1.

During the period 1982-1995 GRASS GIS (Geographic Resources Analysis Support System) was developed as software by the U.S. Army Construction Engineering Research Laboratories (CERL) to support land management in military installations. In 1999 the new development team of GRASS GIS has adopted the GNU GPL license (Blackwell Publishing Ltd. 2004).

Currently GRASS GIS is open source project that is permanent developed for GNU/Linux, Windows, Mac OSX and sponsored by numerous sites worldwide (e. g. Centre for Scientific and Technological Research, in Trento, Italy, http://grass.itc.it). The current stable version of GRASS GIS on Windows is 6.4.x. GRASS GIS is also integrated as a tool in QGIS. GRASS GIS is a hybrid geographic information system for vector, raster, image analysis, modelling and 2D and 3D-visualization.

QGIS and GRASS GIS were released under the GNU General Public License (GPL). This license means "...that users have the freedom to distribute copies of free software (and charge for this service if they wish), that users receive source code or can get, that users can change the software or use pieces of it in new free programs; and that users know they can do these things." (Free Software Foundation, Inc. 1991).

QGIS and GRASS GIS provide a powerful collection of tools for the management, spatial data analysis and visualization. Therefore GRASS GIS and QGIS are used for different applications around the world by academic, governmental agencies and commercial institutions.

In this work we have used the capabilities of those software to demonstrate how raw TCO data can be imported into QGIS and GRASS GIS and how can be modelled in order to create spatial surfaces of global TCO.

Methods

According to Burrough (1986) the values of properties at unsampled locations on the set of observed values at known locations can be estimated through spatial interpolation. Interpolation is therefore, process of estimation unknown values that are located between surrounding known values across an area and is used to create a surface of models a sampled phenomenon. Spatial interpolation procedures are reviewed by different authors, e. g. Burrough (1986), Burrough and McDonnell (2000), Mitasova and Hofierka (1993), Mitasova et al. (1995), Mitas and Mitasova (1999), Cressie (1993). They can be grouped as follow:

- local neighborhood approach (Inverse Distance Weighted interpolation - IDW, Natural Neighbor interpolation, interpolation based on a Triangulated Irregular Network (TIN),
- geostatistics approach (e.g. Kriging),
- variational approach to interpolation and approximation (Thin Plate Spline - TPS function, Regularized Spline with Tension (RST), and other forms of smoothness semi-norm) (Mitas and Mitasova 1999).

According to Chiles and Delfiner (1999) the quality of any analysis depends on interpolation of observed data and is subject to a degree of uncertainty. Different interpolation techniques that are performed on the same data sets can therefore generate different spatial predictions at same locations.

Assessment of error (uncertainty) or comparison of some interpolation methods were presented by different authors and applications, e. g. MacEachren and Davidson (1987), Mitas and Mitasova (1999), Siska and Hung (2005), Collins and Bolstad (1996), Hůnová et al. (2012) and others. According to MacEachren and Davidson (1987) data measurement accuracy, data density, data distribution, and spatial variability had impact on interpolation accuracy.

Siska and Hung (2005) concluded that IDW, Kriging, Thiessen polygons and TIN interpolations performed almost on the same level, but TIN appears to be a leading method in predicting the unknown values on a more uniform, less varied data set (flat surface).

The results of Collins and Bolstad (1996) outline that certain a priori data characteristics (in their research they are temperature range, temperature variance and temperature correlation with elevation), spatial scale, relative spatial density and distribution of sampling locations impact on interpolation and affect the choice of spatial interpolation technique.

The results of Hůnová et al. (2012) confirm the importance of assessment of performance of different interpolation methods.

Generally, can be concluded that the spatial interpolation accuracy is crucial in accurate estimation of different type of sampled data such meteorological, soil, terrain, bathymetry and others and should be took into account in spatial modelling and analysis.

Spatial interpolation procedures that were used in this article are the Inverse Distance Weighted interpolation (IDW) and Regionalized Spline Interpolation with Tension (RST) without focus on estimating the interpolation accuracy, but on methodological approach for spatial modeling in GIS environment.

The IDW interpolation is a local and exact deterministic interpolation technique. The value in an unsampled location is computed as weighted average considering the values of the sample points and the distance between then and the estimated cell. According to Burrough (1986) weights are inversely proportional to a power of distance. That means that points closer to the evaluated cell are more weighted than sample points that are further away. The result is a surface that does not pass through the data points. IDW produces local maxima and minima at the sample points (Mitas and Mitasova 1999).

Spline methods belong to the variational approach for interpolation and approximation (Mitas and Mitasova 1999). They are based on the assumption that the sum of deviations from the sample points should be minimized in order to pass exactly or closely as possible to them and smoothing surface at the same time (Mitasova et al. 1995; Mitas and Mitasova 1999).

The Regionalized Spline Interpolation with Tension (RST) method used in this article incorporates the properties of Thin Plate Spline (TPS) with tension and function with regular second- and possibly higher-order derivatives (Mitas and Mitasova 1988, 1999). The mathematical functions of TPS with tension and RST are presented and discussed in detail by Mitas and Mitasova (1988), Mitasova and Mitas (1993), Mitas and Mitasova (1999). According to Mitasova et al. (1995) and Hofierka et al. (2002) the RST method enables smoothing of noisy data. This interpolation method is implemented in GRASS GIS (Neteler and Mitasova 2004).

Interpolation methods are integrated at most GIS software packages and are used in different applications. For example, interpolation methods are often used in climatology (e.g. Hutchinson 1995; Hofierka et al. 2002; Hancock and Hutchinson 2006; Luo et al. 2008), geomorphology and geomorphometry (e.g. Mitasova and Mitas 1993; Mitasova and Hofierka 1993; Mitasova et al. 2004, Mitasova et al. 2005 and others), and others.

Results

The spatial analysis is the most important functionality of geographic information systems (GIS). Including other GIS capabilities such spatial data processing, storage in geographical database and visualization, GIS is a powerful tool that is widely used currently as technology and method in different applications. The choice of methodological approach in each GIS application depends on the specific goal. Therefore the selection or the elaboration of appropriate work processes has an important role in each GIS project (Tcherkezova 2004).

In this article the following methodological approaches for processing and visualization of global TCO data in QGIS and GRASS GIS environment were demonstrated:

- TCO data processing and visualization using QGIS,
- TCO data processing and visualization using GRASS GIS, and
- TCO data processing and visualization using GRASS GIS as a QGIS tool.

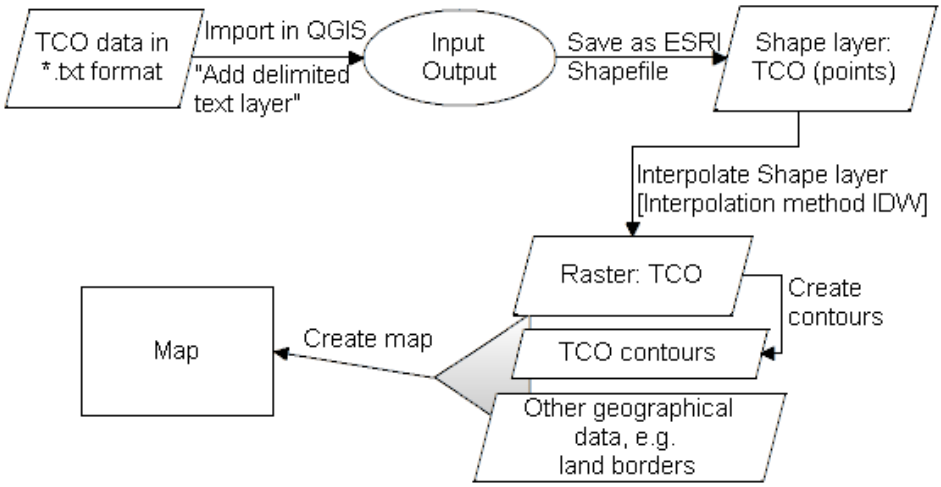

Fig. 1. Flowchart of raw global TCO data processing and spatial modelling in QGIS environment

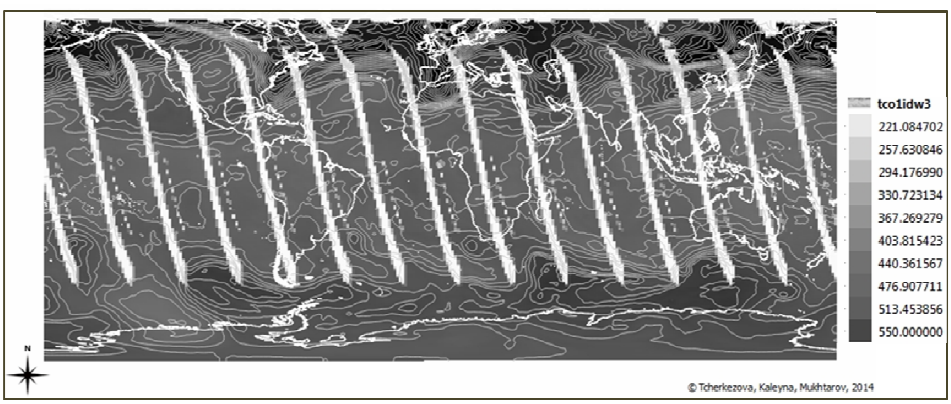

Fig. 2. Global TCO spatial distribution based on IDW interpolation method overlapped with some main TCO contours and land boundaries

Figure 1 shows in detail how to import raw TCO daily data with 'no data' values as delimited text into QGIS and how to generate surface of global spatial distribution using IDW method that is implemented in QGIS. The first step was to open the raw data in Notepad++ a free and source code editor for Windows (http://www.notepad-plus-plus.org/) in order to proof the data format and if necessary to convert it in "delimited text format".

The result is presented in Figure 2 and outlines that the 'no data' values are not interpolated as zero values.

In the Figure 3 were presented three possible work steps for integration of the raw TCO data into GRASS GIS. In the first case the attribute table was transformed in DBF format and imported using the GRASS GIS command db.in.org (File → Import database table → Multiple import formats using OGR). It includes three fields: longitude, latitude and TCO. The imported table was used to create a vector point layer in GRASS GIS

environment (v.in.db , Vector → Generate points → Generate from database). The created vector point layer was used then to interpolate surfaces that models the global TCO spatial distribution using IDW and RST interpolation methods (Raster - Interpolate Surfaces - IDW from vector points whereby the TCO values in the attribute table of the vector layer should be selected as Z value field) and command v.surf.rst (Raster - Interpolate Surfaces - Regularized Spline Tension whereby the TCO values in the attribute table of the vector layer should be also selected as Z value field).

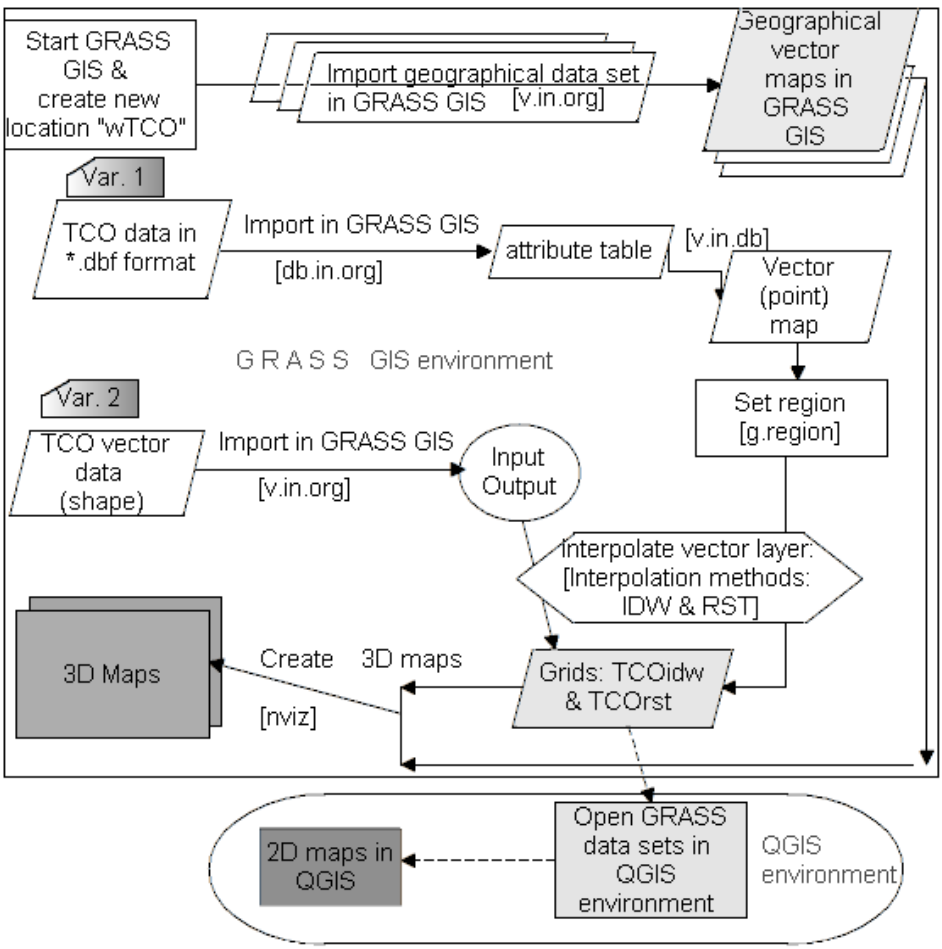

Fig. 3. Flowchart of raw global TCO data processing and spatial modeling in GRASS GIS environment and visualization

The layers that are stored in GRASS GIS geo-database can be opened, analysed and visualized also in QGIS environment (Figure 3 in the ellipse). This is another way to manipulate the geodata combining QGIS and GRASS GIS.

The result of IDW interpolation and created contours was presented as 3D map

using the NVIZ tool for visualization and animation of GRASS data (Figure 4). In the interpolation IDW and RST procedures in GRASS GIS environment the 'no data' values were ignored.

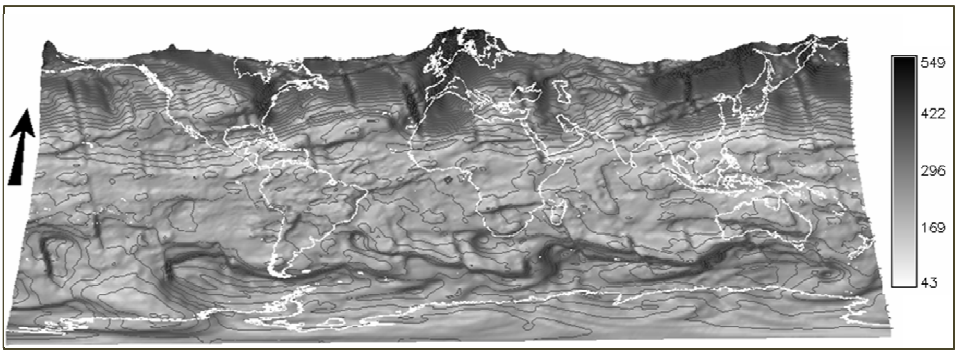

Fig. 4. Spatial model of global TCO which is generated using IDW method in GRASS GIS environment

The three dimensional visualization helps for better understanding the spatial distribution of the Total Column Ozone. We have visualized the interpolated IDW surface of TCO spatial distribution using 'invert grey color' legend (Figure 4).

The figure below shows the result of spatial modelling of Total Column Ozone using Regularized Spline Tension method ignoring 'no data' values (Figure 5). In order to highlight better the differences by close contrast values, the legend was colored in grey using histogram equalization. The raster image was overlapped with land boundaries and created TCO contours.

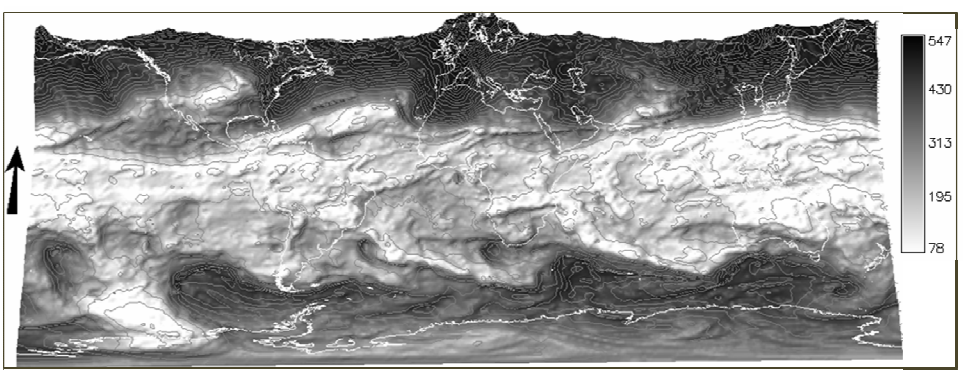

Fig 5. Spatial model of global TCO which is generated using RST method in GRASS GIS environment

Although the results of IDW and RST are visually similar, but there are differences which can be presented trough visual comparison of IDW and RST contours (Figure 6) or through analysis of errors.

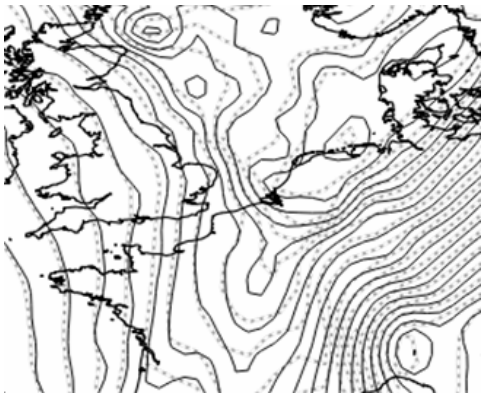

Fig. 6. Differences between IDW and RST interpolation results (black lines: contours of RST interpolation; grey point line style: contours of IDW interpolation)

The results present that the spatial distribution of global TCO can be modelled using different methodological approaches. The import of raw TCO data in table format in QGIS is more user-friendly as their import in GRASS GIS, but the GRASS GIS offers more interpolation methods than QGIS and an easy of access 3D visualization. Additionally, the functionality of GRASS GIS for creation of an own GRASS geodatabase in PERMANENT and users map sets allows using the stored data in QGIS. The stored data in the PERMANENT map set can't be changed or damaged from additional users (Dassau et al. 2004-2005).

For this reasons the mostly appropriate methodological approach includes the following steps:

- Import of raw TCO data in table format in QGIS.
- Save the imported data as vector data (points).
- Import of TCO point vector layer in GRASS GIS.
- Interpolate surface using different interpolation methods in GRASS GIS environment.
- 3D visualization of the results or mapping TCO in QGIS environment.

The results demonstrate that the QGIS and GRASS GIS are appropriate for the article's purposes and offer a realistic alternative to commercial GIS and to other software. The advantages of this use are the following:

- no-cost for software and
- GIS application that allows also more complex spatial analysis of TCO in GIS environment using additional geographic data and analytical tools for spatial analysis.

Conclusions

In this article were demonstrated different methodological approaches for integration, manipulation and interpolation of raw global TCO data using free and open source QGIS and GRASS GIS.

The results show how the global TCO can be modelled in GIS environment. The elaborated flowcharts present in detail the workflow for import, processing and visualization applying QGIS, GRASS GIS and GRASS GIS as a QGIS tool.

The presented methodological approaches can be adopted for modelling of TCO and other meteorological phenomena such as air pollution at regional scale.

This work also link interdisciplinary expertise to help investigation and spatial modelling of TCO at more advanced level which results can be used directly in other studies or for more complex spatial analysis and to help the understanding variation of TCO. Additionally, QGIS and GRASS GIS effort high degree of customisation and users can develop scripts for other interpolation methods.

Acknowledgment. In this work we have used only Free and Open Source Software (QGIS, GRASS GIS and Notepad++) and free available data (OMI Ozone data and Natural Earth land data sets) those links are presented in the references.

References

Burrough, P.A. (1986). Principles of Geographical Information Systems for Land Resources Assessment. Clarendon Press. ISBN 0198545924. 194 p.

Burrough, P.A. and McDonnell, R. (2000). Principles of Geographical Information Systems. Oxford University Press. 333p. Chiles, J.P. and P. Delfiner, 1999. Geostatististics and Modelling Spatial Uncertainty. 1st Edition, Wiley-Interscience, USA. ISBN-13: 978-0471083153. 720p.

Collins, F.C. and Bolstad, P.V. (1996). A Comparison of Spatial Interpolation Techniques in Temperature Estimation. In Proceedings of the Third International Conference/Workshop on Integrating GIS and Environmental Modeling. National Center for Geographic Information Analysis (NCGIA): Santa Fe, NM, Santa Barbara, CA: January 21–25. Available:

Cressie, Noel. A.C. (1993) Statistics for Spatial Dat. John Wiley & Sons, Inc., New York, [revised edition], 900p.

Dassau, O., Holl, S., Neteler, M., and Redslob, M. (2004-2005). Eine Einfürung in den praktischen Umgang mit dem Freien Geographischen Informationssystem GRASS 6.0. Version 1.2. GDF Hannover bR. 157.

Hancock, P.A. and Hutchinson, M.F. (2006). Spatial interpolation of large climate data sets using bivariate thin plate smoothing splines. Environmental Modelling and Software, 21(12). 1684-1694.

Hofierka, J., Parajka, J., Mitasova, H., and Mitas, L.(2002). Multivariate Interpolation of Precipitation Using Regularized Spline with Tension. - Transactions in GIS, 6(2): 135-150.

Hůnová I., Horálek, J., Schreiberová, M., and Zapletal, M. (2012). Ambient Ozone Exposure in Czech Forests: A GIS-Based Approach to Spatial Distribution Assessment. - The ScientificWorld Journal ,Volume 2012, Article ID 123760, 10 pages. Doi:10.1100/2012/123760.

Hutchinson, M.F. (1995). Interpolating Mean Rainfall Using Thin Plate Smoothing Splines. International Journal of Geographical Information Systems, 9(4). 385-403.

Jin, H. , Miyoshi, Y., Pancheva, D., Mukhtarov, P., Fujiwara, H. and Shinagawa, H. (2012) Response of migrating tides to the stratospheric sudden warming in 2009 and their effects on the ionosphere studied by a whole atmosphere-ionosphere model GAIA with COSMIC and

TIMED/SABER observations, Journal of Geophysical Research, VOL. 117, A10323, doi:10.1029/2012JA017650

Luo, W., Taylor, M.C., Parker, S.R. (2008). A comparison of spatial interpolation methods to estimate continuous wind speed surfaces using irregularly distributed data from England and Wales. Int. J. Climatol., 28. 947-959. Doi:101002/joc.1583.

MacEachren, A.M., J.V. Davidson (1987). Sampling and Isometric Mapping of Continuous Geographic Surfaces. - The American Cartographer, Vol. 14, No. 4, 299-320.

Mitas, L., Mitasova, H. (1988). General variational approach to the interpolation problem. - Comput. Math. Application, Vol. 16, No. 12, Pergamon Press, 983-992.

Mitas, L., Mitasova, H. (1999). Spatial Interpolation. In Longley, P., Goodchild, M.F., Maguire, D.J., Rhind, D.W. (Eds.), Geographical Information Systems: Principles, Techniques, Management and Applications, GeoInformation International, Wiley, 481-492.

Mitasova, H. and Hofierka, J. 1993. Interpolation by Regularized Spline with Tension: II. Application to Terrain Modelling and Surface Geometry Analysis. - Mathematical Geology, Vol. 25, No. 6. 657-669.

Mitasova, H., Drake, T.G., Harmon, R.S. and Bernstein, D. (2004). Quantifying rapid changes in coastal topography using modern mapping techniques and GIS. Env. and Engineering Geoscience, vol. 10. 1-11.

Mitasova, H., Mitas, L. (1993). Interpolation by regularised spline with tension: I. Theory and implementation. Mathematical Geology 25: 641–655.

Mitasova, H., Mitas, L., Brown, W.M., Gerdes, D.P., Kosinovsky. I., Baker. T. (1995) Modelling spatially and temporally distributed phenomena: new methods and tools for GRASS GIS. –

Mitasova, H., Overton, M., Harmon, R.S. (2005). Geospatial analysis of a coastal sand dune field evolution: Jockey's Ridge, North Carolina. Geomorphology 72.204–221. Available: www.sciencedirect.com. Last visit: 9th Dec. 2013.

Neteler, M. and Mitasova, H. (2004). Open Source GIS: A GRASS GIS Approach, 2nd Ed. Kluwer International Series in Engineering and Computer Science 773, Springer/Kluwer Academic Press,NY/Boston. ISBN: 1-4020-8064-6. 424p.

Schwartz, S. E. and Warneck, P. (1995). Units for use in atmospheric chemistry. Pure Appl. Chem. 67 (8-9): 1377–1406. doi:10.1351/pac199567081377.

Siska, P. P., Hung, I. K. (2005). Assessment of kriging accuracy in the GIS environment. Available: http://gis.esri.com/library/userconf/proc01/professional/papers/pap280/p280.htm. Last visit: 17th Jan 2014.

Tcherkezova, E. 2004. (2004). GIS-gestützte geomorphologische Untersuchungen an Beispielen aus dem nördlichen Teil der Bucht von Burgas (Schwarzmeerküste, Bulgarien). – Berliner Geographische Studien. Band 52. D 83. Berlin. 191 Seiten mit CD-Rom. ISBN 3 7983 1945 6. 191.

Data sources

Natural Earth: http://www.naturalearthdata.com/. Last visit: 15th Aug 2013.
OMI Ozone: http://ozoneaq.gsfc.nasa.gov/qa/faq_omi.md#g_1. Last visit: 25th Apr 2013

Моделиране пространственото разпределение на глобалното съдържание на озон чрез QGIS и GRASS GIS

Е. Черкезова, П. Калейна, Пл. Мухтаров

Резюме. Тоталното съдържание на озон (TCO) оказва влияние върху атмосферата на Земята. В тази статия измерванията на TCO са използвани за моделиране на пространственото разпределение на TCO в атмосферата, с цел да се наблюдават стойностите на TCO и състоянието на озоновия слой като цяло. Пространствена интерполация позволява екстраполация на големи бази точкови данни за TCO за голями площи и е важен метод за тази цел. Тази статия се фокусира върху моделиране на глобалните данни за TCO, използвайки два метода за пространствена интерполация чрез безплатния отворен софтуера Quantum GIS (QGIS) и GRASS GIS. Основния приоритет на статията е да се представят фигури-таблици, показващи как да се прилагат Quantum GIS и GRASS GIS, как да се прилагат някои методи за пространствена интерполация при използването на географските информационни системи (GIS) в моделирането на пространственото разпределение на TCO в земната атмосфера. Основната цел следователно е, да се покажат различни средства за интегриране на необработените данни за TCO в GIS и моделиране на неговото пространствено разпределение, използвайки безплатения софтуер с отворен код GIS. Резултатите показват, че QGIS и GRASS GIS са подходящи инструменти за моделиране на пространствено разпределение на TCO. Има две основни предимства при използването на GIS: безплатен софтуер и GIS приложение, което позволява още по-сложен пространствен анализ на TCO в GIS среда, с помощта на допълнителни инструменти за пространствен анализ на географски и аналитични данни.

ASSESSMENT OF THE 2012 M_W=5.6 EARTHQUAKE IMPACTS IN THE CITY OF SOFIA

I.Alexandrova

National Institute of Geophysics, Geodesy and Geography, BAS, Akad G.Bonchev street, bl.3, Sofia, Bulgaria, e-mail: i.alex@abv.bg

Abstract: In this work are represented the minimum and the maximum degrees of the seismic impact and the relevant effects on different types buildings on the territory of Sofia caused by the earthquake on 22nd of May 2012 with magnitude Mw=5.7 and I_0=8 MSK. In order to define better the impacts, here are collected and analyzed information and further identification of the damages in Sofia. The observed effects are evaluated using the macroseismic scale MSK-64.

Key words: earthquake, seismic impact, macroseismic intensity, the city of Sofia

Introduction

The Sofia area is the most populated (the population is of more than 1.5 mil. inhabitants), industrial and cultural region of Bulgaria that faces considerable earthquake risk.

The contemporary tectonic activity of the Sofia area is associated predominantly with marginal faults of Sofia graben. The boundaries of the graben are represented by SE-NW fault systems with expressive neotectonic activity. Earthquakes in the Sofia seismic zone seem to be distributed along these fault systems, which have played an active role in the recent geodynamic evolution of the area.

The available historical documents prove the occurrence of destructive earthquakes during the 15th-18th centuries in the Sofia zone (Watzof, 1902). However, the information about the ancient events is very incomplete and uncertain and only an approximate estimation of their location is possible. In 19th century the city of Sofia has experienced two strong earthquakes: the 1818 earthquake with epicentral intensity I_0=8-9 MSK and the 1858 earthquake with I_0=9-10 MSK (recently revised value in terms of EMS98 proves to be the same) (Christoskov et al., 1979). The 1858 earthquake caused heavy destruction to the city of Sofia and the appearance of thermal springs in the western part of the town (Watzof, 1902). After a quiescence of about 50 years a strong event with

M=6.5 occurred in 1905 near the town of Trun in the western marginal part of the zone (Grigorova et al, 1979).

During the 20th century the strongest event occurred in the vicinity of the city of Sofia is the 1917 earthquake with M_S=5.3 and I_0=7-8 MSK. The earthquake caused a lot of damages in the town and changed the capacity of the thermal mineral springs in Sofia and surroundings. The earthquake was felt in an area of 50000 km^2 and followed by aftershocks, which lasted more than one year (Kirov, 1952; Petkov and Christoskov, 1965).

Almost a century later (95 years after the 1917 earthquake) an earthquake of moment magnitude 5.6 (I_0=8 MSK) hit the Sofia seismic zone, on May 22nd, 2012, located at 25 km south west of the city of Sofia. No casualties and severe injuries have been reported. Predominantly moderate (grade2, according to Grünthal, edit., 1998) to substantial (grade3, according to Grünthal, edit., 1998) damages were observed in the city of Sofia and surroundings.

In the present study, distribution of macroseismic effects along the city of Sofia is estimated and analyzed. The approach used in the present study is applied for generation of deterministic scenarios using directly the intensity assessment of the strongest past earthquakes for the cities of Ruse (Solakov et al., 2009a,b) and Plovdiv (Solakov et al., 2011).

Observed macroseismic effects in the city of Sofia

Distribution of macroseismic effects (generated by the 2012 M_W =5.6 earthquake) along the city of Sofia is estimated on the base of documents and reliable information available in the "Archive" department at the Sofia municipality. The intensity map illustrating the distribution of macroseismic intensity (MSK) along the city of Sofia is presented in Fig.1.

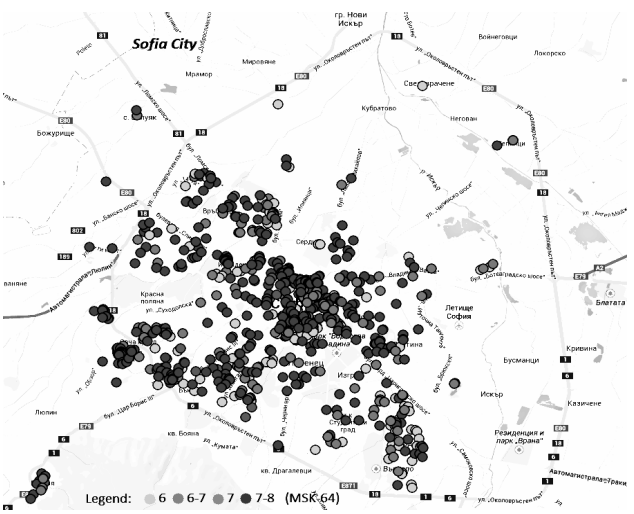

Fig. 1. Observed macroseismic effects (in MSK intensity scale) for the city of Sofia caused by the 2012 (M_W=5.6) earthquake

The figure shows that the intensity values range between 6.0 and more than 7 (MSK).

The highest intensity values (above 7 MSK) are related to old not well maintained buildings that were not reinforced (marked by red spots in Fig.1). Twelve cases of failures of 7-8 degree MSK in Sofia have been documented. Some of the most vulnerable buildings are shown in Figure 2.

Fig.2. Buildings with damages from 7-8 degree

One part of these buildings are uninhabited with unknown owners and self-destructives. Others are municipal property and are used for housing the socially weak families. Additionally these are buildings witch haven't been renovated recently. The third types of buildings with that kind of damages are declared for culture monuments. But because of the lack of clearance whose property they are, they are also uninhabited, strongly damaged from the atmospheric conditions and amortized.

The predominant degree of damage of the buildings in Sofia is 7th (MSK-64), its concentration is focused in the central city part. These are brick houses and buildings built at the beginning of the 20th century (such a house is illustrated in Fig.3).

Fig.3. One example of the damage from 7 degree

Most of these buildings are unkempt – without being done any basic renovation. As a result, the chimneys are with fallen cowls; partly or at half demolished bodies; with crumbled plastering, amenable to falling bricks. There are big pieces of fallen plastering from the facades of the buildings and also tiny cracks on the walls. In about 40 percent of the observed cases there are dislocation and sliding of the tiles from the roofs. The area with impacts from 7th MSK degree is expanding mainly westerly from the central parts of the city (from north-west to south-west, reaching Vladaya neighbourhood, situated in the south-west parts of Vitosha mountain).

Impacts from 6th and 6-7th MSK degree according to MSK experience big part of the schools and the kindergartens in the municipalities situated from south-south-western to north-western part of the city. In the apartment buildings (in these municipalities) regardless of the construction type (panel, monolithic), in the most of the cases the plastering of the walls is broken, the cracks are tiny and insignificant, non-causing influence of the entirety of the building construction. Damages of 7th degree MSK in the buildings are due to reconstructions in the apartments made by their owners like: removal of supporting walls or columns, merging of two apartments in one by making holes for doors in the supporting walls.

Impacts with degree of intensity 6 (MSK) predominates in the south-eastern parts of the city.

Generally, in the north-north-eastern part of the city of Sofia (where districts: Voenna Rampa's industrial zone, Benkovski are located) there are almost no evidences of damages. The same is the situation in the south-eastern parts of the city (districts: Druzhba 1 and 2, The Poligon, Tzarigradski Kompleks).

In the districts at the foot of the Vitosha mountain, where most of the buildings are 2-3 storeyed houses and new blocks (Dragalevtsi, Boyana, Krustova voda, Manastirski Livadi) there are also no information about damages.

Conclusions

Based on about 760 points, values of seismic impacts in which the damages occurred in buildings of the Sofia are determined. The most vulnerable types of buildings are those, built at the beginning of the 20th century and are unkempt. Others, more seriously damaged, are buildings, where the supporting walls and columns have been constructively changed. Such buildings are scattered throughout the city of Sofia.

Acknowledgements. This research was able to be done with the support and cooperation of the employees from "Archive" department at Sofia Municipality. Thanks to their understanding "Seismology" department at NIGGG have list in details with the damages in Sofia after the earthquake on 22nd of May 2012.

References

Christoskov, L., D. Sokerova and S. Rijikova, 1979. New catalogue of the earthquakes in Bulgaria for the period V century BC to XIX century (1899), Geoph. Inst., BAS, Sofia.

Grigorova, E., D. Sokerova, L. Christoskov and S. Rijikova, 1979. Catalogue of the earthquakes in Bulgaria for the period 1900-1977, Geoph. Inst., BAS, Sofia.

Grünthal, G.edit., 1998. European Macroseismic Scale 1998 – EMS 98, ESC, 15, Luxembourg, 99 pp.

Kirov, K.. 1952. Contribution to study of earthquakes in Sofia region, Ann. Main Dep. Geol. and Mining Res., **5**, 407-440.

Petkov, I. and L. Christoskov, 1965. On seismicity in the region of the town of Sofia concerning the macroseismic zoning, Annali Sofia Univ., **58**, 163-179.

Solakov D., S.Simeonova, I.Aleksandrova, I.Popova, G.Georgieva, 2009a. Earthquake Scenarios: cases study for the cities of Rousse and Vratsa. 5th Congress of Balkan Geophysical Society — Belgrade, Serbia10 – 16 May 2009, 6497, computer file on CD

Solakov D., S. Simeonova, L. Christoskov, I. Aleksandrova, I. Popova, and G. Georgieva, 2009b. Earthquake scenarios for the cities of Sofia, Rousse and Vratsa. INFORMATION & SECURITY. An Int. J, 24, 51-64.

Solakov D., S. Simeonova, I. Alexandrova, P. Trifonova, M. Metodiev, 2011. Verification of seismic scenario using historical data-case study for the city of Plovdiv. In Proceedings V.2 (Edts. Grützner C., R. Perez-Lopez, T. Steeger, I.Papanikolaou, K.Reicherter, P.Silva and A.Vött) of 2nd INQUA-IGCP-567 International Workshop on Active Tectonics, Earthquake Geology, Archaeology and Engineering, Corinth, Greece, 39-41

Watzof, S., 1902. Earthquakes in Bulgaria during XIX century, Central Meteorological Station, Imprimerie de I'Etat, Sofia, pp 93. (in Bulgarian and French)

Оценка на въздействията в град София от земетресението на 22-ри май 2012г.

И. Александрова

Резюме. В тази работа са представени минималните и максималните степени на сеизмичното въздействие, както и съответните ефекти върху различни видове сгради на територията на София, причинени от земетресението на 22 Май 2012 с магнитуд Mw = 5.7 и I_0 = 8 MSK. За да се определят по-добре въздействията, тук е събрана и анализирана информация и последващо определяне на щетите в София. Наблюдаваните ефекти са оценени чрез използване на макросеизмична скала MSK-64.

FAULT PLANE SOLUTIONS OF THE 2012 M_W 5.6 PERNIK (SW BULGARIA) EARTHQUAKE AND THE STRONGEST AFTERSHOCKS

V. Protopopova

National Institute of Geophysics, Geodesy and Geography - BAS, Akad. G. Bonchev str., bl.3, Sofia, Bulgaria, e-mail: valia.pr@gmail.com

Abstract: An earthquake with magnitude M_L=5.8 (Mw=5.6) and epicentral intensity I_0= 8 MSK64 occurred in the vicinity of the city of Pernik (SW Bulgaria) on 22nd of May 2012. The earthquake was followed by intensive aftershock activity. In the study the fault plane solutions for 20 earthquakes (the main shock and 19 aftershocks) registered by the national seismological network of Bulgaria are presented. The orientations of the fault plane solutions and spatial distribution of the aftershocks coincide with the NW-SE trend of Pernik-Belchin fault. Additionally, basic geodynamic analysis is performed.

Key words: earthquake, fault plane solution, faulting, geodynamics

Introduction

An earthquake of moment magnitude 5.6 (I_0=8 MSK64) hit the Sofia seismic zone (SW Bulgaria) on May 22nd, 2012. The earthquake is located in the vicinity of the city of Pernik (epicenter coordinates 23.00º E and 42.58º N and 9 km depth) at about 25 km south-west of the city of Sofia. The earthquake was largely felt on the territory of Bulgaria and neighbor countries: northern Greece, FYROM, eastern Serbia and southern Romania. No casualties and severe injuries have been reported. Moderate to heavy damages were observed in the cities of Pernik, Radomir and Sofia and their surroundings. During the 20th century the strongest event occurred in the vicinity of Sofia was the 1917 earthquake of M_S=5.3 and I_0=7-8 MSK64 (Grigorova et al., 1979). The earthquake caused a lot of damages in the town and changed the capacity of the thermal mineral springs in Sofia and surroundings. The earthquake was felt in an area of 50000 km^2 and was followed by aftershocks, which lasted more than a year.

Fourteen days after the 2012 earthquake more than 650 aftershocks were registered, most of them are microearthquakes (M<1.0) (Botev et al., 2013a). The modern digital network allowed providing reliable detection, fast location and precise determination

of the earthquake parameters. The spatial distribution of the aftershock epicenters is presented in Fig.1, and coincides with the NW-SE trend of Pernik-Belchin fault (identified by Karagjuleva et al., 1973).

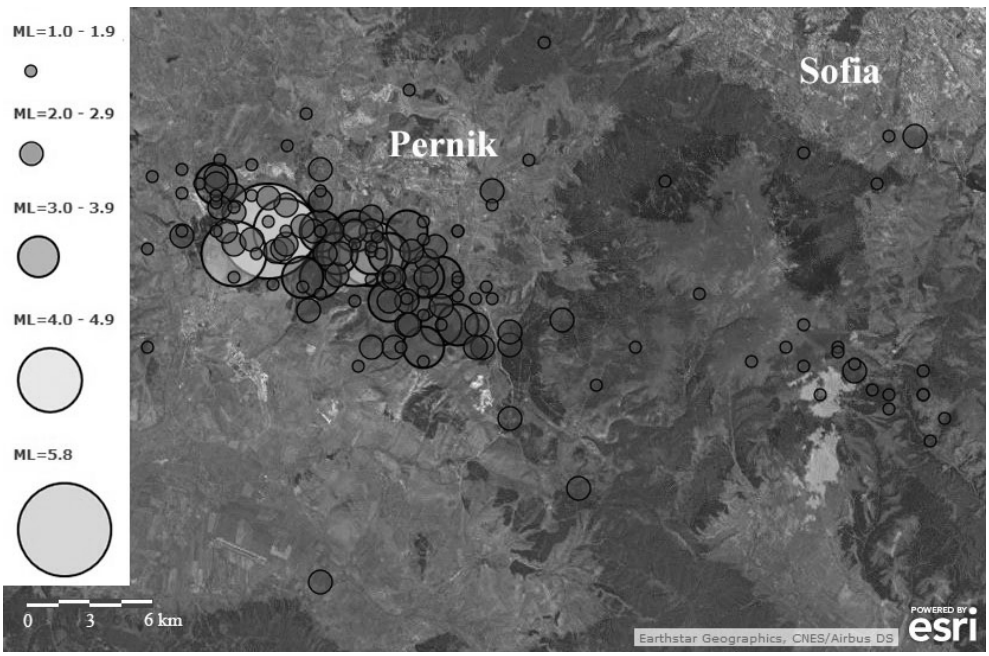

Fig. 1. Epicentral distribution of the events along Pernik-Belchin fault line (Natural Earth - Free vector and raster map data@naturalearthdata.com)

In the study new results of the present state of stress field in southwestern Bulgaria are obtained based on evaluation of 20 earthquake focal mechanisms. The results confirm the recent seimotectomic models for southern Bulgaria (Van Eck and Stoyanov, 1996).

Method and input data

The fault-plane orientations and slip directions of earthquakes can provide important information about fault structure at depth and the stress field in which the earthquakes occur. The source of a small earthquake is typically approximated by a double-couple point source, or focal mechanism, derived from observed P-wave first-motion polarities. A focal mechanism represents two orthogonal nodal planes that divide a reference sphere around the source into four quadrants: the first motion in two of them should be away from the source (cause compression), and in the other two quadrants the first motion should be toward the source (cause dilatation). First-motion-polarities are observed at seismic stations, and the position on the focal sphere for each observation is the

azimuth and take-off angle at which the ray leaves the source, is computed for an assumed hypocenter location and seismic-velocity model (Botev et al., 1996). The computing program for determining the parameters of the seismic events is an adaptation of the widespread product HYPO'71 (Solakov, 1993). A focal mechanism can then be found that best fits the first-motion observations.

For the determination of the earthquake focal mechanisms the program FOCMEC is used (Snoke, 2009). Input data are the polarities of the P wave (the number of input data is in the range 9 – 49), azimuth and take-off angle at which the ray leaves the earthquake source. Output data are all possible orthogonal nodal planes that separate the compressional and dilatational first motions.

Results

Fault plane solutions for the main earthquake and 19 aftershocks with ML ≥ 3 are shown in Fig. 2 and their parameters are presented in Table 1. For the purposes of the present study, all the available focal mechanisms were collected, checked, tested and recalculated according to the definitions by Aki and Richards (1980) and to the procedure described by Christoskov (2007). All polarities were checked as waveforms (data from NOTSSI and ORFEUS database - ftp://www.orfeus-eu.org/pub/data/continuous/2012/), the strike, dip and rake are determined by FOCMEC software (Snoke, 2009) with accuracy up to 10 degrees and the solutions are displayed in lower hemisphere projections.

As it is seen in Fig. 2 and Table 1 for all focal mechanisms the average strike of one of the nodal planes is 311º NW-SE. That predominant nodal plane can be accepted as the main fault in this zone and it has the same NW-SE orientation as the Pernik-Belchin fault with average dipping 50º. If the chosen nodal plane of focal mechanisms is the main, then it is clear that the faulting is typical right-lateral (Kasahara, 1978). The foot-wall block is on the right side of line Pernik-Belchin – Golo Burdo and the hanging-wall block is on the left side - Pernik graben.

All earthquakes are characterized as a normal right-lateral faulting with small strike-slip component, except earthquake № 7, which is thrust faulting with small strike-slip component and earthquake № 16 is clear strike-slip motion. Position of event № 7 is at the end of the Pernik-Belchin fault line and it is the most NW earthquake with determined herein focal mechanism.

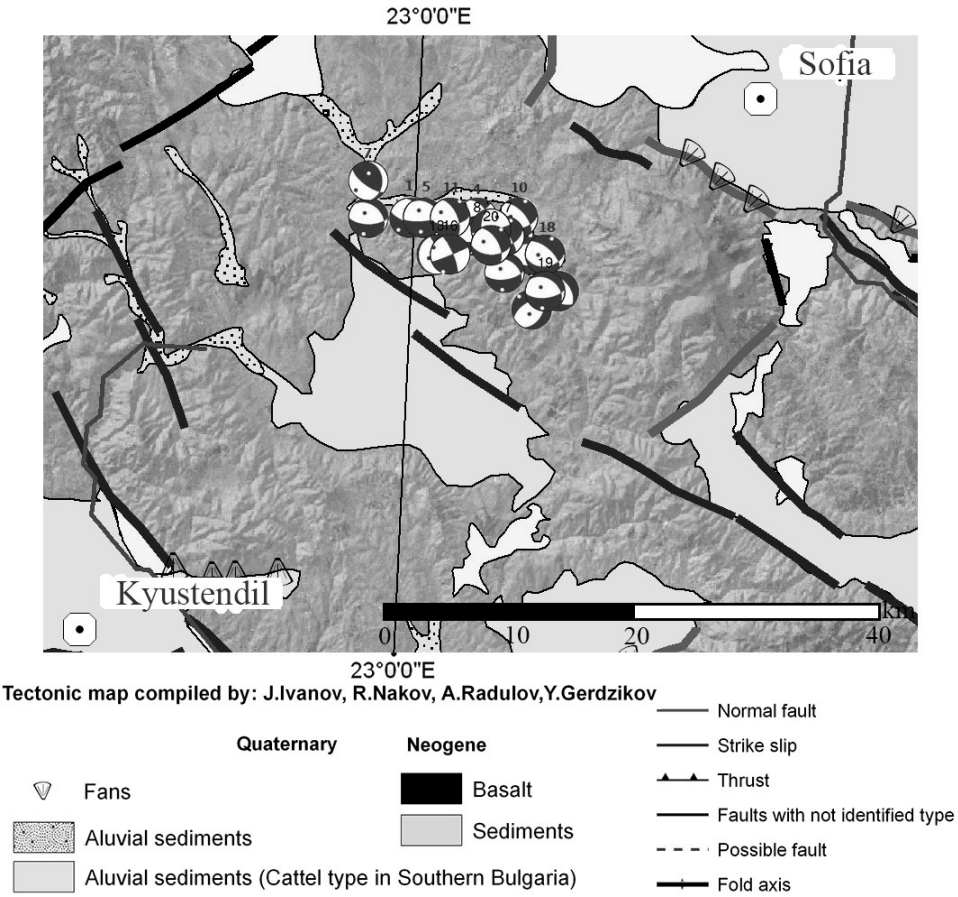

Fig.2 Fault plane solutions of the 2012 MW = 5.6 Pernik earthquake and aftershocks (modified from Ivanov et al., 2008)

Fault plane solutions for the main earthquake of 22 April 2012 with magnitude Mw=5.6 were obtained by forty-nine first motion polarities. The determined by the author focal mechanism is compared with other known solutions shown in Fig. 3 and their parameters are presented in Table 2. The small differences in the solutions determined by World networks are due to the use of different seismic-velocity models, number of first motion polarities, as well as the azimuthal location of the seismic stations around the earthquake epicenter. According to the focal mechanism parameters, the earthquake is characterized as jerk normal fault movement with small strike-slip component, the faulting takes place along a hidden fault plane, caused by extensional regional tectonic stresses (Botev et al., 2013b).

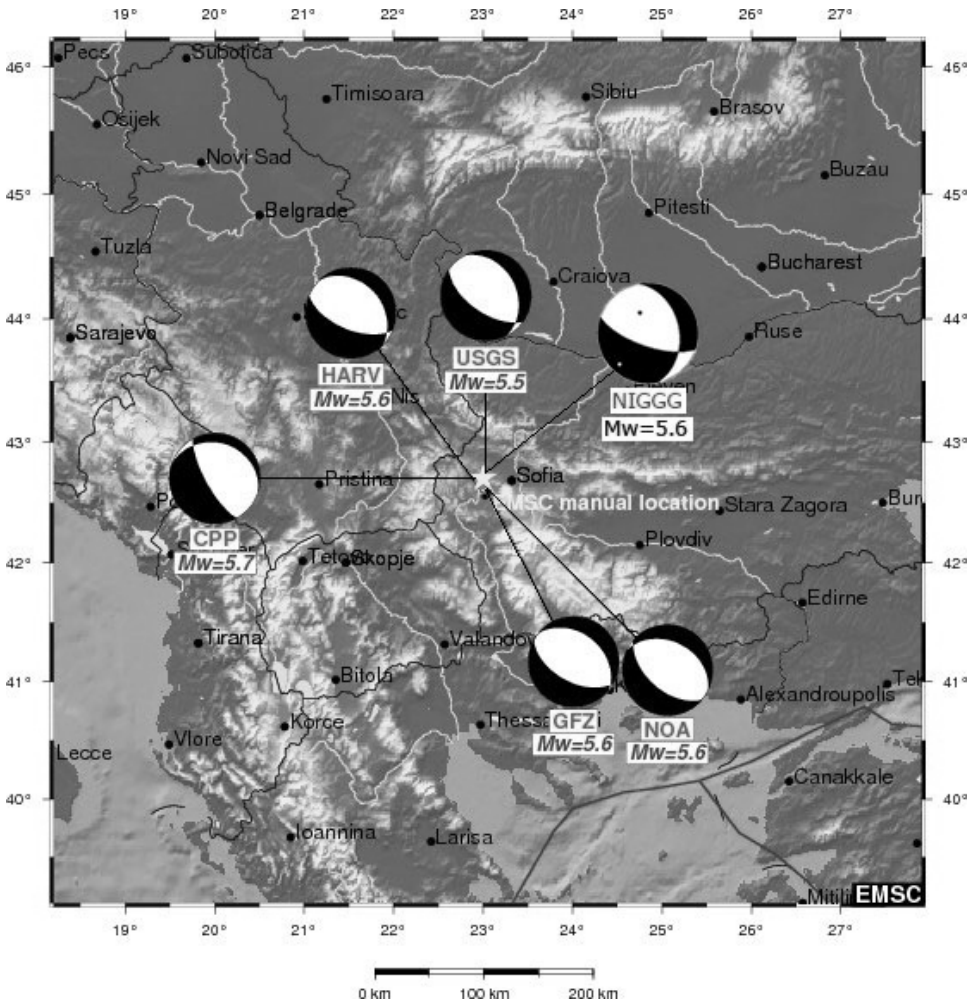

Fig.3 Fault plane solutions of the 2012 MW = 5.6 Pernik earthquake by NOTSSI and European-Mediterranean Seismological Centre (http://www.emsc-csem.org). World networks: NIGGG - National Institute of Geophysics, Geodesy and Geography, Bulgarian Academy of Sciences, Sofia, Bulgaria; CPP - Cal Poly Pomona University, California, United States of America; HARV - Harvard Seismology Group, Harvard University, Cambridge, United States of America; USGS - National Earthquake Information Center, United States of America; NOA - National Observatory of Athens, Greece; GFZ - Seismological Data Center, Potsdam, Germany.

Table 1. Parameters of the nodal planes for the main event and aftershocks. Date is given in year, month, day, origin time in hours:minutes, location is given as latitude (Lat N°) and longitude (Long E°) in degrees, event depth in kilometers (km), local magnitude (ML) is the Bulgarian magnitude. The two fault planes are specified with their azimuth (S1, 2), dip (D1, 2) and rake (R1, 2) in degrees. The focal mechanism principal axis of pressure (P), tension (T) and the null axis (B) are also specified by azimuth (az) and dip-plunge (pl) in degrees.

№	Date	Origin time	Lat N□	Long E□	h km	M_L	S1 [°]	D1 [°]	R1 [°]	S2 [°]	D2 [°]	R2 [°]	Paz [°]	Ppl [°]	Taz [°]	Tp [°]	Baz [°]	Bpl [°]
1	120522	00:00	42.58	23.00	9	5.8	349	38	-36	109	69	-122	337	54	223	15	125	30
2	120522	00:04	42.58	22.97	8	3.9	312	36	-54	90	62	-113	311	63	193	9	103	20
3	120522	00:16	42.56	23.09	13	3.0	279	46	-73	75	46	-107	268	75	178	0	89	11
4	120522	00:43	42.58	23.05	10	3.4	334	45	0	224	90	135	298	30	187	60	63	45
5	120522	01:30	42.58	23.01	9	4.4	316	23	-41	85	75	-107	322	56	190	30	91	15
6	120522	01:34	42.53	23.09	10	3.0	244	55	-66	26	42	-120	204	68	320	1	47	20
7	120522	02:11	42.60	22.97	12	3.0	126	69	66	357	31	137	233	7	359	60	136	22
8	120522	02:13	42.57	23.05	5	4.1	289	43	-24	37	74	-131	263	45	156	31	52	38
9	120522	04:09	42.57	23.04	2	3.2	345	48	-31	97	67	-133	320	48	217	10	119	38
10	120522	04:29	42.58	23.08	15	3.1	318	61	-56	83	44	-135	276	58	25	7	120	30
11	120522	17:07	42.58	23.03	15	3.3	336	60	-35	85	60	-144	288	42	209	2	119	45
12	120523	10:57	42.54	23.11	11	3.0	319	43	-82	128	47	-98	330	84	223	0	133	5
13	120523	11:41	42.56	23.02	2	3.1	186	11	-63	339	80	-95	242	59	70	36	338	5
14	120523	21:59	42.56	23.10	10	3.7	312	63	-62	82	38	-132	267	62	29	10	118	23
15	120529	05:36	42.55	23.07	7	3.4	301	34	-58	83	62	-110	312	66	188	11	94	16
16	120529	07:23	42.56	23.03	6	3.8	337	78	-3	68	87	-168	299	10	198	8	80	77
17	120616	04:51	42.57	23.07	10	3.0	324	74	-45	69	47	-158	278	43	23	15	130	43
18	120714	12:52	42.57	23.06	8	4.3	78	83	-40	174	50	-170	29	32	130	20	250	49
19	120731	00:10	42.54	23.10	7	3.3	306	36	-54	84	62	-113	313	67	188	10	95	19
20	120816	02:11	42.57	23.06	10	3.0	331	58	-49	92	50	-136	297	50	34	2	126	33

Table 2. Parameters of the nodal planes for the main event 22nd of May 2012, origin time 00:00 GMT. The symbols are same as in Table 1, except moment magnitude (M_W) and World networks are the same as Fig. 3.

Network	Lat N□	Long E□	H km	M_w	S1 [°]	D1 [°]	R1 [°]	S2 [°]	D2 [°]	R2 [°]	Paz [°]	Ppl [°]	Taz [°]	Tpl [°]	Baz [°]	Bpl [°]
NIGGG	42.58	23.00	9	5.6	349	38	-36	109	69	-122	337	54	223	15	125	30
CPP	42.70	23.00	9	5.7	288	22	-132	152	74	-75	83	58	230	27	328	15
HARV	42.55	23.00	12	5.6	316	32	-70	113	61	-102	355	72	211	15	119	10
USGS	42.68	23.02	12	5.5	292	41	-104	130	50	-78	95	79	212	4	302	9
NOA	42.60	23.06	10	5.6	296	36	-102	131	54	-81						
GFZ	42.67	23.01	16	5.6	310	37	-80	119	54	-96	1	80	213	8	123	5

Regional stress field

Fig.4 displays the horizontal projections of the individual P (pressure) and T (tension) axes of all twenty earthquake focal mechanisms. The projections of compression (P-axis) are predominantly of NW-SE orientation and are significantly smaller than the axes of extension (T-axis) in NE-SW. The plunge of P-axes varies in the range 10º-84º, about 51° in average, and the plunge of T-axes is in predominant sub-horizontal orientation (0º -60º), about 15° in average. The above pattern indicates for extensional stress field in the studied area.

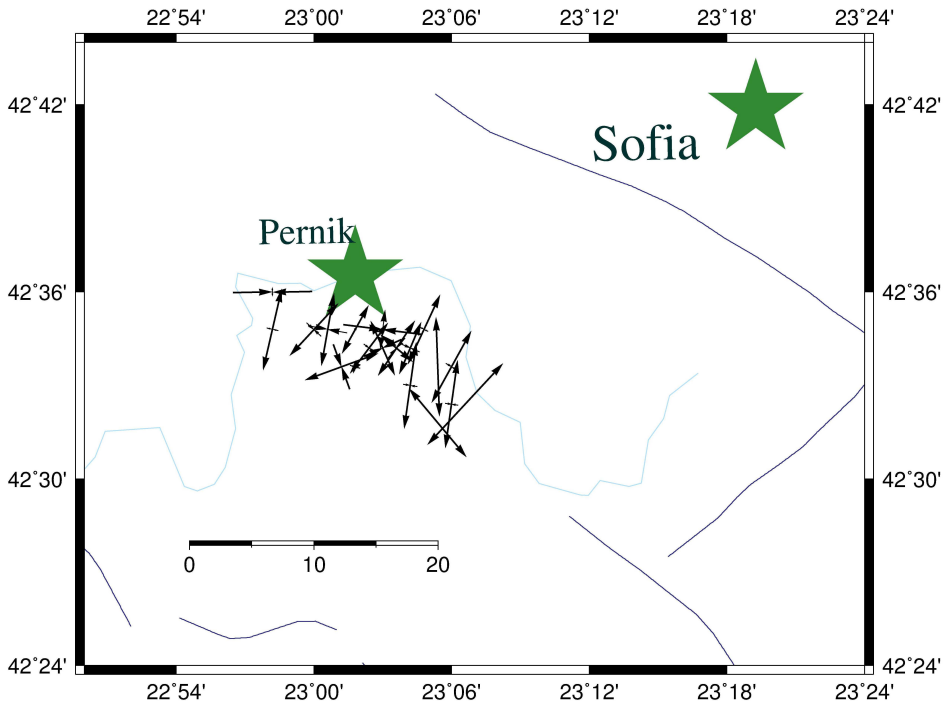

Fig.4 Horizontal projections of the individual P and T axes of the 2012 MW = 5.6 Pernik earthquake and aftershocks focal mechanisms (The Generic Mapping Tools - http://gmt.soest.hawaii.edu/home, the tectonic map is compiled after Barrier et al., 2004 and Georgiev et al., 2007). The stars mark the location of the cities of Sofia and Pernik.

Conclusion

The main result from the focal mechanism determination and the stress orientation analysis shows the prevailing of a normal or extensional stress regime in the studied region. Generally, the tension axes are sub-horizontal and of NE-SW orientation.

The observed sub-horizontal uppercut extensional stress with predominant NE-SW trend of the T-axes is consistent with the general trend of the regional extensional field on

the territory of Bulgaria (e.g., Protopopova et al., 2013). This stress field corresponds to that found in southern Bulgaria (presented by Van Eck and Stoyanov, 1996) and confirms the hypothesis that the neotectonic movements in Balkan Peninsula region are the consequence of the long lasting extensional movements in the inner parts of the Aegean and Central Balkan regions.

Acknowledgements. The author would like to thank Prof. E.Botev and Ass.Prof .S.Simeonova about their scientific and technical support.

References

Aki, K. and P.G.Richards, 1980. Quantative seismology: Theory and Methods, New York, 801.

Barrier, E., N.Chamot-Rooke, G.Giordano, 2004. Geodynamic map of the Mediterranean, Sheet 1-Tectonics and Kinematics, CGMW, France.

Botev, E., D.Dimitrov, I.Georgiev, V.Protopopova, 2013b. Investigation of the 22 May 2012 Earthquake, Pernik, Bulgaria, Proceedings of 7th Congress of Balkan Geophysical Society – Tirana, Albania, 7-10 October 2013, CD.

Botev, E., V.Protopopova, I.Popova, B.Babachkova, S.Velichkova, I.Tzoncheva, S.Dimitrova, V.Boychev, D.Lazarov, P.Raykova, 2013b. Data and analysis of the events recorded by NOTSSI in 2012, Bulgarian Geophysical Journal, Sofia, v.38, 93-102.

Botev, E., V.Treussov, V.Efrimova, 1996. A velocity model of crust and upper mantle of Bulgaria on data of earthquake and explosion records, Bulgarian Geophysical Journal, 22 (2), 49-62

Christoskov, L., 2007. Seismology, part II. Sofia, 198.

Georgiev, I. D.Dimitrov, T.Belijashki, L.Pashova, S.Shanov, G.Nikolov, 2007. Geodetic constraints on kinematics of southwestern Bulgaria from GPS and leveling data, Geological Society, London, Special Publications, 2007; 291: 143-157.

Grigorova E., D.Sokerova, L.Christoskov, Sn.Rizhikova, 1979. Catalogue of the earthquakes in the territory of Bulgaria for the period 1900-1977, Archives of the Geophysical Institute of BAS, Sofia.

Ivanov, J., R.Nakov, A.Radulov, Y.Gerzikov, 2008. Neotectonic Map of Bulgaria, In Project report: Seismic zoning of Bulgaria according to EC8, Part II, Geophysical inst. – BAS, Sofia, pp.187.

Karagjuleva, Ju., E.Bonchev, V.Kostadinov, 1973. Tectonic map of Bulgaria, Geological Inst.BAS

Kasahara, K., 1978, Earthquake mechanics, Tokyo, 54.

Protopopova, V., I.Georgiev, D.Dimitrov, E.Botev, 2013. Fault plane solutions and geodynamics of Bulgarian territory and some adjacent lands, Proceedings of 7th Congress of Balkan Geophysical Society – Tirana, Albania, 7-10 October 2013, CD.

Snoke, J.A., 2009. FOCMEC: FOCal MECanism Determinations, Virginia Tech, Blacksburg, VA, USA, Manual.

Solakov, D., 1993. An algorithm for hypocenter determination of near earthquakes, Bulgarian Geophysical Journal 19 (1), 56-69.

Van Eck, T., T.Stoyanov, 1996. Seismotectonics and seismic hazard modelling for Southern Bulgaria, Tectonophysics, 262, 77-100.

Определяне на механизмите на земетресението край град Перник M_W 5.6 през 2012 година (северозападна България) и по-силните афтършоци

В.Протопопова

Резюме: Земетресение с магнитуд M_L=5.8 (Mw=5.6) и епицентрална интензивност I_0= 8 MSK64 се случи в близост до град Перник (северозападна България) на 22-ри май 2012 г. Земетресението е последвано от интензивна афтършокова активност. В научната публикация са представени 20 определени фокални механизма (главният и 19 афтършока) регистрирани от Националната сеизмологична мрежа. Ориентацията на фокалние равнини на определените механизми и пространственото разпределение на афтършоците съвпада със северозападно-югоизточното направление на разлома Перник-Белчин. Също така е представен основен геодинамичен анализ.

TEMPORAL CHARACTERISTICS OF THE 2012 PERNIK EARTHQUAKE AFTERSHOCK SEQUENCE

P. Raykova

National Institute of Geophysics, Geodesy and Geography, BAS, Akad. G. Bonchev street, bl.3, Sofia, Bulgaria,
e-mail: plamena.raikova@gmail.com

Abstract: Statistical analysis is applied to study temporal pattern of earthquake distribution in aftershock sequence of the 2012 Mw=5.6 Pernik earthquake. On the assumption that aftershocks are distributed in time as a non-stationary Poisson process the maximum likelihood method for estimating the parameters (K, c and p) of the modified Omori formula is used. A transformation from the time scale t to a frequency-linearized time scale τ is applied for testing the goodness of fit between the aftershock occurrence and different statistical models. It is found that the temporal distribution of the Pernik earthquake aftershocks is dominated by the classic power law decay in time.

Key words*:* aftershock, aftershock sequence, aftershock decay rate, southern Bulgaria

Introduction

Study of the space-time distribution of earthquakes is of fundamental importance for understanding the physics of the earthquake generation process. The spatial and temporal clustering of aftershocks is the dominant non-random element of seismicity, so when aftershocks are removed, the remaining activity can be modelled (as first approximation) as a Poisson process (Gardner and Knopoff, 1974). Aftershocks occur after the mainshock and their frequency decays through time with approximately the reciprocal of time elapsed since the main earthquake. The occurrence rate of aftershock sequence in time is empirically well described by the modified Omori formula proposed by Utsu in 1961 (Utsu, 1969). The power-low decay represented by the modified Omori relation is an example of temporal self-similarity of the earthquake source process. Aftershock decay rate (parameter p) may contain information about the mechanisms of stress relaxation and frictional strength heterogeneity, (Mikumo and Miyatake, 1979), but this information can not to be derived without precise characterization of the empirical relations that best fit the

data.

In the present study statistical analysis to examine the temporal pattern of earthquakes in the aftershock sequence of the Mw=5.6 Pernik earthquake is applied. The earthquake occurred on May 22, 2012 in Sofia seismic zone south-western Bulgaria. To estimate the parameters (K, c and p) in the modified Omori formula the maximum likelihood method for the aftershock sequence is used. The goodness of fit between the aftershock occurrence and different statistical models has then been tested on the base of transformation of the time scale t to a frequency-linearized time scale τ. Further the Akaike Information Criterion (Akaike, 1974) is used to select the best model among competing models.

Method and Data

Method

The frequency ***n(t)*** of aftershocks at time ***t*** is well represented by the modified Omori formula (Utsu, 1969):

$$n(t) = K(t+c)^{-p} \qquad (1)$$

where ***t*** is the elapsed time since the occurrence of the main shock, and ***K***, ***p***, ***c*** are constant parameters. The most important parameter ***p***, characterizes the decay of the aftershock activity.

On the assumption that aftershocks are distributed as a non stationary Poisson process with intensity function $\lambda(t;\theta)$, $\theta=(K, p, c)$, Ogata (Ogata, 1983) used the maximum likelihood method to estimate the parameters ***K***, ***c*** and ***p*** in modified Omori formula (1).

The intensity function of the Poisson process $\lambda(t)$ is defined by the relation:

$$\lambda(t)=\lim_{\Delta t\to 0} \text{Prob}\{\text{an event in } [t,t+\Delta t]\}/\ \Delta t \qquad (2)$$

Using the modified Omori formula, the intensity function becomes:

$$\lambda(t, \theta)=K(t+c)^{-p} \qquad (3)$$

An integration of the intensity function $\lambda(t)$ gives a transformation of the time scale t to a frequency-linearized time scale τ (Ogata and Shimazaki, 1984). If the choice of the intensity function $\lambda(t)$ (i.e., the parameters K, c and p) is correct the occurrence of aftershocks becomes the standard stationary Poisson process on the frequency-linearized time axis.

The frequency-linearized time for an aftershock sequence can be defined as:

$$\tau = \Lambda(t) = \int_S^t \lambda(s)ds \qquad (4)$$

The time scale τ is used for testing the goodness of fit between the aftershock occurrence and the selected model. A linear dependence between the observed cumulative number of aftershocks ***(N)*** and τ should be observed if an appropriate model has been selected. Anomalies in the aftershock activity are more evident on the $N(\tau)$ plot than on ***n(t)***. Thus the τ time axis will be used to detect secondary aftershock activity**.**

To select which model fits the observations better, the Akaike Information Criterion (AIC) (Akaike, 1974) is used. The AIC is defined by:

$$AIC=(-2)Max(\ln\text{-likelihood})+2(\text{Number of the used parameters}) \quad (5)$$

A model with a smaller value of AIC is considered to be a better fit to the observations.

Data

All events that satisfy the criteria introduced by Gardner and Knopoff (Gardner, J.K., L.Knopoff, 1974) and modified by Christoskov and Lazarov (Christoskov, L., R. Lazarov, 1981) for the Central Balkans, accepted as aftershocks

$$\log(R_a) = 0.9696 + 0.1243M$$

$$\log(T_a) = -0.62 + 0.56\,M \qquad (M<6.0)$$

$$\log(T_a) = -5.25 + 2.15M - 0.137M^2 \qquad (M\geq 6.0) \quad (6)$$

where M is surface wave magnitude of the main event, Ra is the greatest distance between the main event and aftershock, and Ta is the greatest elapsed time since the occurrence of the main shock.

For the time period May 2012 - May 2013 aftershock sequence of the M_W =5.6 Pernik earthquake is compiled on the base of digital data from NOTSSI (National Operative Telemetric System for Seismological Information). More than 1000 aftershocks occurred in the considered time interval but only about 20% of them are localized (recorded at least at three stations). The majority of the aftershocks are recorded only at seismic station Vitosha (VTS)-the nearest station (at about 15 km from the main shock epicenter). Thus the analyzed sequence comprises 169 (M≥1.0) aftershocks occurred in time interval of 365 days.

Results

The aftershock sequence from 0 to T=365 days after the M_w=5.6 Pernik earthquake applying to the modified Omori formula (1) was analyzed. The maximum likelihood estimates (MLM's) are as follows: K=15.23, c=0.025, p=0.90. The frequency-time distribution of aftershocks is presented in Figure 1.

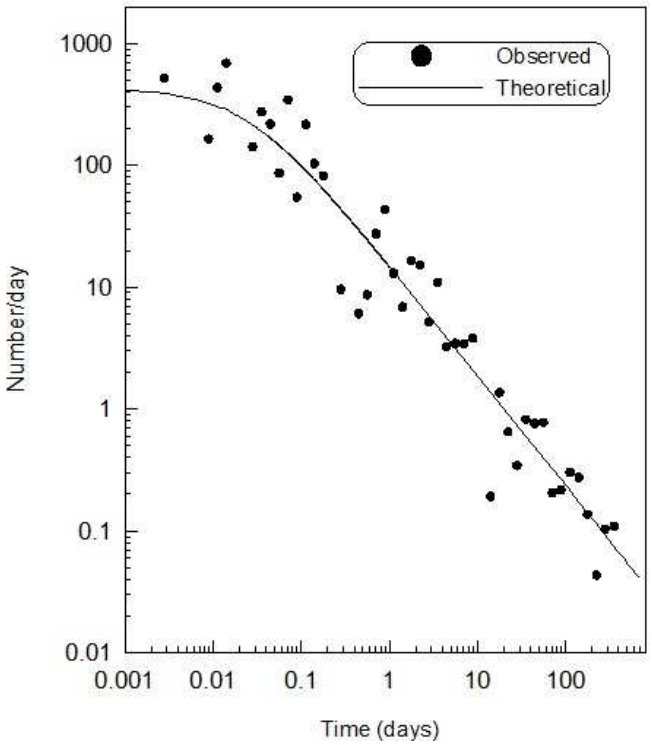

Fig. 1. Frequency - time distribution of aftershocks.

In the figure the observed distribution is compared to the distribution (called theoretical), which is expected as a results from the selected model (in the case, the model is the modified Omori formula). The comparison between empirical and theoretical distribution (Fig.1) shows that as a first approximation the temporal distribution of earthquakes in aftershock sequence of the 2012 M_w=5.6 Pernik earthquake is well described by the modified Omori formula.

The cumulative number of events is plotted against the frequency-linearized time $\boldsymbol{\tau}$ defined in the equation (4) using the MLM's of parameters ***K***, ***p***, ***c*** (presented in Fig. 2). A relatively good agreement between the expected (theoretical) and the observed distribution of the aftershocks can be seen in Figure 2. The figure shows that a nearly linear trend of aftershock decay continues up to 365 days (177 linearized time); thus the modified Omori formula (1) fits largely the observations up to 365 days after the main shock.

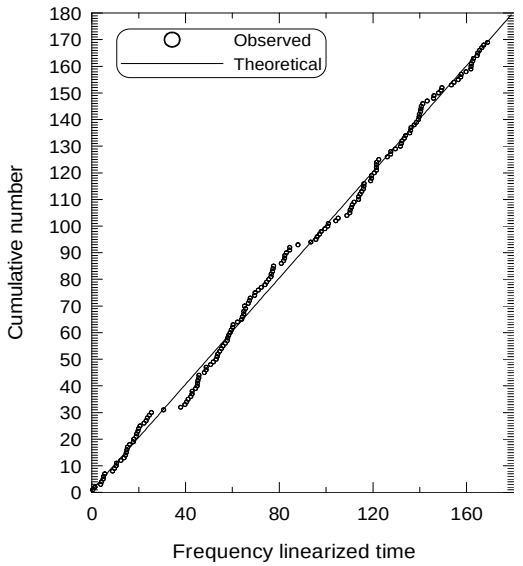

Fig. 2. Plot of cumulative number of events versus frequency linearized time τ.

The figure also suggests the existence of some discrepancies between the observed and expected distributions (S-shaped deviations from the linear trend) – evident periods of decaying and activation of the process. An increase of the cumulative number is observed in the first hours after the main shock (time period of twelve hours 36 aftershocks occurred, among them the strongest one) followed by a decrease in number of events several hours later. The aftershock activity decreases before the 40th day and increases about 10 to 20 days later. This temporal distribution anomaly could be caused by the occurrence of one of the strongest aftershock that occurred 53 days (on July 14, 2012 with M=4.4) after the mainshock.

Consequently two models that take into account the effect of secondary aftershock activity were constructed: 1) the first model with one secondary aftershock sequence after 0.5 days and 2) a combination of one main and two secondary sequences - after 0.5 and 53 days. The same p value for the main and secondary aftershock sequences is assumed for both models.

The maximum likelihood estimate of the parameters in the modified Omori formula, and the selection of a statistical model based on AIC, show that the aftershock sequence of the 2012 Pernik earthquake is best modeled by one ordinary and two secondary sequences, although there remain S-shaped deviation from the linear trend -about 80 day after the main shock.

Discussion and conclusions

The aftershock sequence from 0 to 365 days after the 2012 Pernik earthquake (occurred in Sofia seismic zone – south-western Bulgaria) by fitting it to the modified Omori formula was analyzed. The aftershock sequence of the 2012 earthquake (its

magnitude estimates according to USGS/NEIC are: M_w=5.6; m_b=5.7; M_s=5.2) is compiled on the base of digital data from NOTSSI. For homogeneity a threshold magnitude (the minimum magnitude of aftershocks) of M=1.0 is accepted. Thus the studied sequence comprises 169 aftershocks occurred in time interval of 365 days.

The p value (p=0.90) estimated for the aftershock sequence is in the middle of p value range obtained for aftershock sequences in Bulgaria, i.e., p=0.71-1.17 (Simeonova, Solakov, 1999).

The temporal distribution of the aftershocks following the 2012 M_w=5.6 earthquake is similar to the aftershock sequences in northern Bulgaria obtained by Simeonova and Solakov (1999) - slowly decay in time (p<1.0), without secondary aftershock activity. By contrast, the sequences in south-western Bulgaria are characterized by well expressed secondary aftershock activity and relatively high values of p for the main sequence (p>1) (Simeonova, Solakov, 1999).

The main conclusions are as follows:

- The maximum likelihood estimate of the parameters in the modified Omori formula and the selection of a statistical model based on AIC show that the aftershock sequence of the 2012 Pernik earthquake is best model by one ordinaryand two secondary sequences.
- The temporal pattern of the earthquakes distribution in aftershock sequence of the 2012 M_w=5.6 Pernik quake (occur in south-western Bulgaria) is similar to the temporal distribution of the aftershocks in Northern Bulgaria - slow decay in time (p<1.0), without secondary aftershock activity.
- It can be assumed that aftershocks are generated in slowly relaxing environment with low heterogeneity.

References

Akaike, H., 1974. A new look at the statistical model identification, IEEE Trans. Autom. Control AC-19, 716-723.

Christoskov, L., and R. Lazarov, 1981. General considerations on the representativeness of theseismological catalogues with a view to the seismostatistic investigations, Bulg.Geoph. J., 3, 58-72 (in Bulgarian).

Gardner, J.K., and L. Knopoff, 1974. Is the sequence of earthquakes in southern California, with aftershock removed, Poissonian, Bull. Seism. Soc. Am., 64, 1363-1367.

Mikumo, T., and T. Miyatake, 1979. Earthquake sequences on a frictional fault mode with non-uniform strengths and relaxation times. Geophys. J. R. Astr. Soc. 59, 497-522.

Ogata, Y., 1983. Estimation of the parameters in the modified Omori formula for aftershock sequences by the maximum likelihood procedure, J.Phys. Earth, 31, 115-124.

Ogata, Y., and K. Shimazaki, 1984. Transition from aftershock to normal activity: the Rat Islands earthquake aftershock sequence, BSSA, 74, 1984, 1757-1765.

Simeonova, S., and D. Solakov, 1999. Temporal characteristics of some aftershock sequences in Bulgaria, Annali di Geofisica, 42, 5, 821-832.

Utsu, T., 1969. Aftershocks and earthquake statistics (I) - Some parameters which characterize an aftershock sequence and their interaction, J. Fac. Sc., Hokaido Univ., Ser. VII (Geophys.), 3, 129-19.

Времеви характеристики на афтършоковата активност след земетресението от 2012 около град Перник

Пл.Райкова

Резюме. Статистическият анализ се прилага за изучаване времевия модел наафтършоковата активност последвала след земетресението през 2012 Mw = 5.6 в района на град Перник. Въз основа на предположението, че вторичните трусове са разпределени във времето като нестационарен Поасонов процес се използва модифицираната формула на Омори за оценяване на параметрите (K, c и p). Трансформацията на времета скала t в честота-линеализирана скала τ се прилага за определяне на най- добрата връзка между афтършоковата активност и различни статистически модели.

ON THE MONITORING OF THE SEISMIC ACTIVITY IN THE TERRITORY OF BULGARIA AND SURROUNDINGS

E.Botev, D.Solakov, L.Christoskov

NIGGG of BAS, Akad. G. Bonchev street, bl.3, Sofia, Bulgaria, e-mail: ebotev@geophys.bas.bg

Abstract. Generalized analysis of the monitoring of the seismicity over the territory of Bulgaria and its very adjacent lands for the last 32 years is proposed. More than 32 000 seismic events with magnitude M > 0.5 are localized in this region since 1981 – the time of the modern National Seismological Network starting operated. Catalog of earthquakes with magnitude M>4.0 is applied. The time and space variation of the seismicity is traced out by the consequential analysis of the epicentral distributions around the seismic zones for each 5-years period during the time operation of the National Seismological Network. Some more or less clear expressed grouping of epicenters of strongest earthquakes around the main Quaternary active fault structures is established, as well as some kind of "migration" of the strong seismicity during the time – from north-east to south-west and vise versa.

Key words: Bulgaria, seismic monitoring, seismicity

The earthquake monitoring in Bulgaria is carried out by the National Seismic Network (NSN), part of the Seismological Department of the National Institute of Geophysics, Geodesy and Geography of Bulgarian Academy of Sciences (NIGGG of BAS). The network was run in 1980 and nowadays consists of 23 stations (16 permanent seismic stations and two local networks) – Fig.1. After 2005 NSN is developed as fully digital seismic network.

The main tasks of NSN are:

- to provide reliable recording and transfer of seismological data;
- to ensure rapid hypocenter and magnitude estimation and notification of the governmental authorities, media and broad public in case of felt or damaging earthquakes on the territory of Bulgaria;
- to provide a modern basis for seismological studies in Bulgaria

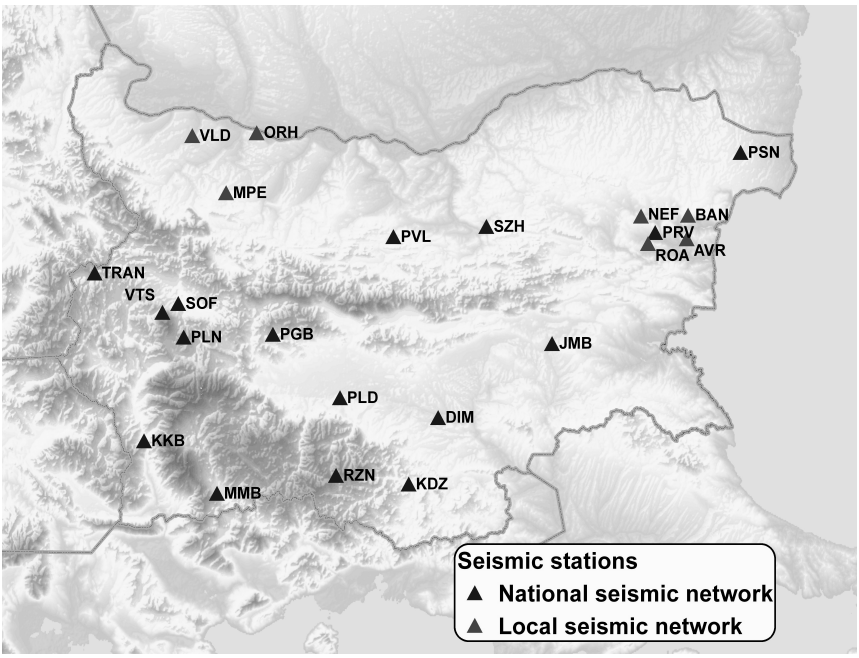

Fig.1. Modern seismological network of Bulgaria

At the National Digital Center (NDC) the data are automatically and manually processed and interpreted. Unified duration magnitude Md (up to 2006) and magnitudes based on P and S wave amplitudes (since 2006) are calculated. Both estimates of earthquake hypocenter parameters and magnitude, as well as station data are archived on a disc storage system. Additional information from foreign Balkan stations is used in hypocentral estimations. The monitoring process at the NDC also includes an assessment of the impact on the people and the buildings due to earthquakes and the relevant information is send to the responsible governmental bodies. In a case of a strong earthquake on the Balkans, the seismologist sends Bulgarian data to the neighboring and international seismological centers. Macroseismic information for about 30% of all events with magnitude M>3.0 is included in seismological catalogue. Epicentral intensity Io is published for events with compiled isoseismal maps.

The present study contains generalized results concerning the seismic events recorded by the NSN after 1981. The expanded seismic information, the analysis and evaluation of the space-time and energy earthquake distribution give possibilities to study the space-time correlations with other geophysical parameters for earthquake prediction purposes.

The evaluation of the main seismic event parameters is performed by a computer program (Solakov , 1993) based on HYPO'71 (Lee, W. H. K. and J. C. Lahr, 1972). The energy parameters of the events are presented mainly by the magnitude M calculated according to the record's duration by the formula (Christoskov and Samardjieva, 1983).

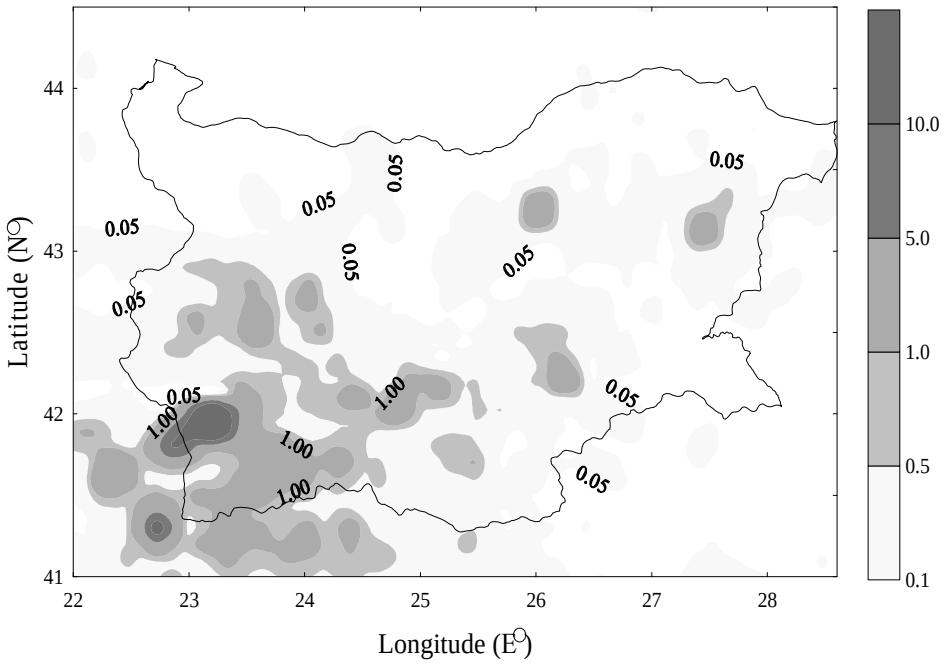

Fig.2. Epicentral density (events/100km^2/year) of the seismic events recorded after 1981 (M>0.5)

The focal mechanism parameters are obtained applying FOCMEC program (Snoke, 2009). The existing seismic network in Bulgaria provides a possibility to locate seismic events different magnitude threshold levels of local, regional and long distance earthquakes: M=1.5 for the territory of Bulgaria, M=3.0 for the central part of the Balkans, M=5.0 for long distance events.

More than 32000 events are localized on territory of Bulgaria and adjacent regions during the last 32 years – on Fig.2 the space distribution of the epicentral density is

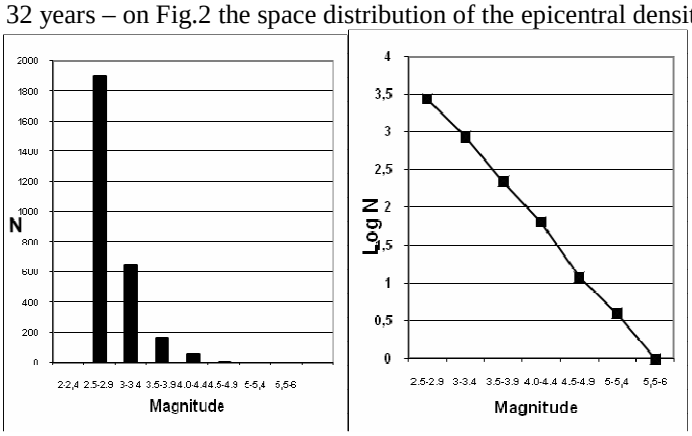

Fig.3. Magnitude-frequency and cumulative LogN-magnitude distributions of the earthquakes with magnitude M > 2.5

presented. The strongest earthquake is realized in Central Western Bulgaria with magnitude M_w=5.6. The maximum number of events is occurred in South-western part of the region of interest. Almost 97.3percentage of the events are micro earthquakes - with magnitude less than 3.0. For the analysis of the seismicity in Bulgaria during the period of National Seismic Network operation (since1981) catalogue of the earthquakes with M>2.5 have been used (Archives of NIGGG; Botev et al., 1991-2012; Solakov&Simeonova/eds/,1993).

The magnitude-frequency distribution (Fig. 3a) of the earthquakes with magnitude M > 2.5 shows that the number of the events increases with the decrease of magnitude: 1 event of M > 5.5, 3 event of M > 5.0, 7 of M=4.5-5, 54 of M=4-4.5, 162 of M=3.5-4, 646 of M=3-3.5 and 1904 of M=2.5-3. The cumulative magnitude-frequency dependence (log(N)=a ± bM) or so called Guttenberg – Richter relation (1965) is presented on the diagram on Fig. 3b. A linear distribution of the events with magnitude M> 1.5 is observed. The distribution line has coefficients a = 5.93 and b = 1.09. The value b is approximately in the range of the corresponding values from the standard dependence for longer periods and stronger events which means that some equilibrium between our period of investigation and the whole period with all strong events is available.

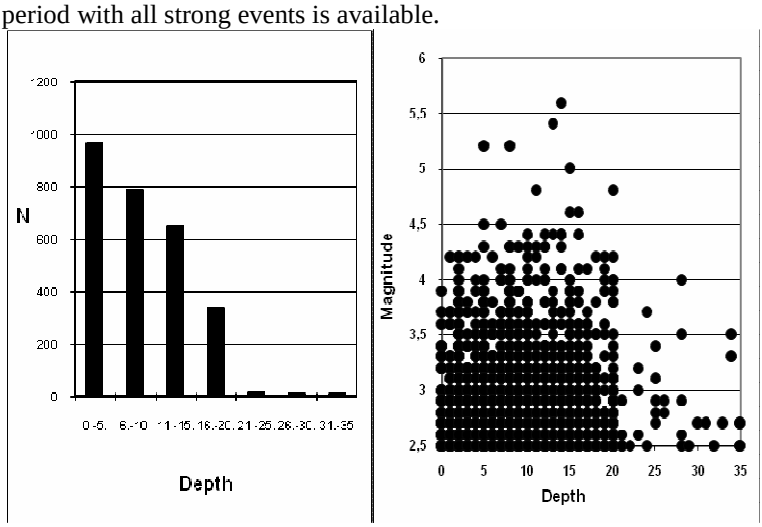

Fig.4. Depth and Depth-magnitude distributions of the events with magnitude M > 2.5

Depth distribution of the events with magnitude M > 2.5 shows that the hypocenters of the earthquakes are concentrated in the subsurface 20 km depth interval; they reach down to 30-35 km depth for a few events mainly in the SW part of Bulgarian territory. The smooth increasing in the events number with the depth's decreasing to 0-5 km is probably an evidence for availability of very small quantity of unidentified industrial explosions. The distribution of the events' strength (magnitude) in depth does not permit distinguishing any depth "floor"; the stronger events can be traced out within a large depth interval – from 5 to 20 km , the maximal events – 13-15 km.

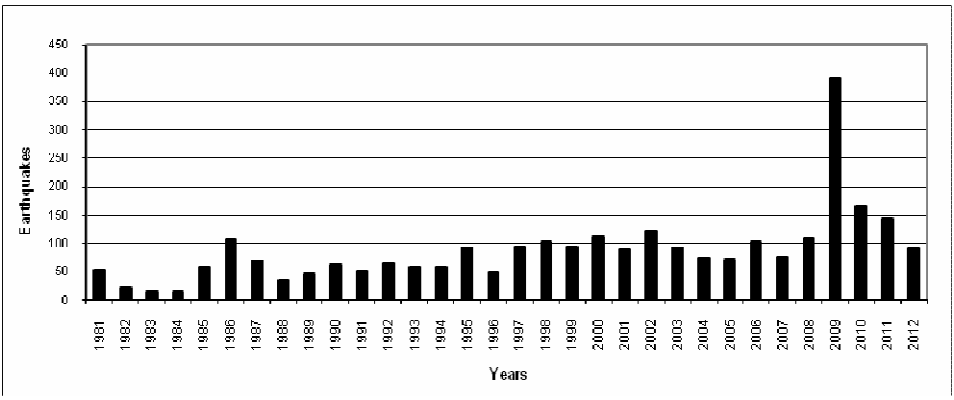

Fig.5. Time - distribution of the events with magnitude M > 2.5

From the time distribution of the events with M > 2.5 it is remarkable that in the last years (after 1997) the frequency of the events is stable higher in comparison with the previous years. The increased number of events during 1986 is due to the aftershock sequences of the Strazhitza earthquakes (magnitudes 5.1 and 5.4). The increased number during 1997 and 1998 is due to a swarm sequence in Rila mountain. The significantly increased number of events in 2009 due to the Valandovo aftershock sequence with main event magnitude M=5.2.

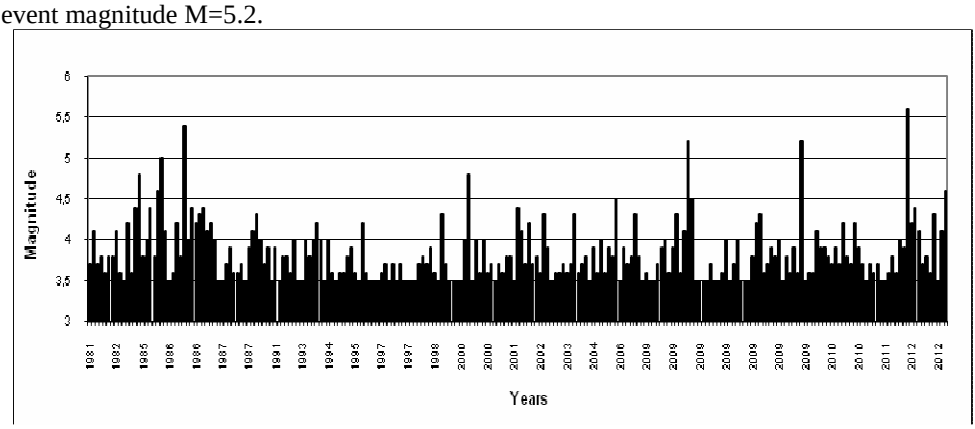

Fig.6. Magnitude – time distribution of the events with magnitude M > 3.5

The magnitude – time distribution of the strongest events (with magnitude M > 3.5) shows the typical decreasing of M in the time for the aftershock series of the strongest earthquakes (Fig.6.). This "energy" distribution of the earthquakes does not allow the establishment of a quasi-periodic peculiarity of the seismicity, but in the same time confirms an idea for some kind of a periodicity. As it will be seen in the next part, this periodicity will be associated with the "migration" of the strong seismicity during the last 32 years – from north-east to south-west and vise versa.

The time and space variation of the seismicity could be traced out by the consequential analysis of the epicentral distributions of the each about 5-years period during the NSN operating (Fig.7.).

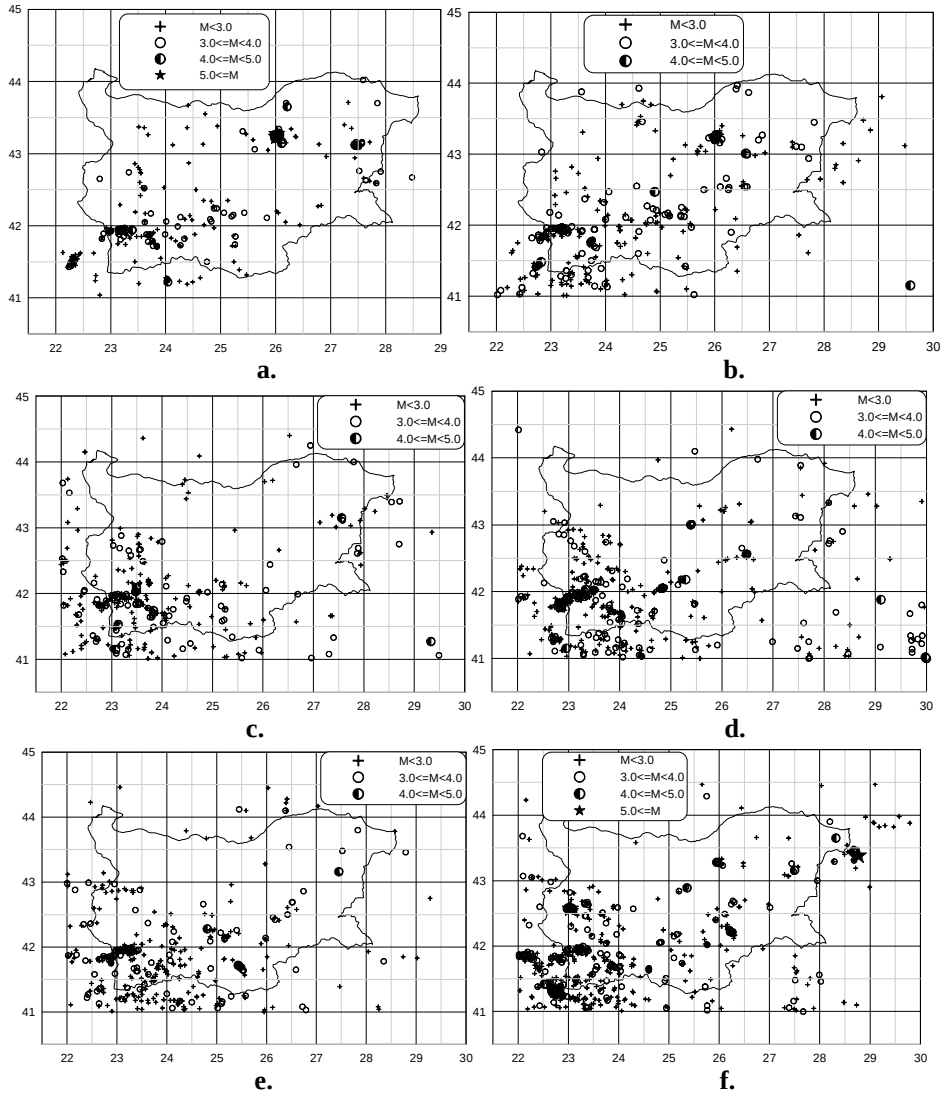

Fig.7. Epicentral distribution of the events with M>2.5 during a)1981-1986,b)1987-1992, c)1993-1997, d)1998-2002, e)2003-2007 and f)2008-2112

From the analysis of the epicentral distributions in the pictures of Figs7(7a, 7b,…., 7f) it is seen that relatively stronger seismicity is observed only during the first and the last time period (Figs 7a and 7f) where the epicenter locations are presented by more specific symbols. Only on these two figures earthquakes with magnitude M >4.5 are observed – with only one exception in Fig7e for Kardzhaly M=4.6 event. The most specific feature of the seismicity during the first time period (Fig.7a) is the NE-SW oriented 1986 Strazhica sequences (Mmax =5.4) in the eastern edge of the Gorna Orjahovitza zone in the central northern Bulgaria and the grouping of epicentres in Provadia zone without strongest

seismicity (Mmax=4.3), in the mainland of NE Bulgaria. With similar specific picture of seismic activation is characterized the seismicity during the last time period (Fig.7f), but now the stronger is the 2009 activation in NE part of Bulgarian territory – Shabla zone in northern Black sea coast (Mmax=5.2). But the strongest event for whole Bulgarian territory occurs after all this activity of Central and Eastern North Bulgaria – in May 2012 by the relatively short Pernik sequence (Mmax=5.6) the strongest seismic activity migrates to the central parts of West Bulgaria.

As a whole the rest lower seismicity shows very similar features on the pictures of all Figs7. The epicentral distribution of the events with M>2.5 is relatively diffuse –the eppicenters of smaller arthquakes are not clearly grouped around the well known active geotectonic structures. Relatively outlined zones of grouping of the epicentres could be marked at the background of everywhere distributed epicenters of the weak seismicity during the last 32 years. The most active zone is the Struma area, in the southwestern part of the investigated region. Some other active zones are those of Plovdiv, Yambol, Kardzhali and Sofia. Very long swarm of seismic activity is observed after 2008 in the region around the Monastery uplift. Nevertheless the most significant feature of all pictures of Figs7 is the dominated biggest concentration of epicentres in southwestern parts of the investigated territory.

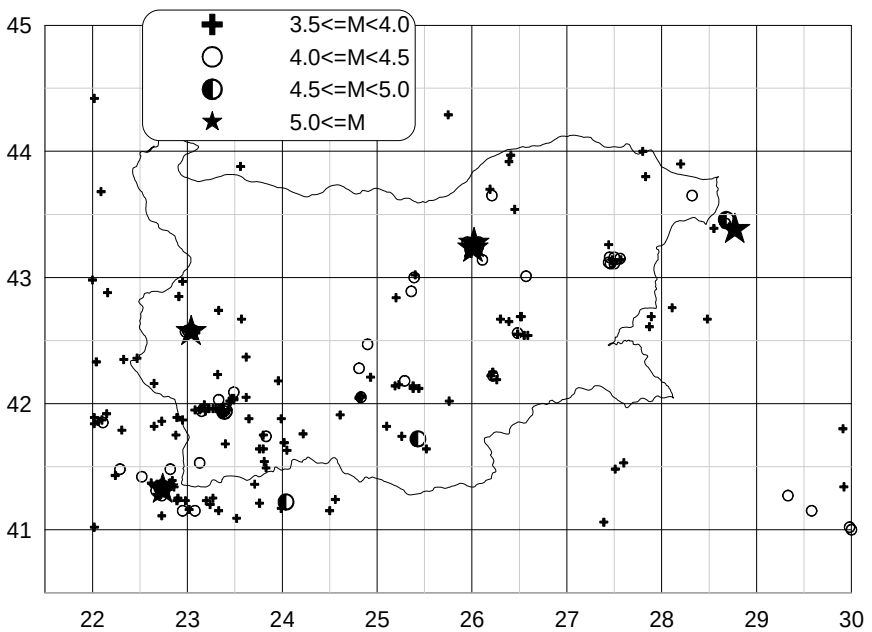

Fig.8. Strong seismicity during 1981 – 2012 (M > 3.5)

There is some correlation between the space distribution of the epicenters of the strong events (Fig.8, events with magnitude M>3.5) and the main Quaternary active fault sources in Bulgarian territory. It is no so clear that Moesian platform is characterized by the lowest seismic activity (like a platform) - on the contrary, several of the strongest Bulgarian events with M>5.0 and many aftershocks are realized in the central part of North Bulgaria

and to the north in the Black sea coast. The biggest concentration of epicenters is observed in western part of Rhodopian super unit (SW Bulgaria). Some grouping of events is seen in western and central part of the Srednogorie zone (Central Bulgaria). The epicenters show one very active south-western part of the investigated territory. The most active region of the state's territory here is the Kroupnik zone. It is to be stressed also on the seismicity tothe south of the Greek-Bulgarian border where many quakes are localized along the Middle-Mesta lineament. Some other polygons of activation can be fixed in the inner part of the Rhodope Mountain, in the region of Pernik (around Sofia zone), in the central parts of the Northern Bulgaria, in the northern Black sea coast and in the regions of Provadia, Jambol, Plovdiv and Kardzhali. The parameters of strongest events in these regions could be finding in the Table1.

Table 1. List of earthquakes with M ≥ 4.0 in Bulgaria and very adjacent lands

Year	Month	Day	Hour	Minute	Latitude (°N)	Longitude (°E)	Depth (km)	Magnitude
1981	7	23	6	15	43.12	27.44	8	4.1
1982	8	27	9	58	43.65	26.21	19	4.1
1983	11	10	17	28	43.11	27.46	10	4.2
1984	12	3	9	29	41.94	23.39	12	4.4
1984	12	3	10	26	41.94	23.39	11	4.8
1985	6	12	14	5	43.11	27.50	12	4.0
1985	9	28	14	50	41.48	22.29	10	4.4
1985	11	9	23	30	41.22	24.04	16	4.6
1986	2	21	5	39	43.27	26.02	15	5.0
1986	2	21	6	18	43.26	25.97	16	4.1
1986	5	15	16	45	41.94	23.15	19	4.2
1986	12	7	14	17	43.23	26.01	13	5.4
1986	12	7	14	53	43.14	26.11	20	4.0
1986	12	7	17	26	43.22	25.98	14	4.4
1986	12	8	14	44	43.26	26.03	20	4.2
1986	12	12	19	29	43.27	26.05	12	4.3
1986	12	17	22	1	43.28	26.07	14	4.4
1986	12	18	7	16	43.23	26.06	14	4.1
1986	12	18	17	16	43.25	26.07	18	4.2
1987	12	1	9	54	43.26	26.03	15	4.0
1989	10	25	15	27	43.01	26.57	17	4.1
1990	1	31	10	16	41.48	22.82	12	4.3
1990	6	10	11	36	41.15	29.58	19	4.0
1992	8	24	21	43	42.47	24.90	20	4.0
1993	3	27	23	47	41.15	23.08	12	4.0
1993	4	21	16	53	43.15	27.56	8	4.0
1993	12	12	17	21	41.27	29.33	3	4.2
1993	12	16	9	22	41.53	23.13	11	4.0
1994	3	21	21	42	42.09	23.49	10	4.0
1996	2	1	17	43	41.74	23.83	1	4.2
1998	12	11	15	9	42.18	25.29	14	4.3
2000	4	2	18	57	41.02	29.98	10	4.0
2000	6	6	2	42	41.88	29.11	20	4.8
2000	8	22	11	40	41.00	30.00	2	4.0

Year	Month	Day	Hour	Minute	Latitude (°N)	Longitude (°E)	Depth (km)	Magnitude
2000	8	28	5	16	43.00	25.39	8	4.0
2001	8	13	14	26	42.56	26.48	16	4.4
2002	2	18	10	19	42.03	23.33	10	4.1
2002	4	5	13	13	42.05	24.83	11	4.2
2002	7	31	4	5	41.15	22.95	11	4.3
2003	12	17	23	15	43.16	27.45	9	4.3
2004	9	10	17	46	42.28	24.81	15	4.0
2006	2	20	17	20	41.72	25.43	7	4.5
2008	4	15	3	43	42.89	25.36	10	4.3
2009	5	5	17	39	41.85	22.11	7	4.0
2009	5	24	14	29	41.35	22.71	8	4.3
2009	5	24	14	34	41.33	22.73	2	4.1
2009	5	24	16	17	41.32	22.74	5	5.2
2009	5	24	16	23	41.33	22.74	5	4.5
2009	5	24	18	50	41.32	22.71	7	4.0
2009	5	25	7	59	41.31	22.67	4	4.0
2009	5	31	22	7	43.28	25.95	2	4.2
2009	6	1	8	3	41.27	22.73	5	4.3
2009	6	15	9	56	41.31	22.76	5	4.0
2009	8	5	7	49	43.38	28.77	8	5.2
2009	11	30	5	48	43.43	28.67	14	4.1
2010	8	20	2	34	42.22	26.22	6	4.2
2010	10	7	19	51	43.16	27.50	2	4.2
2011	10	11	19	49	43.65	28.32	28	4.0
2012	5	22	0	0	42.57	23.04	14	5.6
2012	5	22	0	4	42.57	22.98	4	4.2
2012	5	22	1	30	42.58	23.00	13	4.4
2012	5	22	2	13	42.58	23.07	12	4.1
2012	7	14	12	52	42.57	23.06	8	4.3
2012	8	27	16	26	41.42	22.52	7	4.1
2012	12	3	18	58	43.46	28.68	15	4.6

From the analysis of the strong seismicity it is seen that the most seismic area in Bulgaria is situated in the Struma structural province in South-west Bulgaria. As usually, the largest concentration of epicenters is marked in the Kroupnik seismic source zone. This zone is characterized by faults transversal to the Struma lineament. One of the strongest crustal event for all Europe (M>7.8 in 1904) and about 30% of the present day weak seismicity are localized here. The biggest frequency of the earthquakes in Kroupnik zone is associated with the tectonic activity of Simitly quaternary depression, first of all with the activity of the Kroupnik fault. As it had been said, the seismic activation here has a transversally orientation in relation to the first order Strouma fault zone. Transversal faulting process can be marked in the region of Kovatchevitza, crossing the Upper Mesta fault zone. Transversally to the Strouma fault lineament is the seismicity in the SW corner of the region, and it is associated with the Belasitza and Stroumeshnitza faults. The activity in Central Bulgaria is associated with: Sub-Balkan fault lineament in the northern board of Sofia depression; the faults in the southern board of the Upper Thracia depression (the north flank of Rhodopes) and Tundzha fault linement in Yambol zone. The activity in the

central part of North Bulgaria is associated with the eastern border of Strazhitza depression and the southern one of the Ressenski trough. The seismicity in Provadia region is associated with the eastern border of the Provadia depression which is cross lying to the Fore-Balkan fault lineament. The relatively rare but strong seismicity in the Shabla zone on the Black sea coast during the last three years is associated with the activity of Kaliakra fault lineament in the sea aquatory.

Conclusions

The analysis of the instrumentally observed seismicity after the starting of NSN operation makes evident:

- The energetic level of the observed seismicity for the period 1981-2012 is relatively low – 97.3% from the all about 32000 seismic events are microearthquakes (M<3.0); the maximum magnitude event (M=5.6) is located in Pernik region – Central West Bulgaria.

- The magnitude-frequency distribution of earthquakes shows that the earthquake catalogue is complete for events of M > 2.5.

- The slope of the averaging straight line of the recurrence relationship of events shows some convenience between the weak and relatively stronger events from the whole seismic history of Bulgaria.

- The epicenter distribution of the events with M > 2.5 is relatively diffuse –the epicenters of all microearthquakes are not clearly grouped around the well known active geotectonic structures.

- Probably due to the high accuracy of determinations of epicenters for the stronger earthquakes (M>3.5), some more or less clear expressed grouping of epicenters around the main Quaternary active fault structures is established.

References

Botev E., B. Babachkova, B. Dimitrov, S. Velichkova, I. Tzoncheva, K. Donkova, S. Dimitrova (1991, 1991, 1992, 1992, . . . 2012, 2012) Preliminary data on the seismic events recorded by NOTSSI in January - June 1991 (July – December 1991), …, (July – December 2012). *Bulg. Geophys. J., v.v.18, 18, ... 36, 37 (NN1, 2, 3, 4).*

Christoskov L. and E. Samardjieva, 1983. Investigation on the duration of the seismic signals like a energetic characteristic of the earthquakes. *BGJ, vol.IX, N1*.

Lee, W. H. K. and J. C. Lahr, 1972. HYP071: A computer program for determining hypocenter, magnitude, and first motion pattern of local earthquakes, *Open File Report, U. S. Geological Survey*, 100 pp.

Solakov, D., 1993. An algorithm for hypocenter determination of near earthquakes. Bulg. Geophys. J. 19 (1), 56-69

Solakov D. and Simeonova S. /eds/ , 1993. Bulgaria catalogue of earthquakes 1981-1990. *BAS, Geophysical Institute, Seismological department, Sofia, pp 38.*

Snoke J.A, 2009. FOCMEC: FOCal MECanism Determinations. *VirginiaTech,Blacksburg, VA, USA.*

Върху мониторинга на сеизмичната активност на територията на България и прилежащите земи

Е.Ботев, Д.Солаков, Л.Христосков

Резюме. Предлаганата публикация съдържа обобщена информация за мониторинга на сеизмичната активност на територията на България и непосредственно прилежащите земи. Повече от 32 000 земетресения с магнитуд M > 0.5 са локализирани в този район след 1981 г. – времето на влизане в действие на съвременната Национална Сеизмологична Мрежа. Предлага се и каталог на най-силните земетресения с магнитуд M>4.0. Сеизмогенните прояви се обсъждат по отделни сеизмични зони в пространството и по петгодишни периоди във времето. Установено е повече или по-малко изявено групиране на епицентрите на най-силните земетресения около основните кватернерно активни разломи и обособени миграционни процеси на сеизмичната активност.

DATA AND ANALISIS OF THE EVENTS RECORDED BY NOTSSI IN 2013

E.Botev, V.Protopopova, I.Popova, Bl.Babachkova, S.Velichkova, I.Aleksandrova, Pl.Raykova, Vl.Boychev

Geophysical Institute, BAS, Akad. G. Bonchev street, bl.3, Sofia, Bulgaria, e-mail: ebotev@geophys.bas.bg

Abstract. A map of epicentres of 1622 earthquakes that occurred during 2013 in the Balkan Peninsula (sector outlined by latitude $\varphi = 37^0 - 47^0$N and longitude $\lambda = 19^0 - 30^0$E) is presented. Expert generalized analysis of the seismicity over the territory of Bulgaria and its very adjacent lands (with more then 930 localized events) is proposed. Catalog of earthquakes with magnitude M>2.5 is applied.

Key words: Balkan Peninsula, Bulgaria, seismicity

The present scientific communication contains generalized information on the results of collection, processing and analysis of the data about the seismic events recorded by the National Operative Telemetric System for Seismological Information (NOTSSI) in 2013. The expanded information about the realized seismicity is suggested as a natural generalization and supplementation of the monthly compilations of the preliminary seismological bulletin of NOTSSI. The analysis and evaluation of the space, time and energy distribution of the seismicity, periodically been made, open up possibilities for searching for time correlations with the parameters of different geophysical fields aiming to find out eventual precursor anomalies.

The recording and space localization of the seismic events in NOTSSI during 2013 is realized by means of the new digital network (Solakov et al., 2005). The routine processing and acquisition of the initial data is organized in a real time duty regime. The operations are fulfilled by the authors of this communication. In such a way the main goal of NOTSSI, namely the seismicity monitoring in order to help the authorities' and social reaction in case of earthquakes felt on the territory of the country, is realized. The computing procedure for determining the parameters of the seismic events is an adaptation of the widespread product HYPO'71 (Solakov , 1993). The energy parameters of the events are presented mainly by the magnitude M calculated according to body wave amplitudes (Christoskov et al., 2011a, Christoskov et al., 2011b) and the record's duration by the

formula (Christoskov and Samardjieva, 1983).

$$M = 1.92 + 2.72\log\tau - 0.026\Delta$$

The focal mechanism parameters are obtained by means of a program FOCMEC (Snoke, 2009). The high sensitivity of the seismographs allows recording and processing of a great number of long distance earthquakes. As a result of the achieved experience in the authors interpretation work, different magnitude's lower threshold for successful determination of local, regional and long distance earthquakes is established: M=1.5 for the territory of Bulgaria, M=3.0 for the central part of the Balkans, M=5.0 for long distance events. The precision of the epicenter's determination is different; except on the distance it depends also on the specific position of the epicenter in relation to the recording network. The parameters of seismic events occurring at a distance more than 100-150 km outside the territory of Bulgaria should be accepted only informatively and cannot be used for responsible seismotectonic investigation.

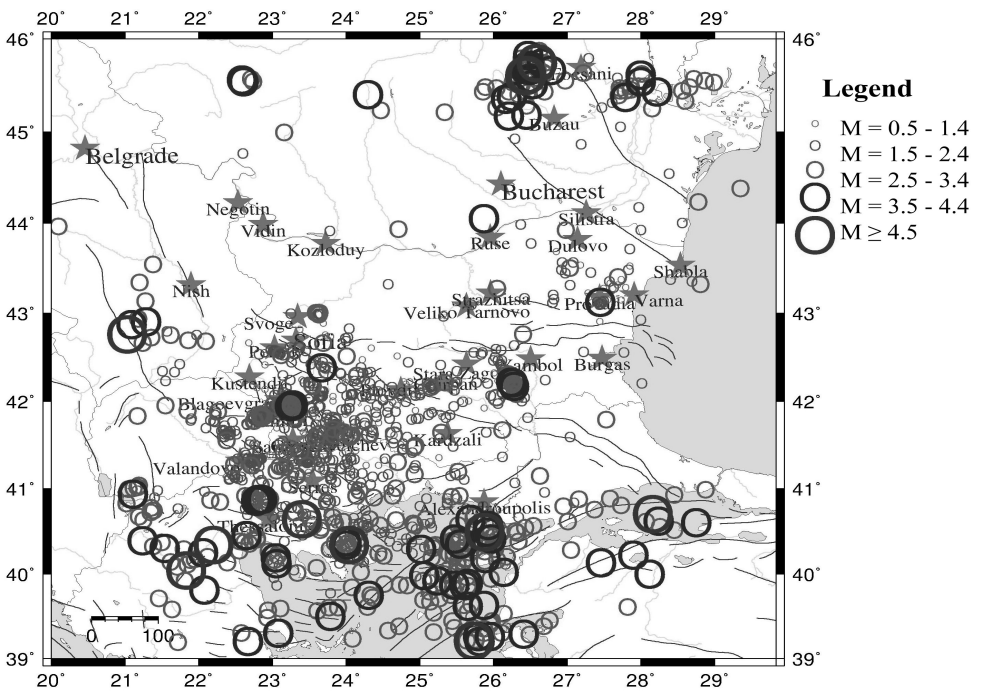

Fig.1. Map of epicenters in Central Balkans during 2013 (The Generic Mapping Tools - http://gmt.soest.hawaii.edu/home, the tectonic map is compiled after Barrier et al., 2004).

For the period of observations presented in this communication, the primary data about 2000 local, regional, distant earthquakes and industrial explosions on the territory of Bulgaria are recorded, classified and processed (as a work bulletin) in NOTSSI. After comprehensive analysis of the records and application of the above mentioned calculation procedures it is established that 1622 of all registered earthquakes are in the Balkan

Peninsula region outlined by geographic latitude 37^0 - 47^0 N and longitude 19^0 - 30^0 E. The epicenters of the earthquakes differentiated by magnitude levels are plotted on Fig.1. The number of the events in the magnitude interval M=0.5-1.9 is 788, in M=2-2.9 - 632, in M=3-3.9 - 175, in M=4-4.9 – 26 earthquakes. During this not so active period there is 1 event with magnitude M=5.0.

As a whole, the seismic situation in the study part of the Balkans during 2013 is characterized by not so high activity - 1622 events against 1508 in 2012, 1829 in 2011, 2401 in 2010, 2744 in 2009, 1775 in 2008, and around 1100- 1400 for most of the previous years. The maximum realized earthquake is with magnitude Ms=5.0 while this value for the previous years is lower then five, as a rule, except 2011 – M=5.8 and 2012 - M=5.6. It can be noted that the observed tendency of high increase of the activity compared with the former years is partly due to the high level of earthquake activation in Marmara sea, Central Greece, Serbia, Romania, and also due to increase of number of microearthquekes in the territory of Bulgaria.

The strongest event outside Bulgaria during the study period occurred in the region situated to the south of Marmara sea (Turkey) with magnitude M=5.0. Shakable effects because of outside attack (Vranchea source zone in Romania) during the study period occurred 3 times in north-eastern Bulgaria (intensity III in towns of Ruse, Tutrakan and Silistra).

As a whole, events with M<3.0 which occur outside Bulgaria are difficult to be localized by the national seismological system; consequently, not all of them have been marked on the scheme in Fig.1.

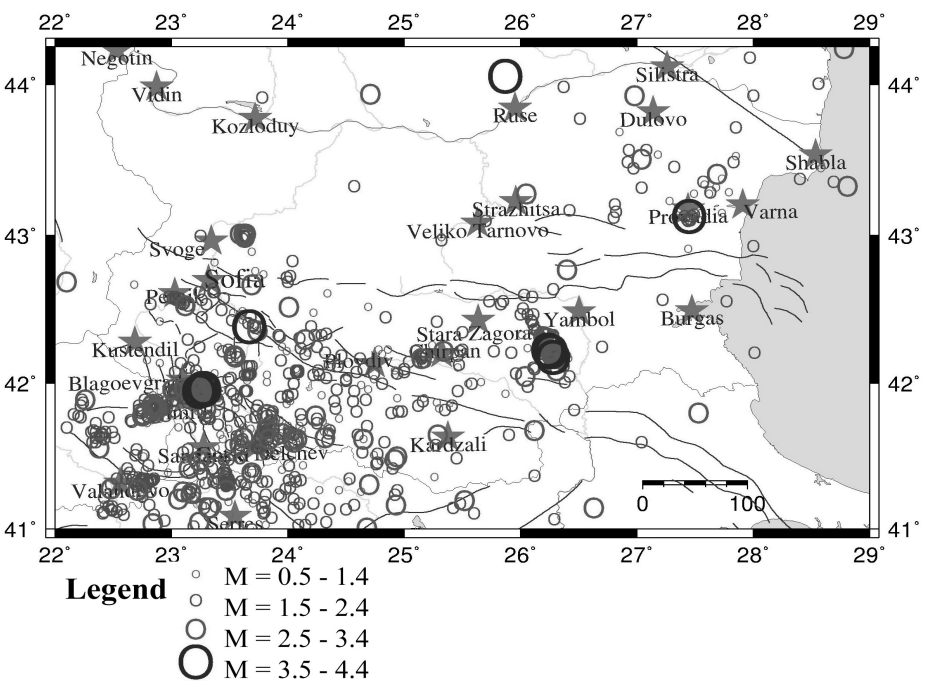

Fig.2. Map of epicentres in Bulgaria and adjacent lands during 2013

Fig.2 illustrates the seismicity just in the territory of Bulgaria and nearby lands ($\varphi = 41^0 - 44.3^0$N, $\lambda = 22^0 - 29^0$E). The earthquakes are differentiated by magnitude intervals. The seismic stations are also noted in the same figure by triangles. The parameters of relatively stronger earthquakes are presented in Table 1.

Table 1. List of earthquakes with M ≥ 2.5 in Bulgaria and adjacent lands during 2013

Date	Time	Coordinates		H,km	M
3.1.2013	1:26:31.3	41.21	23.06	1	2.7
3.1.2013	2:28:37.3	41.91	23.25	2	2.5
4.1.2013	1:26:32.3	41.26	23.1	6	2.8
13.1.2013	14:21: 7.2	41.89	22.26	5	2.8
15.1.2013	10:34:57.1	42.53	23.12	11	2.9
17.1.2013	2:16:23.2	41.01	24.68	14	2.6
20.1.2013	1:59:55.5	42.67	23.69	10	2.6
23.1.2013	18: 1:59.6	41.42	23.15	4	2.7
26.1.2013	7:13:45.9	41.17	24.93	2	2.5
26.1.2013	8:26:40.2	41.92	23.27	2	2.6
27.1.2013	18:37:13.4	41.8	27.53	2	2.8
5.2.2013	21:43:32.3	41.97	23.34	2	2.8
5.2.2013	6: 6:12.8	41.79	23.82	5	2.9
6.2.2013	22:45:19.9	43.33	28.81	2	3.4
11.2.2013	8:29:22.6	41.96	23.22	0	2.5
17.2.2013	16: 5:47.2	42.69	22.1	2	2.9
8.3.2013	18: 5:43.3	42.05	26.04	2	2.6
12.3.2013	17: 1: 6.9	42.36	23.74	5	2.5
21.3.2013	14:29:23.5	41.94	23.21	4	2.9
23.3.2013	18: 0:13.8	42.17	25.15	1	2.6
25.3.2013	17: 2:19.8	42.09	26.31	6	2.9
28.3.2013	13:13:37.8	44.24	28.78	4	2.5
9.4.2013	2:38:51.3	41.69	23.82	8	2.5
9.4.2013	6:59:23.4	42.23	26.24	6	3.7
9.4.2013	7: 3:42.5	42.27	26.2	4	3.4
9.4.2013	7: 9:56.9	42.26	26.2	2	2.9
9.4.2013	7:24:43.8	42.2	26.28	3	2.5
10.4.2013	2:14:59.4	42.23	26.25	2	2.5
14.4.2013	14:30:45.8	42.14	26.29	2	3
24.4.2013	23:17:16.2	41.89	23.22	15	2.5

28.4.2013	10:27: 8.9	42.22	25.34	2	2.6
28.4.2013	22:18:35.3	42.32	26.2	1	2.9
29.4.2013	0: 8: 0.5	42.23	26.26	5	3
29.4.2013	6:19:36.1	42.21	26.26	5	2.9
2.5.2013	19:49:19.9	41.31	24.7	11	2.7
4.5.2013	2:20:28.2	42.31	26.23	10	2.5
5.5.2013	6:38:55.8	41.04	22.84	2	2.7
7.5.2013	1:31: 9.0	41.15	23.33	3	2.5
8.5.2013	9:27:46.2	41.43	23.38	8	3.2
9.5.2013	7:31: 2.8	41.97	23.23	5	2.5
14.5.2013	19:22: 3.2	41.15	26.63	15	2.5
17.5.2013	13:40:26.6	42.22	26.25	5	3.9
23.5.2013	21:47:53.5	41.2	25.52	2	2.5
26.5.2013	2:28:52.8	43.28	26.05	3	2.7
3.6.2013	14: 7:38.7	41.25	23.17	2	2.5
5.6.2013	13: 3:22.0	43.94	24.71	6	2.9
5.6.2013	17: 4:53.2	41.97	23.26	2	2.5
5.6.2013	3:46:41.6	41.83	23.3	8	2.6
6.6.2013	11: 6: 4.5	41.97	23.11	2	2.9
11.6.2013	12:46:36.8	41.15	23.32	2	2.8
4.7.2013	22:47:21.9	41.97	23.24	2	2.5
5.7.2013	13: 0:18.6	41.97	23.25	2	2.7
8.7.2013	11:24:51.1	41.97	23.26	1	3
8.7.2013	18:16:50.8	41.97	23.24	1	2.7
9.7.2013	17: 6:37.9	42.19	26.27	5	3
9.7.2013	17:12: 0.4	42.22	26.26	10	3.7
9.7.2013	18:11:38.4	42.18	26.28	8	3.7
10.7.2013	2:17: 3.6	41.96	23.26	2	2.7
10.7.2013	21:33: 7.5	42.23	26.24	4	2.5
10.7.2013	5:58: 5.6	41.97	23.27	2	2.6
10.7.2013	8:52:31.1	42.22	26.25	1	2.5
11.7.2013	12: 3:19.9	42.17	26.3	5	2.8
11.7.2013	6:29:37.1	42.18	26.29	5	3
11.7.2013	7:56:20.2	41.5	24.94	9	2.5
17.7.2013	19:25:22.3	41.58	23.59	7	2.6
19.7.2013	14:19:42.9	41.63	23.62	2	2.5

27.7.2013	1:24:25.5	41.97	23.28	2	3.6
27.7.2013	1:48:32.2	41.96	23.28	2	3.8
27.7.2013	12:14:31.6	41.97	23.26	2	2.7
27.7.2013	17:32:21.6	41.97	23.24	6	2.6
27.7.2013	3:17: 0.7	41.97	23.27	2	3.7
27.7.2013	3:20:10.2	41.97	23.27	2	3.3
27.7.2013	3:21:55.2	41.95	23.24	2	3.7
27.7.2013	3:30:55.4	41.98	23.27	2	2.8
27.7.2013	3:40: 2.6	41.97	23.27	2	2.8
27.7.2013	3:51:21.7	41.96	23.25	6	2.9
27.7.2013	5:36:33.8	41.96	23.27	2	2.6
5.8.2013	13:42:55.3	41.98	23.17	10	2.7
9.8.2013	19:55:17.5	43.93	26.98	20	2.8
11.8.2013	14:26:35.1	41.98	23.26	8	2.8
13.8.2013	6:14:35.0	43.13	27.45	5	3.6
14.8.2013	11:29:21.7	42.99	23.63	9	3.1
14.8.2013	12:52:54.6	42.99	23.63	12	3.4
21.8.2013	15:39:25.7	43.01	23.62	10	2.5
22.8.2013	15:29:27.7	41.97	23.26	8	2.6
27.8.2013	3:25:39.6	41.48	24.92	14	2.6
28.8.2013	6:48:49.9	41.62	24.05	13	3.3
28.8.2013	8:43:43.2	41.6	24.05	15	3.4
29.8.2013	4: 6:15.8	44.06	25.87	20	4.1
30.8.2013	4:14:58.7	41.62	24.08	10	2.7
1.9.2013	21:22:57.7	41.86	22.84	12	2.7
1.9.2013	21:26:21.0	41.85	22.83	11	2.6
7.9.2013	16:21:59.0	43	23.63	10	2.7
8.9.2013	18: 8: 0.6	41.66	23.95	13	3
10.9.2013	18:56:39.0	43.01	23.59	10	3
10.9.2013	19:28:48.7	41.65	25.29	14	3.3
15.9.2013	19:53: 0.9	43.01	23.64	10	2.9
20.9.2013	10:48:10.9	41.84	22.86	20	2.9
20.9.2013	4:23:50.7	41.83	22.88	20	2.8
20.9.2013	4:45:21.4	41.82	22.84	15	2.7
22.9.2013	12:27: 1.1	42.39	23.67	15	3.7
23.9.2013	13:15:58.3	43.51	27.04	30	2.8

24.9.2013	14:38:22.9	41.27	23.47	13	2.6
29.9.2013	4:18:54.4	41.96	23.01	12	2.6
4.10.2013	13:44:41.9	42.77	26.4	5	2.9
14.10.2013	21:44: 6.6	41.79	22.76	8	3
15.10.2013	4: 5:50.3	41.79	22.76	5	2.6
16.10.2013	2:29: 6.7	41.62	23.84	2	2.5
17.10.2013	9:17:46.3	42.2	26.29	14	2.5
24.10.2013	10:10:43.5	41.05	23.24	18	2.7
26.10.2013	11:44:19.7	43.41	27.69	15	3.1
5.11.2013	8:50:57.6	42.3	24.15	12	2.5
6.11.2013	16: 0:33.2	41.78	22.75	9	2.8
10.11.2013	0: 1:25.7	41.63	24.32	1	2.5
10.11.2013	20:43:57.8	41.39	23.69	14	2.5
19.11.2013	16:50:54.5	41.62	24.65	17	3
22.11.2013	6:43:56.5	42.18	23.55	24	2.6
22.11.2013	9:28:46.1	41.68	26.12	2	2.5
23.11.2013	6:43:56.3	42.19	23.54	19	2.6
26.11.2013	14:18:58.8	41.78	24.24	11	2.5
4.12.2013	21:13:14.0	41.56	22.38	15	2.8
10.12.2013	2:35:37.6	41.28	22.48	12	3.2
15.12.2013	9:13: 0.0	41.47	23.24	15	2.8
19.12.2013	23:24:57.9	42.52	24.01	20	2.9
30.12.2013	11:33:33.2	41.27	22.71	8	3.3

On the territory of Bulgaria relatively normal activity of earthquakes is observed during 2013 – 1124 events are observed, against 932 in 2012, 1205 in 2011, 1607 in 2010, 2017 in 2009 and 1079 in 2008. The earthquakes of a magnitude higher than 3.0 are in normal amount – 32 events compared with an averaged number of about 20-35 for most of the all previous years (exception is 2009 with 147 events because of the aftershocks of Valandovo M=5.2 earthquake).

The maximum realized magnitude is Ms=4.1 in the region of Giurgiu (Rumania), next to the border with Bulgarian territory. This event is the highest earthquake for this region, in comparison with the maximum magnitude in the course of previous years. It is felt with maximum intensity of III-IV degree of MSC scale in the town of Rouse on 29 August 2013. The strongest Bulgarian event during 2013 (with magnitude M=3.9) occurs on 17 May and caused macroseismic effects with intensity of IV degree of MSC scale in the village of Skalitza – close to the Monastery uplift in Southeast Bulgaria.

As usual, the largest concentration of the epicenters in the other regions of Bulgarian territory during 2013 is marked in the southwestern part of the investigated

region (presented in Fig.2). The Kroupnik seismic source is known with the strongest crustal earthquakes in Europe (M=7.8, 7.1) for the last 160 years. In 2013 about 40 events of M<3.0 and only 3 of M≥3.0 occurred in this region. The strongest earthquake for the south-western part of Bulgarian territory is with magnitude M=3.8, it is felt on 27 July in Kroupnik region (village of Gradevo) by intensity of V degree of MSC scale.

The other Bulgarian seismic sources in 2013 are relatively not so active than during the previous years. They produced not more than 15 earthquakes affecting different localities in this country by intensity of up to IV degrees of MSC scale. The maximum number of felt earthquakes is occurred around the Monastery uplift. About six cases of magnitudes more than 3.0 aroused shocks of intensity three or more are felt in Skalitza village. A relatively significant seismic impact is associated with the Mesta earthquake source zone in the southwestern Bulgaria. In the rest part of the Bulgarian territory the felt events caused excitation of lesser intensity during 2013.

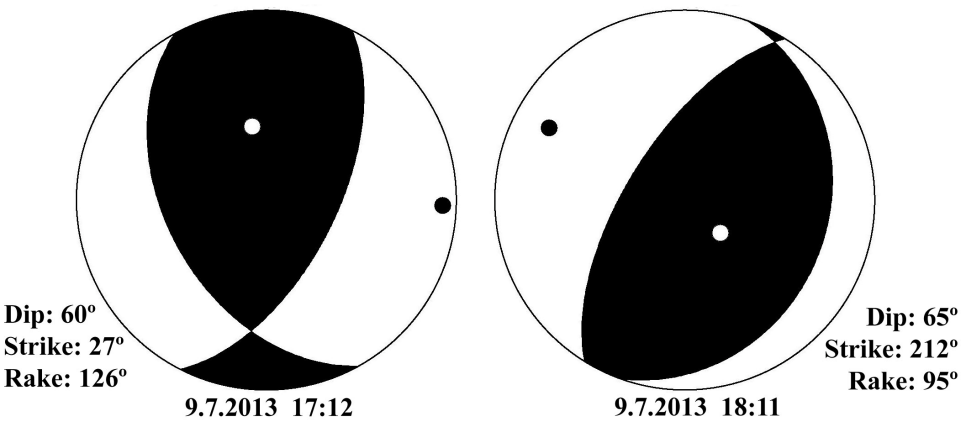

Fig.3. Focal plane solution of earthquakes at Monastery Uplifts (09.07.2013, 17:12 and 18:11 GMT)

For the determination of the earthquake mechanism the program FOCMEC is used. Input data are the polarities of the P wave. Twenty three first motion polarities data from seismological stations in Bulgaria and surrounding area taken from NOTSSI and ISC database (ftp://www.orfeus-eu.org/pub/data/continuous /2013/) are included in the double - couple focal mechanism - Fig.3. The solution is displayed on lower hemisphere. The polarities from ISC are check as waveform. The strike, dip and rake are determined in accuracy up to 10 degree. The earthquake is characterized as a normal faulting, with very small strike-slip component. The fault plane solutions of the some other events are with very bad quality because of a low number of polarities.

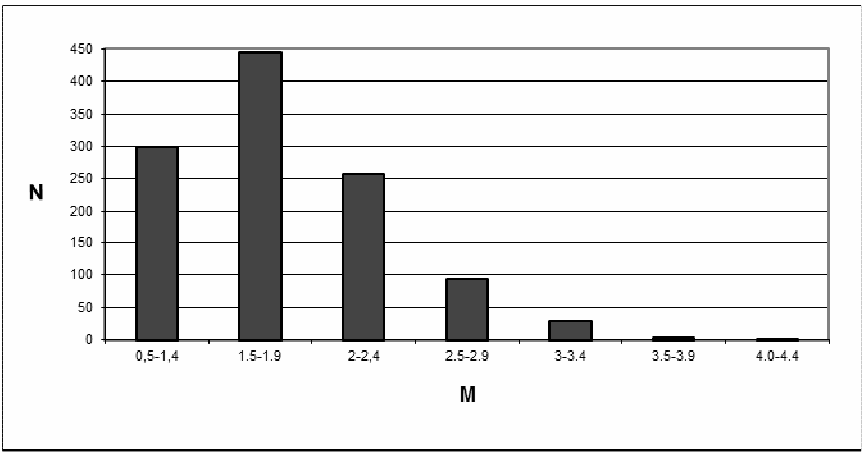

Fig.4. Magnitude - frequency distribution of the earthquakes

A detailed analysis of seismicity in the individual seismic zones is hard to be fulfilled because of the insufficient quantity of events and the narrow magnitude range of the earthquakes. The joint statistics of all the events in Fig.2 characterize predominantly the seismicity parameters of the southwestern part of the territory under investigation.

The magnitude-frequency distribution for the entire data set is presented in Fig.4. The number of localized events increases with the magnitude decreasing: for M= 4.0-4.5 is 1 event, M=3.5-3.9 is 8 events, for M=3.0-3.4 is 28 events, for M=2.5-2.9 - 96, for M=2.0-2.4 - 252 and so on. The abrupt diminishing of the number of earthquakes in the first interval (M<1.5) in Fig.4 determines also the registration power of the seismic stations network. It can be supposed that the magnitude sample for levels with M > 1.5 is comparatively closer to the reality for the bigger part of the Bulgarian territory.

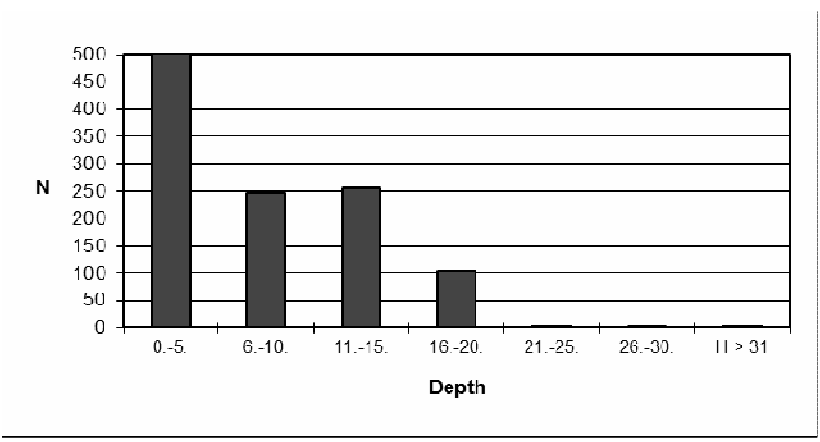

Fig.5. Depth - frequency distribution of the earthquakes

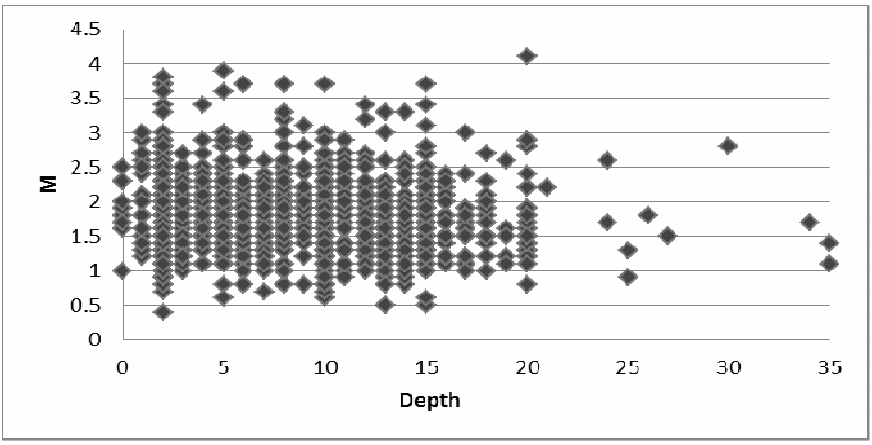

Fig.6. Magnitude - depth dependence

The picture of the depth distribution in Fig.5 shows that the majority of events occur down to 15 km depth. The number of events does not decrease smoothly with increase of the depth. It is possible the established predominating depth (from 0 to 5 km) to be also due to the presence of small number of unidentified industrial explosions. In the same time the number of events in the interval 11-15 km is bigger than this in the previous interval. The magnitude distribution of the events in depth (Fig.6) does not permit to note some differentiation of depth "floors" with the increase of magnitude – the relatively the same maximums can be traced out for the depth intervals down to 20 km depth. As usual the strongest event is deep situated at 20 km depth.

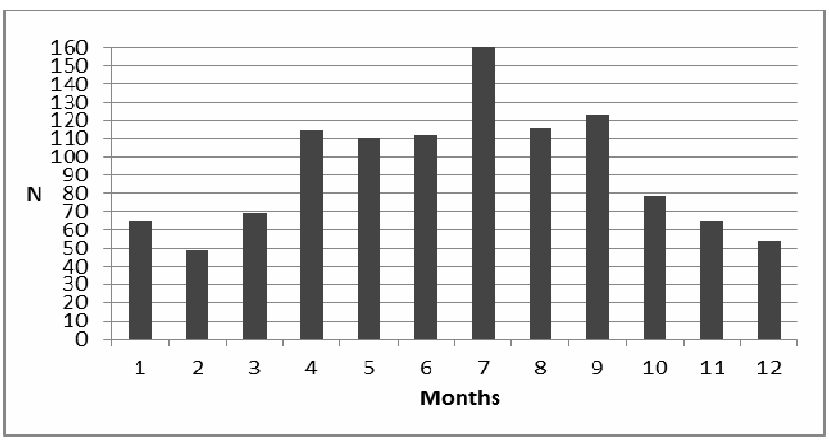

Fig.7. Time distribution of the earthquakes.

Fig.7 illustrates the distribution of seismicity in time according to the number of events per months. The biggest earthquake's amount is displayed in July, when about 160 earthquakes occurred, and it is associated with a swarm activity around of 27 July maximal

earthquake in southwest Bulgaria. The lowest earthquake quantity is in February, around 50 events.

Additionally, about 1000 distant earthquakes have been recorded in the period under study, as well as more than 900 industrial explosions, processed and classified in the preliminary monthly bulletins. In order to identify the artificial seismic sources the methodical approach described by Deneva et al. (1988) and some information about the quarry sites in Bulgaria have been used.

Acknowledgements: The authors owe their gratitude to the engineering staff for the perfect software and hardware ensuring of NOTSSI.

References

Barrier, E., N.Chamot-Rooke, G.Giordano, 2004. Geodynamic map of the Mediterranean, Sheet 1-Tectonics and Kinematics, CGMW, France.

Christoskov L. and E. Samardjieva, 1983. Investigation on the duration of the seismic signals like a energetic characteristic of the earthquakes. *BGJ, vol.IX, N1*.

Christoskov L., L. Dimitrova, D. Solakov. 2011a. Magnitude determinations of P wave by digital broadband seismometers of NOTSSI network for local and regional events. Compres rendus de l'Acade'mie bulgare des Sciences, Vol 65, No5, pp.653-660

Christoskov L., L. Dimitrova, D. Solakov. 2011b. Digital broadband seismometers of NOTSSI for practical magnitude determinations of P waves. BGS. v.XXXVIII, N1-4/2011, ISSN 1311-753X, 62-72.

Deneva D. et al., 1988. On the discrimination between industrial explosions and weak earthquakes using records of local seismics networks. *Proc. of conference in Liblice, 1988*, Praha.

Snoke J.A, 2009. FOCMEC: FOCal MECanism Determinations. VirginiaTech, Blacksburg, VA, USA, 2009, Manual.

Solakov, D., 1993. An algorithm for hypocenter determination of near earthquakes. Bulg. Geophys. J. 19 (1), 56-69

Solakov, D. et all., 2005. National Seismological Network – state and development. Proceedings of Scientific-practical conference on management in extraordinary situations and people protection, BAS, Sofia, 2005, 265-272.

Данни и анализ на сеизмичните събития регистрирани от НОТССИ през 2013

Е.Ботев, В.Протопопова, И.Попова, Бл.Бабачкова, С.Величкова, И.Александрова, Пл.Райкова, Вл.Бойчев

Резюме. Предлаганото научно съобщение съдържа обобщена информация за резултатите от събирането, обработката и анализа на първичните данни за сеизмичните събития, регистрирани от Националната Оперативна Телеметрична

Система за Сеизмологична Информация (НОТССИ) през 2013 г. Представена е карта на епицентрите на общо 1622 земетресения в частта от Балканския полуостров, ограничена от географска ширина 37^0 - 47^0 N и дължина 19^0 - 30^0 E. По-подробно се анализира сеизмичността за територията на България и прилежащите й земи (повече от 930 сеизмични събития в район с координати $\lambda = 22^0$ - 29^0E и $\varphi = 41^0$ - 44.5^0N). Предлага се и каталог на земетресенията с магнитуд M>2,5. Сеизмогенните прояви се обсъждат по зони, сравнени със съседни периоди време.

OBJECTIVE ASSESSMENT OF THREE STORM CASES OVER THE MEDITERRANEAN BASED ON NCEP-NCAR REANALYSIS DATA

H. Chervenkov

National Institute of Meteorology and Hydrology, blvd Tsarigradsko Shose 66, Sofia 1784, Bulgaria, e-mail: hristo.tchervenkov@meteo.bg

Abstract. The cyclones are dominant synoptic-scale features of the atmospheric circulation in the mid-latitudes influencing strongly the local weather, in particular causing severe weather events. The Mediterranean region is the most discernible secondary maximum of the cyclonic activity in the Northern hemisphere. Applying some base mathematics and well-known relations from the theoretical meteorology on the gridded NCEP-NCAR reanalysis datasets, an illustrative case study of three very intense storms in semi-automatic way is performed.

Key words: Mediterranean cyclones, Case study, cyclonic circulation, quantitative climatology

Introduction

Cyclones represent the most important manifestation of the mid-latitude high-frequency variability, and play a fundamental role in the atmospheric large-scale horizontal (and vertical) mixing and in modulating the air–sea interaction. Cyclonic circulations, due to their frequency, duration and intensity, play an important role in the weather and climate over the entire Mediterranean region (Radinovic, 1987). A large spectrum of environmental variables and phenomena are associated with cyclones in the Mediterranean region. Wind, pressure, temperature, cloudiness, precipitation, thunderstorms, floods, waves, storm surges, landslides, avalanches, air quality and even the fog and visibility in the Mediterranean are influenced by the formation and passage of cyclonic disturbances. The Mediterranean area, although located to the south of the main Atlantic storm track that more directly affects western and northern Europe, is quite frequently subjected to sudden events of extreme and adverse weather, often having high social and economic impacts. (Lionello et al., 2006).

Better understandings of spatial and seasonal variability of Mediterranean cyclones as well as the mechanisms leading to cyclogenesis (lysis) are a major concern for the meteorology of the region, especially for those cyclones related to severe weather. Pioneering studies that include climatology of cyclones, cyclogenesis and track patterns in the Mediterranean are those by Pissarski (1955), Pettersen (1956) and Klein (1957). Information about mesoscale cyclones can be obtained from manual analyses. In these analyses, the analyst takes into account information, not present in the objective analysis, from conceptual models and, in some cases, from satellite imagery. The cyclones can be detected and characterized in these analyses by hand. However, the manual technique presents some disadvantages because it is very laborious and it is difficult to apply to long periods of time and to large areas. Also, the systematic computation of certain parameters is difficult as the domain of the cyclones is often too constrained. Furthermore, this method inevitably entails a certain degree of subjectivity. The subjectivity of the analyst affects the detection and location of the cyclones as well as some parameters such as the geostrophic vorticity or the lifetime of the cyclones. These difficulties would disappear if an automated method was used (Picornell et al., 2001). Based on the availability of hemispheric gridded data sets from observations, analysis and global climate models, objective cyclone identification methods were developed and applied to these data sets in the recent decades (see Ulbrich et al., 2009 for a comprehensive review). An expression of the common drive for estimation of the current progress in the field was the IMILAST project - a community effort to intercompare extratropical cyclone detection and tracking algorithms, whose main aim was to reveal those cyclone characteristics that have been robust between different schemes and those that differ markedly (e.g., Neu et al. 2013). Since 1990 (Alpert et al., 1990), most of the studies on climatology of the Mediterranean cyclones are based on objective analyses and objective techniques aimed at detecting and tracking the cyclones (see Lionello et al., 2006 for a comprehensive review). MEDEX (MEDiterranean EXperiment on cyclones that produce high-impact weather in the Mediterranean) is a Research and Development Project, framed into the World Weather Research Program of the World Meteorological Organization, whose main objective is to increase knowledge and improve forecasting of cyclones that produce high-impact weather in the Mediterranean (Genovés et al. 2006).

Mean goal of the presented short paper is to reveal the basic physical and mathematical approach that more or less is incorporated in almost all modern objective cyclone climatologies. Part of the possibilities of the methodology is demonstrated of three very intense storms that produce high-impact weather, especially over the eastern part of the domain. The numerical analysis is performed in semi-automatic way.

The paper is structured as follows: the second chapter is dedicated to the description of the methodology. The third chapter describes the choice of the dataset as well as the performed calculations. The core of the paper is in the fourth chapter, where the results are exposed and discussed. Summarizing remarks are listed and briefly commented on in the conclusion.

Methodology

Following Radinovic (1987) the horizontal domain of a cyclone is defined as the area of positive (in the North hemisphere) vorticity around the cyclone centre, bounded by the zero-vorticity line. After the paper of Sinclair (1997), many authors use the cyclonic circulation as main estimator of the cyclone strength. The author's opinion is that the circulation is a physically the most consistent measurement of cyclone strength because, as stated by Sinclair (1997), it takes into account both the size and rotation rate of the system. The reasons for using this parameter in front of any other (like the pressure or the vorticity in the core point of the low) as a measure of the cyclone strength were detailed and referenced in Picornell et al. (2001) and Campins et al. (2006), and coincident with those argued by Sinclair.

According the definition, the flux Φ of some vector (in our case the wind velocity u) trough area S is equal to:

$$\Phi_u = \iint_S \vec{u}.d\vec{s} \tag{1}$$

Applying the Stokes theorem, which states equivalence between the circulation C, defined as the line integral of the vector around a closed path L_s and the flux of the vector's vorticity trough the area, bounded by this path area S, we can write:

$$C = \oint_{L_s} \vec{u} \cdot d\vec{r} = \iint_S (\vec{\nabla} \times \vec{u}) \cdot d\vec{s} \tag{2}$$

Due to the fact that the dot product between the horizontal vorticity components $(\vec{\nabla} \times \vec{u})_x$, $(\vec{\nabla} \times \vec{u})_y$ and the surface element $d\vec{s}$ is equal to zero, the cross product in the right side of equation (2) can be replaced with the vertical vorticity component, traditionally marked in the meteorology with ξ:

$$\xi := (\vec{\nabla} \times \vec{u})_z = \frac{\partial v}{\partial x} - \frac{\partial u}{\partial y} \tag{3}$$

The integral on the right side of equation (2), namely the vorticity flux Φ_ξ according equation (1), can be estimated as follows:

$$\Phi_\xi = \iint_S (\vec{\nabla} \times \vec{u}).d\vec{s} = \iint_S \xi.d\vec{s} \approx \overline{\xi} \iint_S d\vec{s} = \overline{\xi}.S_c \tag{4}$$

Thus, C is roughly equal to the area S_c enclosed by the curve L_s times the mean vorticity $\overline{\xi}$ over the area. If obtained separately, as shown in the next chapter, S_c can be used as additional measure of the cyclone's magnitude. Assuming circular shape with diameter D_c

of the cyclone and movement with constant tangential velocity v_τ along this circle, we can obtain:

$$C = \oint_{L_s} \vec{u} \cdot d\vec{r} = v_\tau \oint_{L_s} d\vec{r} = \pi v_\tau D_c = 2v_\tau \sqrt{\pi S_c} \tag{5}$$

finally:

$$v_\tau = \frac{C}{2\sqrt{\pi S_c}} = \frac{\Phi_\xi}{2\sqrt{\pi S_c}} \tag{6}$$

Thus the computation of the cyclonic circulation, as measure of its strength, is in natural way connected with the calculation of other significant quantities as the size/diameter and representative velocities (linear or angular - most often the mean tangential velocity along the cyclone's boundary). The SI-unit of measure of the vorticity flux is $m^2.s^{-1}$ or, for convenience in the meteorology, CU, where 1 CU=10^7 $m^2.s^{-1}$. For example, if the cyclonic area is 1000000 square kilometers (approximately a circle with diameter 1128 km, which is typical value for North Atlantic cyclones or very big Mediterranean ones) and the mean vorticity trough this domain is 5.10^{-5} s^{-1}(CVU), the circulation will be 5 CU and, according the second relation in (6), the mean tangential velocity v_τ along the boundary will equal 14 m/s.

The main difficulty with circulation calculations lies in defining the region of cyclonic airflow associated with each vertex (i.e. cyclone center), especially in cases of multi-core depressions, when many centers share a common zero-vorticity line. Basic idea in most algorithms is: starting from the cyclone centre, a search is made radially outward looking for the location where $\xi = 0$. In the study of Picornell et al. (2001) the points where the (geostrophic in this case) vorticity is zero are searched along the east, north, west and south directions (principal axes) and they are joined by means of four portions of ellipse. The initial horizontal domain of the cyclone is then obtained by adding the four quarters of elliptical areas, limited by the portions of ellipse and the principal axes ('pseudo-ellipse'). More precisely, in other studies (Sinclair, 1997; Campins et al., 2006) the search is performed along more radial axes (i.e. with smaller angular increment) but generally such procedures requires interpolation between the gridnodes which can be very computationally demanding.

Original authors idea is to estimate the size and the circulation of the cyclone without explicit determination of the zero-vorticity line. Thus, let n_{ij} be the number of corners of the gridcell with lower left corner at the grid point with indexes *i* and *j*, where the vorticity ξ_{ij} is positive. Obviously, n_{ij} can take only five values: 0, 1, 2, 3 and 4. The values 0 and 4 are in the cases when this gridcell is completely in or out of the area, occupied by the cyclonic flow and if n_{ij} is equal to 1, 2 or 3, the zero-vorticity line, whose

exact position is not known, splits the gridcell. The idea is to estimate the 'cyclonic part' of the gridcell's area Δs_{ij}^{c} as:

$$\Delta s_{ij}^{c} := \frac{n_{ij}\Delta s_{ij}}{4} \approx \frac{n_{ij}\Delta y(\Delta x_{j} + \Delta x_{j+1})}{8} \tag{7}$$

Here Δy is the cell side along the meridian, Δx_{j} and Δx_{j+1} are the cell sides along the model's parallel with index *j* and *j+1* as shown on figure 1.

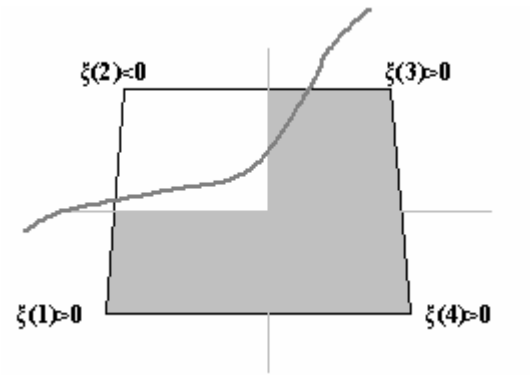

Fig. 1 Schematic illustration of the proposed method. The zero-vorticity line (shown in bold) crosses the gridcell and thus *n=3*. The 'cyclonic part' (grayed) of the gridcell is estimated as ¾ from the whole and the average cyclonic vorticity-$(\xi_1+\xi_3+\xi_4)/3$

Continuing the upper idea, the average positive (cyclonic) vorticity in the gridcell is equal to:

$$\overline{\xi^{c}_{ij}} := \begin{cases} \dfrac{\sum\limits_{i,j,\xi_{ij}>0} \xi_{ij}}{n_{ij}}, & n_{ij} \neq 0 \\ 0, & n_{ij} = 0 \end{cases} \tag{8}$$

Finally, we can obtain the cyclonic vorticity flux trough the gridcell:

$$\Phi_{ij}^{c} = \overline{\xi_{ij}^{c}}.\Delta s_{ij}^{c} \tag{9}$$

Keeping in mind that the flux is an additive quantity, the total one over a certain region can be obtained by simple summing of single shares over the calculated by equation (9) contributions for all gridcells included in this region. In particular, it is possible to estimate the flux of an individual cyclone by summing the gridcell fluxes over the area which includes this object. The borders can be found inspecting the vorticity sign around the corresponding vorticity maximum. Obviously such approach lacks accuracy. However, due

mainly to its simplicity, it can be used for case studies of well isolated structures as demonstrated later.

Used data and performed calculations

The data used in this study are the time series of 6-h wind produced during National Centers for Environmental Prediction (NCEP) National Centre for Atmospheric Research (NCAR) 40-year reanalysis project (Kalnay et al., 1996), converted in plain ASCII format in the Climatic Research Unit, University of East Anglia. The data set consists of grid point values of the 850 Hpa level real (not geostrophic!) wind for Quarter-Spherical Window (0°N-90°N; 90°W-90°E) in a grid of 2.5°×2.5°, allowing the study of synoptic scale cyclones. The modeling domain extends between latitudes 22.5°N and 55.0°N, and longitudes 12.5°W and 47.5°E including completely the Mediterranean, the surrounding territories and the Black Sea. The finite difference method is applied to calculate the vorticity field. The reasons for selection of this isobaric level are manifold, but will be not discussed here. One of the main merits of the chosen approach, based on the above proposed method, is the indicative force of the vorticity flux over a certain area – first, it is a very robust integral (over the space) criterion of absence or presence of cyclonic activity there and, if such is present, of its magnitude. Thus the maximums of the time-series of the overall (i.e. the integrated over the whole domain) flux can be treated as rough proxy for cyclonic activity at the corresponding time. In such a fashion an outstanding peaks that correspond to very intense lows, as this shown on figure 2, can be easily detected.

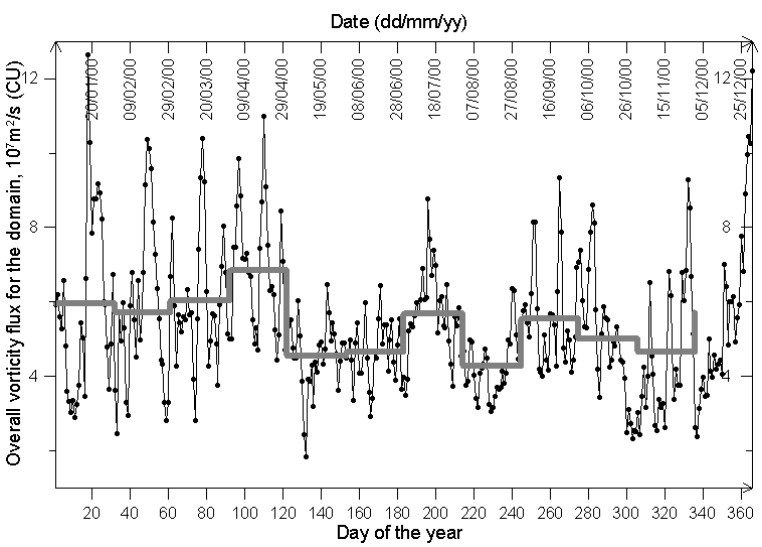

Fig. 2 Time series for the overall cyclonic flux trough the domain for the year 2000. The step plot shows the monthly averages. The very high value on the right ridge of the figure reveals strong activity in day 366 (31 December).

Resolving this task using other methods can be very time-consuming. The computation of these time series for the full 66-year (1948-2013) time span of the dataset reveals the first, second and third maximums of the daily average, which are on the 03.02.1954, 07.02.2012 and 08.02.1996 and are equal to 18.0 CU, 16.4 CU and 15.7 CU correspondingly. Next necessary step is to find the positions of all vorticity maximums for the time frame of interest, which are potential cyclone centers. The traditional manner of detecting the location, respectively of the value, of the maxima is performed automatically: The vorticity in each node is compared with that in all eight surrounding grid points, followed by interpolation within the gridcell, as illustrated in one other case (not observed here further) on figure 3

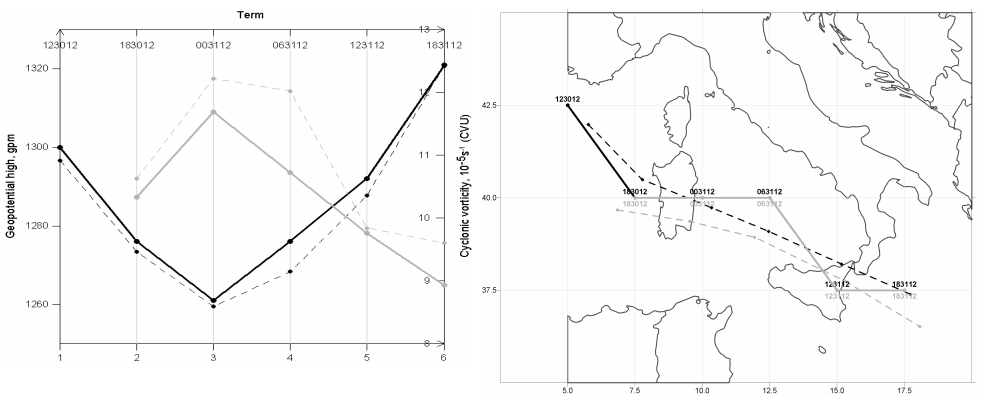

Fig. 3 (Left) Time series (time lebel: hhddmm, year 2000) of the 850 Hpa geopotential high (in black) and cyclonic vorticity (in gray) of the selected cyclonic center. (Right) Corresponding tracks. The solid lines on both panes connect the non-interpolated (i.e. gridnode value and position) and the dashed – the interpolated values. The value and position of the vorticity centre at 123012 is not computed in this case due to the absence of derivate (respectively vorticity) at the left domain border.

The maximal value of the vorticity for a single vertex is calculated for the one, detected on 21.01.1981 18 UTC and is equal to 13.2 CVU. Although the tracking of individual systems is out of the scope of this work, the created digital maps with vorticity maximums allow performing such a task for short intervals in semi-automatic manner. Thus, applying the most widely used (Ulbrich et al., 2009) nearest-neighbor search and inspecting consecutive time frames, the tracks of the selected lows for four time steps before and four time steps after (or 48 hours as a whole) the moment of maximal core-point vorticity, are constructed as shown on figure 4. The most important feature, the determination of the region of cyclonic airflow, is performed using the prescribed in the previous section method. A simple four-directional search along horizontal and vertical axes, obtaining a rectangular area, occupied by the low is applied. Further, the cyclone 'size' and intensity is obtained by summarizing automatically the cyclonic part of the cell and fluxes trough every gridcell, contained in this area in accordance with Eq. (7) – (9). Finally, applying Eq. (5) and (6) the diameter D_c and mean tangential velocity v_τ are calculated.

Results and comments

Only a first sight about the representation of some calculated features for the selected storms will be addressed, following partly the presentation manner in Genovés et al. (2006).

All of the four observed cases correspond to very deep one- or multi-core lows and at least three among them are reason for severe weather over broad regions in Southeast Europe (for the case from 2012 see, for instance Chervenkov (2012), no documentation has been found at the moment of writing this paper for the case in 1954). The synoptical treatment of these events, however, is out of the scope of the present work. The cyclone from the case in 1996 is dynamically of very complex structure – an extremely elongated (roughly from Greenland in the northwest to Crete in the southeast) depression with multiple circulation vertices. To apply the simple relations, as the equation above, to such a structure, even for rough judgments, can lead to serious discrepancies. Thus, only the three cases from 1954, 1981 and 2012 are treated further. Table 1 summarizes the main obtained results according the mean features of the selection.

According the classification of Guijarro et al. (2006), moderate cyclones are those with circulation greater or equal than 4 and less than 7 CU and grater than 7 – as a strong. Analyzing the SL-geostrophic vorticity, Genovés et al. (2006) finds that the maximum of the circulation's probability density function is located around 3 GCU. The 90% of the cyclones have values of circulation below 6 GCU and 7 GCU, respectively, in the western and eastern Mediterranean, when only the moments of maximum development of the cyclones are considered. Trigo et al. (1999) reveals, that, depending of the sub region and the season (the variability is significant!), the Mediterranean cyclone radii are roughly between 300 and 600 km. Applying these quantitative criteria, the selected cases can be really judged as severe manifestation of cyclonic activity in the Mediterranean. Table 1 shows that all of the cyclones occurred in winter, which is in the accordance with the well-known fact for annual maximum of the cyclonic activity during this season.

Table 1 Main features of the selected cyclones according column caption

	Case 1	Case 2	Case3
Time, hh dd/mm/yyyy	06 UTC 02/02/1954	18 UTC 21/01/1981	18 UTC 06/02/2012
Location, Lat., Long.	40.88N; 11.58E	35.55N; 18.80E	36.72N; 20.76E
Maximal vorticity, CVU	10.4	13.2	12.8
Circulation, CU	15.7	12.5	14.2
Cyclonic size S_c, 10^3 km^2	7919	4140	5410
Equivalent diameter D_c, km	3175	2296	2334
Mean tangential velocity v_t, m/s	15.7	12.5	19.5

The storm in 2012 produced heavy snowfalls over a big part of the Balkan Peninsula and additionally very strong winds with gusts (and resultant high waves) on the western Black Sea coast, causing various damages on the infrastructure. The cyclones in 1954 and 2012 have a similar African origin and the 1981 event corresponds to a Genoa cyclone. The last case is investigated deeper by Genovés et al. (2006) and it is placed in the third place in the severity storm rank-list, where the ordering criterion was the maximal

geostrophic circulation. They have obtained a storm track relatively near (qualitatively compared indeed) to the one on figure 2 and term of maximum development/ maximal circulation 21.01.1981 12 UTC and 13.77 geostrophic circulation units (CGU) respectively. These values are also close to their analogs in Table 1 despite the different method and dataset (ERA40) used in the study.

Concluding this section, it is worth commenting the case 1954. Here, the procedure of bounding the cyclonic air flow reveals that the zero-vorticity line is closed inside the domain, but the corresponding calculated circumference is not. The reason is the zonal elongation of this low. Thus, the depicted circle underestimates the cyclone size in the west-east and overestimates it in the south-north direction. This example, together with the remarks for the cyclone in February 1996, shows that estimation of the characteristics based on simple averages has to be performed carefully and the more correct interpretation of the quantities from (4) are 'equivalent by circular form' rather than 'mean' one.

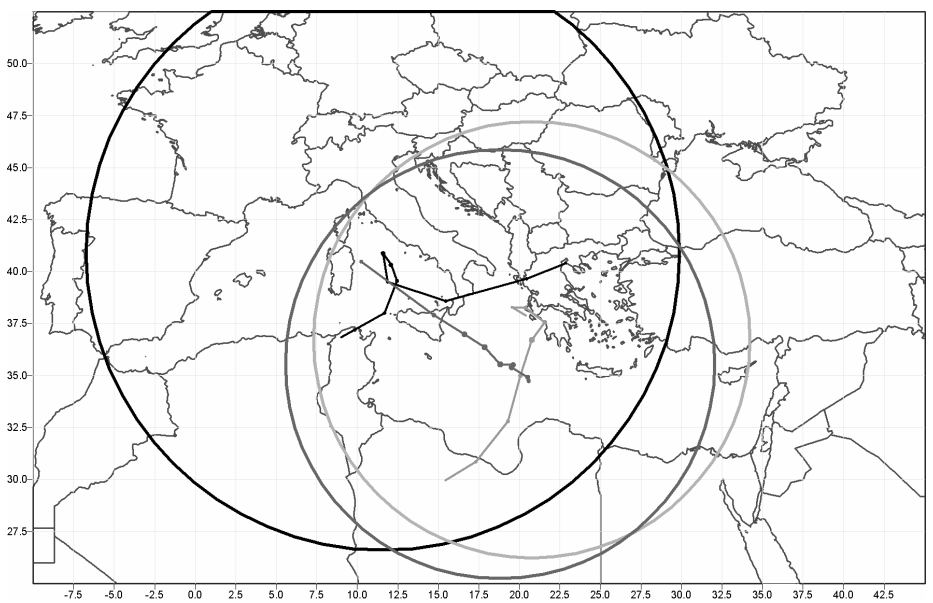

Fig. 4 Figure 4 Obtained 48-hour tracks and cyclones circumferences (according Table 1) centered over the moment of the maximal core-point vorticity for the cases 1954 (in black), 1981 (in dark grey) and 2012 (in light grey). The size of the location symbols for each time step is proportional (same scale for all cases) to the core-point vorticity magnitude.

Conclusion

The paper is concise presentation of some of the base mathematics and physical ideas, which are in the fundamental of the objective assessment of the cyclonic features. In the last decades this, most used approach, has proved his efficiency in obtaining and for analyzing detailed statistics of extratropical weather systems, in particular Mediterranean

ones. Consequently many detailed databases were produced; some of them freely-available (see, for example, the web-page of MEDEX: medex.inm.uib.es). The presence nowadays of long-term gridded datasets, from reanalysis projects and/or global circulation models from one hand and the increased computational resources from other, determines the prevailing role of the approach also in the future. The work demonstrates that even with the proposed, fairly simplified indeed, method; meaningful quantitative estimations can be achieved. Such results are widely used in many sinoptical, climatological, hydrological and etc. studies. Finally, it is worth to emphasize, that the dynamically oriented research has to continue further, especially in the hydro-meteorological institutes in the dense-populated Mediterranean countries, due to the high theoretical and socio-economical importance of the phenomena.

Acknowledgments. To NCEP-NCAR for providing free of charge data and to the Climatic Research Unit, University of East Anglia for the reformatting of these data in convenient form and its further online redistribution.

References

Alpert P, Neeman BU, Shay-El Y (1990) Climatological analysis of Mediterranean cyclones using ECMWF data. TellusA 42:65–77

Campins J, Jansà A, Genovés A 2006 Three-dimensional structure of western Mediterrenean cyclones Int. J. Climatol. 26: 323–343

Chervenkov H 2012 The Winter of 2011/2012 – Synoptical Aspects and Weather Events Proc. of IX-th scientific-technical conference "ECOLOGY and HEALTH", Plovdiv, 17 May 2012, pp. 511-516

Genovés A, Campins J, Jansà A 2006 Intense storms in the Mediterranean: a first description from the ERA-40 perspective Adv Geosciences, 7, 163–168

Guijarro J. A., Jansà A, Campins J 2006 Time variability of cyclonic geostrophic circulation in the Mediterranean Adv Geosciences, 7, 45–49

Kalnay E, Kanamitsu M, Kistler R, Collins W, Deaven D, Gandin L, Iridell M, Saha S, White G, Woolen J, Zhu Y, Chelliah M, Ebisuzaki W, Higgins W, Janowiak J, Mo KC, Ropolewski C, Wang J, Leetmaa A, Reynolds R, Jenne R, Joseph D 1996 The NCEP/NCAR 40-year reanalysis project. Bull Am Meteorol Soc 77:437–471

Klein, W.H. 1957 Principal tracks and frequencies of cyclones and anticyclones in the Northern Hemisphere. U.S. Weather Bur., Res. Paper num. 40

Lionello P., Bhend J., Buzzi A., Della-Marta P. M., Krichak S., Jansà A, Maheras, P., Sanna, A., Trigo, IF., and Trigo, R. 2006 Cyclones in the Mediterranean region: climatology and effects on the environment Developments in Earth and Environmental Sciences, Elsevier, 4, 325–372

Neu U., M.G. Akperov, N. Bellenbaum, R. Benestad, R. Blender, R. Caballero, A. Cocozza, H.F. Dacre, Y. Feng, K. Fraedrich, J. Grieger, S. Gulev, J. Hanley, T. Hewson, M. Inatsu, K. Keay, S.F. Kew, I. Kindem, G.C. Leckebusch, M.L.R. Liberato, P. Lionello, I.I. Mokhov, J.G. Pinto, C.C. Raible, M. Reale, I. Rudeva, M. Schuster, I. Simmonds, M. Sinclair, M. Sprenger, N.D. Tilinina, I.F. Trigo, S. Ulbrich, U. Ulbrich, X.L. Wang, H. Wernli, 2013 IMILAST – a community effort to intercompare extratropical cyclone detection and tracking algorithms. Bull. Amer. Meteor. Soc., 94, 529–547

Sinclair MR 1997 Objective identification of cyclones and their circulation intensity, and climatology. Weather Forecasting 12:595–612

Pettersen S. 1956 Weather Analysis and Forecasting, Vol I. McGraw-Hill: New York, 428.

Picornell MA, Jansà A, Genovés A, Campins J 2001 Automated database of mesocyclones from the Hirlam (INM)-0,5° analyses in the Western Mediterranean. Int J Climatol 21:335–354

Pisarski, A. 1955 The Mediterranean cyclones and their impact on the weather in Bulgaria (in Bulgarian) Hydrology and Meteorology (issue of the Bulgarian Institute of Meteorology and Hydrology) vol II, no. 6

Radinovic, D. 1987 Mediterranean cyclones and their influence on the weather and climate, WMO, PSMP Rep. Ser. num 24

Ulbrich U, Leckebusch G. C., Pinto J. G. 2009 Extra-tropical cyclones in the present and future climate: a review Theor Appl Climatol 96:117–131

Trigo IF, Davies TD, Bigg GR 1999 Objective climatology of cyclones in the Mediterranean region. J Clim 12:1685–1696Saka O., M. Itonaga, T. Kitamura, , 1982. Ionospheric control of polarization of low- latitude geomagnetic micropulsations at sunrise. *J. of Atm. and Terr. Phis.*, 44, No. 8, 703-712.

Обективен разбор на три случая с бури над Средиземнорието, основан на данните от реанализа на NCEP-NCAR

Хр. Червенков

Резюме: Циклоните са доминиращата особеност със синоптичен мащаб на циркулацията на умерените ширини като оказват силно влияние на метеорологичното време, в частност обуславяйки опасни обстановки. Средиземноморието е най-ясно различимият район - вторичен максимум на циклоналната активност в Северното полукълбо. Като се прилагат някои основни математически съотношения и добре познати зависимости от динамичната метеорология, е проведен обективен разбор на три случая с интензивни циклонални бури главно с демонстративна цел.

Information for Contributors

Submission of a paper implies that it has not been published previously and is not under consideration for publication elsewhere.

Typescript. All parts of the paper must be typed double-spaced on good quality white paper A4 (210 x 297mm) with at least 2.5 cm margins at top, bottom, and sides. Each page of the typescript should be numbered on the bottom in the right corner.

Authors are expected to supply 2 clean copies in English or Bulgarian. Please use correct English or Bulgarian spelling, punctuation, grammar, and syntax. The metric system must be used throughout; use of appropriate SI units is encouraged.

Paper length. Paper should be written in the most concise form. Occasionally long papers (over 15p.) are accepted, particularly those of a review nature.

The typescript should be arranged as follows:

1. Title page including authors' names and affiliations
2. Abstract and key words
3. Text (including tables and figures)
4. Reference list

Abstract. The abstract should be in a single paragraph (250 words or fewer). State the nature of the investigation and summarize its important conclusions. References must not be cited in the abstract. The abstract should be suitable for separate publication in a Web site.

Mathematics. All characters available on a standard typewriter must be typewritten in the equations as well as in text. Special attention should be paid to single couples of the kind: vv, pρ, mμ, nη. Distinction should be made between the letter O and the numeral 0; between the letter I and the numeral 1; between k and kappa.

Alignment of symbols must be unambiguous. Superscripts and subscripts should clearly be in superior or inferior position. Fraction bars should extend under the entire numerator. Displayed equations should be numbered consecutively throughout the paper; the number (in parentheses) should be to the right of the equation.

References. A complete and accurate reference list is of major importance. Only works cited in the text should be included in the reference list. References are cited in the text by the last name of the author and the year: (Jones, 1990). If the author's name is part of the sentence, only the year is bracketed. References are arranged alphabetically by the last names of authors. Multiple entries for a single author are arranged chronologically. Two or more publications by the same author in the same year are distinguished by a, b, c after the year.

Tables. Tables should be typed as authors expect them to look in print. Every table must have a title. Column headings must be arranged so that their relation to the data is clear. Each table must be cited in the text.

Illustrations. All illustrations should be inserted in the text, suitable for the camera-ready reproduction (which may include reduction). Each figure must be cited in numerical order in text and must have figure legend. Please do not draw with hairlines. The minimum line width is 0.2 mm (i.e. 0.567pt).

Electronic submission. Authors must submit an electronic copy of their paper with the final version of the manuscript. The electronic copy should match the hardcopy exactly.

Authors will receive more detailed information when the article is accepted for publication so that requirements for the camera-ready presentation are fulfilled.